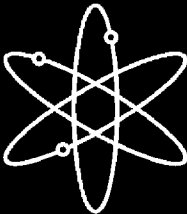
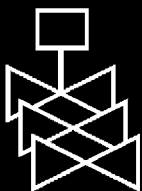


Air Oxidation Kinetics for Zr-Based Alloys



Argonne National Laboratory



**U.S. Nuclear Regulatory Commission
Office of Nuclear Regulatory Research
Washington, DC 20555-0001**



AVAILABILITY OF REFERENCE MATERIALS IN NRC PUBLICATIONS

NRC Reference Material

As of November 1999, you may electronically access NUREG-series publications and other NRC records at NRC's Public Electronic Reading Room at <http://www.nrc.gov/reading-rm.html>. Publicly released records include, to name a few, NUREG-series publications; *Federal Register* notices; applicant, licensee, and vendor documents and correspondence; NRC correspondence and internal memoranda; bulletins and information notices; inspection and investigative reports; licensee event reports; and Commission papers and their attachments.

NRC publications in the NUREG series, NRC regulations, and *Title 10, Energy*, in the Code of *Federal Regulations* may also be purchased from one of these two sources.

1. The Superintendent of Documents
U.S. Government Printing Office
Mail Stop SSOP
Washington, DC 20402-0001
Internet: bookstore.gpo.gov
Telephone: 202-512-1800
Fax: 202-512-2250
2. The National Technical Information Service
Springfield, VA 22161-0002
www.ntis.gov
1-800-553-6847 or, locally, 703-605-6000

A single copy of each NRC draft report for comment is available free, to the extent of supply, upon written request as follows:

Address: Office of the Chief Information Officer,
Reproduction and Distribution
Services Section
U.S. Nuclear Regulatory Commission
Washington, DC 20555-0001
E-mail: DISTRIBUTION@nrc.gov
Facsimile: 301-415-2289

Some publications in the NUREG series that are posted at NRC's Web site address <http://www.nrc.gov/reading-rm/doc-collections/nuregs> are updated periodically and may differ from the last printed version. Although references to material found on a Web site bear the date the material was accessed, the material available on the date cited may subsequently be removed from the site.

Non-NRC Reference Material

Documents available from public and special technical libraries include all open literature items, such as books, journal articles, and transactions, *Federal Register* notices, Federal and State legislation, and congressional reports. Such documents as theses, dissertations, foreign reports and translations, and non-NRC conference proceedings may be purchased from their sponsoring organization.

Copies of industry codes and standards used in a substantive manner in the NRC regulatory process are maintained at—

The NRC Technical Library
Two White Flint North
11545 Rockville Pike
Rockville, MD 20852-2738

These standards are available in the library for reference use by the public. Codes and standards are usually copyrighted and may be purchased from the originating organization or, if they are American National Standards, from—

American National Standards Institute
11 West 42nd Street
New York, NY 10036-8002
www.ansi.org
212-642-4900

Legally binding regulatory requirements are stated only in laws; NRC regulations; licenses, including technical specifications; or orders, not in NUREG-series publications. The views expressed in contractor-prepared publications in this series are not necessarily those of the NRC.

The NUREG series comprises (1) technical and administrative reports and books prepared by the staff (NUREG-XXXX) or agency contractors (NUREG/CR-XXXX), (2) proceedings of conferences (NUREG/CP-XXXX), (3) reports resulting from international agreements (NUREG/IA-XXXX), (4) brochures (NUREG/BR-XXXX), and (5) compilations of legal decisions and orders of the Commission and Atomic and Safety Licensing Boards and of Directors' decisions under Section 2.206 of NRC's regulations (NUREG-0750).

DISCLAIMER: This report was prepared as an account of work sponsored by an agency of the U.S. Government. Neither the U.S. Government nor any agency thereof, nor any employee, makes any warranty, expressed or implied, or assumes any legal liability or responsibility for any third party's use, or the results of such use, of any information, apparatus, product, or process disclosed in this publication, or represents that its use by such third party would not infringe privately owned rights.

Air Oxidation Kinetics for Zr-Based Alloys

Manuscript Completed: March 2004
Date Published: June 2004

Prepared by
K. Natesan, W.K. Soppet

Argonne National Laboratory
9700 South Cass Avenue
Argonne, IL 60439

S. Basu, NRC Project Manager

Prepared for
Division of Systems Analysis and Regulatory Effectiveness
Office of Nuclear Regulatory Research
U.S. Nuclear Regulatory Commission
Washington, DC 20555-0001
NRC Job Codes Y6707 and Y6512



Air Oxidation Kinetics for Zr-Based Alloys

by

K. Natesan and W. K. Soppet

Abstract

An experimental program was conducted to generate data on the air oxidation kinetics of unirradiated cladding of Zr-based alloys (such as Zircaloy-4, Zirlo, and M5) with an oxide layer that is representative of the current inventory of spent fuel discharged after a medium or high level of fuel burnup. The oxide layer that forms on the cladding while in the spent fuel pool was simulated by a preoxidation step in a steam environment for 140 h at 550°C for Zircaloy-4 and Zirlo and for 427 h at 550°C for M5. This resulted in an oxide thickness in the range of 25-30 μm for all three alloys. The steam-preoxidized specimens were subsequently oxidized in air at temperatures in the range of 300-900°C. Oxidation tests in air emphasized temperatures in the range of 300-600°C, which is representative of cladding heatup in the event of a partial or full draining of spent fuel pool coolant. The maximum air oxidation times ranged between 300 h at 600°C and \approx 1000 h at 300°C. Weight change and oxide thickness measurements were made on the specimens exposed at various times to establish the kinetics of the scaling process as a function of temperature. Bare capsules of the three alloys were also exposed in air for comparison of the oxidation behavior of the alloys with and without steam preoxidation. Limited tests were conducted at 400 and 600°C to evaluate the oxidation performance of Zircaloy-4 in a low-oxygen high-nitrogen environment. Isothermal oxidation tests were also conducted with tube specimens of steam-preoxidized Zircaloy-4 with internal pressures in the range of 50-400 psig at 600 to 900°C. Extensive metallography was used on the tested specimens to examine the oxide scale development, pin-hole rupture morphology, and oxide cracking propensity. The data indicate that the oxide thickness is somewhat larger in the tests conducted with high internal pressure than that obtained in the absence of it, especially at 600 and 700°C. The increase is attributed to microcracks in the oxide (and associated oxidation) that result from increased deformation in the specimen due to pressurization. Weight change and oxide thickness data, generated in the present program, were used to develop correlations to depict the air oxidation behavior of the alloys as a function of time and temperature. The results showed that the correlation, developed for Zircaloy-4 from the oxidation data generated in the current project, is in fair agreement with that based on Nureg1 and Powers. The predictions based on Nureg2 and CODEX correlations for Zircaloy-4 are several orders of magnitude lower than those based on current work, especially at lower temperatures. A comparison of the oxidation data for Zirlo with those for Zircaloy-4 showed that the post-breakaway rates are somewhat lower for Zirlo at $T \leq 500^\circ\text{C}$; however, the rates are higher for Zirlo than for Zircaloy-4 at $T \geq 600^\circ\text{C}$. The oxidation rates (in the post-breakaway region) for M5 are consistently lower than for other two alloys at 500 and 600°C. Oxide scale thickness data, developed on the three materials during air exposure, are used to evaluate the time- and temperature-dependence of oxidation of cladding of typical wall thickness.

Contents

Abstract	iii
Executive Summary.....	xv
Foreword.....	xvii
Acknowledgments.....	xix
1 Introduction	1
2 Experimental Procedure	2
2.1 Materials	2
2.2 Specimen Geometry	4
2.3 Steam Exposure of Capsule Specimens	5
2.4 Air Exposure.....	5
2.5 Oxidation Tests with Internal Pressure	9
2.5.1 Steam Exposure.....	9
2.5.2 Air Exposure	9
3 Results for Zircaloy-4	13
3.1 Preoxidation in Steam	13
3.2 Air Oxidation of Steam-Preoxidized Capsules	18
3.2.1 300-600°C.....	18
3.2.2 700-900°C.....	21
3.2.3 Oxygen Analysis	22
3.3 Air Oxidation of Bare Alloy	23
3.3.1 300-600°C.....	23
3.3.2 700-900°C.....	24
3.4 Oxidation in Low-Oxygen Environment.....	25
3.5 Effect of Internal Pressure on Air Oxidation.....	26
4 Results for Zirlo.....	40
4.1 Preoxidation in Steam	40
4.2 Air Oxidation of Steam-Preoxidized Capsules	41
4.2.1 300-600°C.....	41
4.2.2 700-900°C.....	45
4.2.3 Oxygen Analysis	46
4.3 Air Oxidation of Bare Alloy	46
4.3.1 300-600°C.....	46
4.3.2 700-900°C.....	47
5 Results for M5.....	49
5.1 Preoxidation in Steam	49
5.2 Air Oxidation of Steam-Preoxidized Capsules	50
5.2.1 300-600°C.....	50
5.2.2 700-900°C.....	55
5.2.3 Oxygen Analysis	56
5.3 Air Oxidation of Bare Alloy	56
5.3.1 300-600°C.....	56
5.3.2 700-900°C.....	57

6	Correlations for Oxidation Kinetics	59
6.1	Zircaloy-4.....	59
6.1.1	Oxidation Rate Correlation	59
6.1.2	Comparison with Nureg Correlations.....	62
6.2	Oxidation Rate Correlations for Zirlo.....	65
6.3	Oxidation Rate Correlations for M5.....	69
6.4	Oxidation Comparison between Zircaloy-4, Zirlo, and M5	72
6.5	Comparison with Nureg Correlations	72
6.6	Oxide Thickness Growth	75
7	Summary and Conclusions.....	78
7.1	Zircaloy-4.....	78
7.2	Zirlo.....	79
7.3	M5.....	80
	References.....	81
	Appendix.....	83

Figures

2.1	Ring, 75-mm capsule and 150-mm tube specimens used for various tests in the study	4
2.2	Steps involved in the fabrication of tube specimens for air oxidation tests on steam-preoxidized Zircaloy-4 with internal pressure.....	4
2.3	Test facility used for steam preoxidation of Zircaloy-4, Zirlo, and M5 specimens	6
2.4	Specimens of Zircaloy-4 before and after oxidation in steam	6
2.5	Specimen assembly with 75-mm-long capsule specimens of Zircaloy-4 after 140 h oxidation in steam at 550°C	7
2.6	Capsule specimens and rings of Zirlo before and after oxidation in steam for 140 h at 550°C.....	7
2.7	150-mm-long specimens of Zircaloy-4 after oxidation in steam for 140 h at 550°C.....	10
2.8	Zircaloy-4 specimen after steam oxidation, sleeve grinding, and ends drilling.....	10
2.9	Experimental setup for air oxidation studies on Zircaloy cladding tubes with internal pressure.. ..	11
2.10	Steam-preoxidized Zircaloy-4 specimen assembled in the pressure test facility for air oxidation study	11
2.11	Schematic of a test facility for isothermal long-term air oxidation testing under internal pressure....	12
2.12	Magnified view of the specimen assembly used in air oxidation testing with internal pressure.....	12
3.1	Weight change during oxidation of Zircaloy-4 in a steam environment	14
3.2	SEM photomicrographs of cross sections of Zircaloy-4 ring specimens after oxidation in steam for different times at 594°C.....	14
3.3	SEM photomicrographs of cross sections of Zircaloy-4 ring specimens after oxidation in steam for different times at 550°C.....	15
3.4	SEM photomicrographs of cross sections of Zircaloy-4 ring specimens after oxidation in steam for different times at 500°C.....	15
3.5	SEM photomicrographs of cross sections of Zircaloy-4 ring specimens after oxidation in steam for different times at 400°C.....	16
3.6	Variation in oxide thickness as a function of exposure time during steam oxidation of Zircaloy-4 ring specimens.....	16
3.7	Weight change during steam oxidation of Zircaloy-4 capsule specimens for 140 h at 550°C.	17
3.8	Oxide thickness developed on ring and capsule specimens of Zircaloy-4 after oxidation in steam at 550°C.....	17
3.9	Temperature dependence of the rate constant for the steam oxidation of Zircaloy-4.....	17
3.10	Weight change during air oxidation of steam-preoxidized Zircaloy-4 capsule specimens at several temperatures	18
3.11	SEM photomicrographs of cross sections of steam-preoxidized Zircaloy-4 capsule specimens after oxidation in air for different times at 600°C.....	19
3.12	SEM photomicrographs of cross sections of steam-preoxidized Zircaloy-4 capsule specimens after oxidation in air for different times at 500°C.....	19
3.13	SEM photomicrographs of cross sections of steam-preoxidized Zircaloy-4 capsule specimens after oxidation in air for different times at 400°C.....	20

3.14	SEM photomicrographs of cross sections of steam-preoxidized Zircaloy-4 capsule specimens after oxidation in air for different times at 300°C.....	20
3.15	Oxide thickness for air oxidation of steam-preoxidized Zircaloy-4 capsule specimens at several temperatures	21
3.16	Weight change during air oxidation of steam-preoxidized Zircaloy-4 capsule specimens at several temperatures	21
3.17	Weight change during oxidation of steam-preoxidized Zircaloy-4 capsule specimens at 700, 800, and 900°C	22
3.18	Oxide thickness calculated from the weight change data for air oxidation of steam-preoxidized Zircaloy-4 capsule specimens at 700, 800, and 900°C	22
3.19	Weight change during oxidation of bare Zircaloy-4 capsule specimens at 300, 400, 500, and 600°C	24
3.20	Oxide thickness calculated from the weight change data for air oxidation of bare Zircaloy-4 capsule specimens at 300, 400, 500, and 600°C.....	24
3.21	Weight change during oxidation of bare Zircaloy-4 capsule specimens at 700, 800, and 900°C.....	25
3.22	Oxide thickness calculated from the weight change data for air oxidation of bare Zircaloy-4 capsule specimens at 700, 800, and 900°C	25
3.23	Weight change during oxidation of steam-preoxidized Zircaloy-4 capsule specimens in air and in 2.5 vol.% O ₂ -N ₂ gas mixture at 400 and 600°C	26
3.24	Steam-preoxidized Zircaloy-4 specimen setup with an internal Ar pressure of 400 psi in Test 4.....	27
3.25	Steam-preoxidized Zircaloy-4 specimen with an internal Ar pressure of 400 psi after 22 h elapsed time and at the end of Test 4 at ≈40 h.....	27
3.26	Steam-preoxidized Zircaloy-4 specimen after air oxidation with internal Ar pressure of 400 psi in Test 4.....	29
3.27	Micrograph of a steam-preoxidized Zircaloy-4 specimen after air oxidation with internal Ar pressure of 400 psi in Test 4, showing a region with an elongated-fissure crack.....	29
3.28	Steam-preoxidized Zircaloy-4 specimen with an internal Ar pressure of 400 psi after elapsed times of 17 and 34 h in Test 5.....	29
3.29	Steam-preoxidized Zircaloy-4 specimen with internal Ar pressure of 400 psi after oxidation in air for 47 h in Test 5.	30
3.30	Zircaloy-4 specimens tested with internal pressure of 400 and 200 psig at 600°C.....	30
3.31	Zircaloy-4 specimens tested with internal pressure of 400 and 200 psig at 700°C.....	30
3.32	Zircaloy-4 specimens tested with internal pressure of 175 and 100 psig at 800°C.....	30
3.33	Zircaloy-4 specimens tested with internal pressure of 100 and 50 psig at 900°C	30
3.34	Microphotographs of oxide developed on Zircaloy-4 specimens tested with internal pressure of 400 and 200 psig at 600°C	31
3.35	Microphotographs of oxide developed on Zircaloy-4 specimens tested with internal pressure of 400 and 200 psig at 700°C	31
3.36	Microphotographs of oxide developed on Zircaloy-4 specimens tested with internal pressure of 175 and 100 psig at 800°C	31
3.37	Microphotographs of oxide developed on Zircaloy-4 specimens tested with internal pressure of 100 and 50 psig at 900°C.....	31

3.38	SEM photomicrographs of the cross sections of a steam-preoxidized Zircaloy-4 specimen with an internal pressure of 400 psi, after 43-h oxidation in air at 600°C.....	32
3.39	SEM photomicrographs of the cross sections of a steam-preoxidized Zircaloy-4 specimen with an internal pressure of 200 psi, after 5.9-h oxidation in air at 700°C.....	33
3.40	SEM photomicrographs of the cross sections of a steam-preoxidized Zircaloy-4 specimen with an internal pressure of 100 psi, after 1.18-h oxidation in air at 800°C	33
3.41	Microphotographs indicating failure region in Zircaloy-4 specimens tested with internal pressure of 400 and 200 psig at 600°C.....	33
3.42	Microphotographs indicating oxide fracture leading to failure in Zircaloy-4 specimens tested with internal pressure of 400 and 200 psig at 600°C.....	34
3.43	Microphotographs indicating failure region in Zircaloy-4 specimens tested with internal pressure of 400 and 200 psig at 700°C.....	34
3.44	Microphotographs indicating oxide fracture leading to failure in Zircaloy-4 specimens tested with internal pressure of 400 and 200 psig at 700°C.....	34
3.45	Microphotographs indicating failure region in Zircaloy-4 specimens tested with internal pressure of 175 and 100 psig at 800°C.....	35
3.46	Microphotographs indicating oxide fracture leading to failure in Zircaloy-4 specimens tested with internal pressure of 175 and 100 psig at 800°C.....	35
3.47	Microphotographs indicating failure region in Zircaloy-4 specimens tested with internal pressure of 100 and 50 psig at 900°C	35
3.48	Microphotographs indicating oxide fracture leading to failure in Zircaloy-4 specimens tested with internal pressure of 100 and 50 psig at 900°C.....	36
3.49	Variation in pressure and temperature for air oxidation tests conducted at 600°C on steam-preoxidized Zircaloy-4 with initial internal pressures of 400 and 200 psig	36
3.50	Variation in pressure and temperature for air oxidation tests conducted at 700°C on steam-preoxidized Zircaloy-4 with initial internal pressures of 400 and 200 psig	36
3.51	Variation in pressure and temperature for air oxidation tests conducted at 800°C on steam-preoxidized Zircaloy-4 with initial internal pressures of 175 and 100 psig.	37
3.52	Variation in pressure and temperature for air oxidation tests conducted at 900°C on steam-preoxidized Zircaloy-4 with initial internal pressures of 100 and 50 psig.	37
3.53	Oxide thickness data obtained for steam-preoxidized Zircaloy-4 specimens that were air oxidized with and without internal pressure at 600 and 700°C.....	37
4.1	Weight change during steam oxidation of Zirlo capsule specimens for 140 h at 550°C.....	40
4.2	Calculated oxide thickness for Zirlo capsule specimens oxidized in steam for 140 h at 550°C.....	40
4.3	Weight change during air oxidation of steam-preoxidized Zirlo capsule specimens	41
4.4	SEM photomicrographs of cross sections of steam-preoxidized Zirlo after oxidation in air for 40, 80, 151, and 304 h at 600°C	42
4.5	SEM photomicrographs of cross sections of steam-preoxidized Zirlo after oxidation in air for 50, 100, 261, and 429 h at 500°C.....	43
4.6	SEM photomicrographs of cross sections of steam-preoxidized Zirlo after oxidation in air for 73, 150, 300, and 602 h at 400°C.....	43
4.7	SEM photomicrographs of cross sections of steam-preoxidized Zirlo after oxidation in air for 101, 300, 602, and 1013 h at 300°C	44

4.8	Oxide thickness for air oxidation of steam-preoxidized Zirlo capsule specimens at several temperatures.....	44
4.9	Weight change during air oxidation of steam-preoxidized Zirlo capsule specimens at 700, 800, and 900°C	45
4.10	Oxide thickness calculated from the weight change data for air oxidation of steam-preoxidized Zirlo capsule specimens at 700, 800, and 900°C.....	45
4.11	Weight change during oxidation of bare Zirlo capsule specimens at 300, 400, 500, and 600°C	47
4.12	Oxide thickness calculated from the weight change data for air oxidation of bare Zirlo capsule specimens at 300, 400, 500, and 600°C.....	47
4.13	Weight change during oxidation of bare Zirlo capsule specimens at 700, 800, and 900°C.....	48
4.14	Oxide thickness calculated from the weight change data for air oxidation of bare Zirlo capsule specimens at 700, 800, and 900°C	48
5.1	SEM photomicrographs of cross sections of M5 after oxidation in steam for 28, 140, 188, and 427 h at 550°C.....	49
5.2	Weight change during steam oxidation of M5 capsule specimens for 427 h at 550°C.....	50
5.3	Calculated oxide thickness for M5 capsule specimens oxidized in steam for 427 h at 550°C	50
5.4	Weight change during air oxidation of steam-preoxidized M5 capsule specimens	51
5.5	SEM photomicrographs of cross sections of steam-preoxidized M5 after oxidation in air for 41, 86, 161, and 305 h at 600°C	52
5.6	SEM photomicrographs of cross sections of steam-preoxidized M5 after oxidation in air for 51, 100, 246, and 407 h at 500°C.....	53
5.7	SEM photomicrographs of cross sections of steam-preoxidized M5 after oxidation in air for 73, 167, 300, and 600 h at 400°C.....	53
5.8	SEM photomicrographs of cross sections of steam-preoxidized M5 after oxidation in air for 98, 336, 599, and 1003 h at 300°C.....	54
5.9	Oxide thickness for air oxidation of steam-preoxidized M5 capsule specimens at several temperatures.....	54
5.10	Weight change during air oxidation of steam-preoxidized M5 capsule specimens at 700, 800, and 900°C	55
5.11	Oxide thickness calculated from the weight change data for air oxidation of steam-preoxidized M5 capsule specimens at 700, 800, and 900°C.....	55
5.12	Corrected weight change during oxidation of bare M5 capsule specimens at 300, 400, 500, and 600°C	57
5.13	Oxide thickness calculated from the weight change data for air oxidation of bare M5 capsule specimens at 300, 400, 500, and 600°C.....	57
5.14	Weight change during oxidation of bare M5 capsule specimens at 700, 800, and 900°C.....	58
5.15	Oxide thickness calculated from the weight change data for air oxidation of bare M5 capsule specimens at 700, 800, and 900°C	58
6.1	Temperature dependence of rate constant for the air oxidation of steam-preoxidized Zircaloy-4 capsule specimens in the temperature range 300-600°C	60
6.2	Temperature dependence of rate constant for the air oxidation of bare Zircaloy-4 capsule specimens in the temperature range 400-600°C.....	60

6.3	Temperature dependence of rate constant for the air oxidation of steam-oxidized Zircaloy-4 capsule specimens in the temperature range 300-900°C	61
6.4	Temperature dependence of rate constant for the air oxidation of bare Zircaloy-4 capsule specimens in the temperature range 400-900°C	61
6.5	Temperature dependence of rate constant for oxide growth during air oxidation of steam-preoxidized Zircaloy-4 capsule specimens in the temperature range of 300-600°C.	61
6.6	Temperature dependence of rate constant for oxide growth during air oxidation of steam-preoxidized and Zircaloy-4 capsule specimens in the temperature range of 300-900°C	62
6.7	A comparison of the temperature dependence of the oxidation rate constant for air oxidation of steam-preoxidized Zircaloy-4 at 300-600°C derived from this project with those based on Nureg1, Nureg2, and CODEX.	63
6.8	A comparison of the temperature dependence of the oxidation rate constant for air oxidation of bare Zircaloy-4 at 400-600°C derived from this project with those based on Nureg1, Nureg2, and CODEX.....	63
6.9	A comparison of the temperature dependence of the oxidation rate constant for air oxidation of steam-preoxidized Zircaloy-4 at 300-900°C derived from this project with those based on Nureg1, Nureg2, and CODEX.	64
6.10	A comparison of the temperature dependence of the oxidation rate constant for air oxidation of bare Zircaloy-4 at 400-900°C derived from this project with those based on Nureg1, Nureg2, and CODEX.....	64
6.11	A comparison of the temperature dependence of the oxidation rate constant for air oxidation of steam-preoxidized and bare Zircaloy-4 at 300-900°C derived from this project with those based on Nureg1, Nureg2, and CODEX	65
6.12	Temperature dependence of rate constant for the air oxidation of steam-preoxidized Zirlo capsule specimens in the temperature range of 300-600°C.....	66
6.13	Temperature dependence of rate constant for the air oxidation of bare Zirlo capsule specimens in the temperature range of 300-700°C.....	67
6.14	Temperature dependence of rate constant for the air oxidation of steam-preoxidized Zirlo capsule specimens in the temperature range of 300-900°C.....	67
6.15	Temperature dependence of rate constant for the air oxidation of bare Zirlo capsule specimens in the temperature range of 300-900°C.....	68
6.16	Temperature dependence of rate constant for oxide growth during air oxidation of steam-preoxidized Zirlo capsule specimens in the temperature range of 300-600°C	68
6.17	Temperature dependence of rate constant for oxide growth during air oxidation of steam-preoxidized Zirlo capsule specimens in the temperature range of 300-900°C	69
6.18	Temperature dependence of rate constant for the air oxidation of steam-preoxidized M5 capsule specimens in the temperature range of 300-600°C	70
6.19	Temperature dependence of rate constant for the air oxidation of steam preoxidized and bare M5 capsule specimens in the temperature range of 300-600°C.....	71
6.20	Temperature dependence of oxide scale growth rate constant for the air oxidation of steam-preoxidized M5 capsule specimens in the temperature range of 300-900°C.....	71
6.21	Temperature dependence of rate constant for the air oxidation of steam-preoxidized Zircaloy-4, Zirlo, and M5 capsule specimens in the temperature range of 400-600°C	73

6.22	Temperature dependence of rate constant for the air oxidation of steam-preoxidized Zircaloy-4, Zirlo, and M5 capsule specimens in the temperature range of 400-900°C	73
6.23	Temperature dependence of rate constant for oxide growth rate during air oxidation of steam-preoxidized Zircaloy-4, Zirlo, and M5 capsule specimens in the temperature range of 400-900°C...	74
6.24	A comparison of the temperature dependence of the oxidation rate constant for air oxidation of steam-preoxidized Zircaloy-4, Zirlo, and M5 at 400-600°C derived from this project with those for Zircaloy-4, based on Nureg1, Nureg2, and CODEX	74
6.25	A comparison of the temperature dependence of the oxidation rate constant for air oxidation of steam-preoxidized Zircaloy-4, Zirlo, and M5 at 400-900°C derived from this project with those for Zircaloy-4, based on Nureg1, Nureg2, and CODEX	75
6.26	Oxide thickness growth as a function of exposure time in air at several temperatures for steam-preoxidized Zircaloy-4	76
6.27	Oxide thickness growth as a function of exposure time in air at several temperatures for steam-preoxidized Zirlo	76
6.28	Oxide thickness growth as a function of exposure time in air at several temperatures for steam-preoxidized M5	76
6.29	Comparison of oxide thickness growth for steam-preoxidized Zircaloy-4, Zirlo, and M5 as a function of exposure time in air at 500 and 600°C	77
6.30	Cladding wall thickness oxidized in air at 500 and 600°C for initially steam-preoxidized Zircaloy-4, Zirlo, and M5	77

Tables

2.1	Chemical composition of Zircaloy-4 used in the study.....	2
2.2	Chemical composition of Zirlo used in the study	3
2.3	Chemical composition of M5 used in the study	3
2.4	Test matrix for oxidation of steam-preoxidized Zircaloy-4 in air at 300-600°C.....	7
2.5	Test matrix for oxidation of bare Zircaloy-4 in air at 300-600°C.....	7
2.6	Exposure times for air oxidation of steam-preoxidized and bare Zircaloy-4 in air at 700-900°C.....	8
2.7	Test matrix for oxidation of steam-preoxidized Zirlo in air at 300-600°C	8
2.8	Test matrix for oxidation of bare Zirlo in air at 300-600°C.....	8
2.9	Exposure times for air oxidation of steam-preoxidized and bare Zirlo capsules in air at 700-900°C.....	8
2.10	Test matrix for oxidation of steam-preoxidized M5 in air at 300-600°C	8
2.11	Test matrix for oxidation of bare M5 in air at 300-600°C	8
2.12	Exposure times for air oxidation of steam-preoxidized and bare M5 capsules in air at 700-900°C ...	8
2.13	Test matrix for air oxidation of steam-preoxidized Zircaloy-4 with internal pressure	10
3.1	A comparison of the oxygen concentration values calculated from the weight change data with the measured values for steam-preoxidized Zircaloy-4 specimens after air oxidation	23
3.2	Oxidation rates for steam-preoxidized Zircaloy-4 in air and in low-O ₂ environments	26
3.3	Air oxidation test data on steam-preoxidized Zircaloy-4 with internal pressure.....	38
3.4	Oxide thickness data developed during air oxidation of steam-preoxidized Zircaloy-4 with internal pressure.....	39
4.1	Oxidation rates in air for steam-preoxidized Zirlo and Zircaloy-4 specimens.....	41
4.2	A comparison of the oxygen concentration values calculated from the weight change data with the measured values for steam-preoxidized Zirlo specimens after air oxidation.....	46
5.1	Oxidation rates in air for steam-preoxidized Zircaloy-4, Zirlo, and M5 specimens	51
5.2	A comparison of the oxygen concentration values calculated from the weight change data with the measured values for steam-preoxidized M5 specimens after air oxidation.....	56

Executive Summary

The kinetics of cladding oxidation in air environment is important in many safety-related studies. For example, in a pressurized thermal shock event, the reactor pressure vessel may be breached leading to air intrusion in the core and consequent oxidation of relatively cold fuel cladding. Another example is structural failure of dry storage and transportation cask, which may result in air intrusion and consequent interaction with spent fuel rods. In both cases, knowledge of air oxidation kinetics of cladding at relatively low temperatures is essential in assessing and determining the margin for clad integrity.

The objective of this program is to obtain experimental data on the air oxidation kinetics of unirradiated Zircaloy-4, Zirlo, and M5 cladding with an oxide layer that is representative of the current inventory of spent fuel discharged after a medium or high level of fuel burnup. Experiments were conducted in which Zircaloy-4 ring specimens were exposed in a steam environment at several temperatures and for various time periods. Based on a detailed analysis of weight change and oxide thickness data from these tests, steam exposure time of 140 h and temperature of 550°C were selected to simulate the oxide layer ($\approx 25\text{-}30\ \mu\text{m}$ in thickness) on the Zircaloy-4 and Zirlo cladding in spent fuel pool. Steam exposure time of 427 h and temperature of 550°C were selected to simulate the oxide layer on the M5, since the oxidation rate was lower for M5 than for the others.

The steam-preoxidized specimens were subsequently oxidized in air at temperatures in the range of 300-900°C. Oxidation tests in air emphasized temperatures in the range of 300-600°C, which is representative of cladding heatup in the event of a partial or full draining of spent fuel pool coolant. The maximum air oxidation times ranged between 300 h at 600°C and ≈ 1000 h at 300°C. Weight change and oxide thickness measurements were made on the specimens exposed at various times to establish the kinetics of the scaling process as a function of temperature. Bare capsules of Zircaloy-4, Zirlo, and M5 were also exposed in air for comparison of the oxidation behavior of the cladding with and without steam preoxidation.

Results showed that the initial oxide scale developed in steam was adherent and crack free in all three alloys but tended to crack when exposed in air at 600°C. The thickness of the oxide developed during air exposure increased significantly with time and the transverse cracks persisted over the entire thickness of the scale. The growth rate for oxide at 500°C in air was much less, and the scales exhibited virtually no cracks even after an exposure time of 400 h at 500°C. The oxidation rates in air for steam-preoxidized specimens were minimal to negligible at 400 and 300°C after exposure times of 600 and ≈ 1000 h, respectively. The data showed that in the pre-breakaway region, oxygen ingress into Zirlo occurs at a higher rate than in Zircaloy-4. In the post breakaway region, the rates for Zirlo are somewhat lower than for Zircaloy-4 at $T \leq 500^\circ\text{C}$; however, at $T \geq 600^\circ\text{C}$, the rates for Zirlo are higher than for Zircaloy-4. The air oxidation rates for M5 are substantially lower than the rates observed for Zircaloy-4 and Zirlo.

Limited tests were conducted at 400 and 600°C to evaluate the oxidation performance of Zircaloy-4 in a low-oxygen high-nitrogen environment. At 600°C, the weight change data showed that the rates are somewhat lower in the low- O_2 environment when compared with those in air. The rates were almost the same in both environments at 400°C.

Isothermal oxidation tests were also conducted with tube specimens of steam-preoxidized Zircaloy-4 with internal pressures in the range of 50-400 psig at 600 to 900°C. Extensive metallography was used on the tested specimens to examine the oxide scale development, pin-hole rupture morphology, and oxide cracking propensity. The data indicated that the oxide thickness is somewhat larger ($\approx 20\%$ in post breakaway region) in the tests conducted with high internal pressure than that obtained in the absence of it, especially at 600 and 700°C. The

increase is attributed to microcracks in the oxide (and associated oxidation) that results from increased deformation in the specimen due to pressurization.

Weight change and oxide thickness data, developed in the present program, were used to develop correlations to depict the air oxidation behavior of the alloys as a function of time and temperature. The results showed that the correlation developed for Zircaloy-4 from the oxidation data generated in the current project is in fair agreement with that based on Nureg1 and Powers. The predictions based on Nureg2 and CODEX correlations for Zircaloy-4 are several orders of magnitude lower than those based on current work, especially at lower temperatures. Correlations, based on measured oxide thickness, were used to predict the oxide thickness on the cladding as a function of temperature and exposure time for steam-preoxidized cladding (with an initial 25-30- μm -thick oxide). Results showed that the Zircaloy4 cladding would develop an additional oxide of 100 μm in 150 h at 600°C and ≈ 50 μm in 1000 h at 500°C, due to air ingress. Under similar conditions, Zirlo would develop an oxide of 170 μm at 600°C, 150 h and 55 μm at 500°C, 1000 h. The values for M5 are 65 μm at 600°C, 150 h and 45 μm at 500°C, 1000 h. Data and correlations for Zirlo, and M5, developed in this project, are applicable to the advanced claddings for use under high burnup conditions.

Foreword

The kinetics of cladding oxidation in air environment is important in many safety-related investigations. For example in a pressurized thermal shock event, the reactor pressure vessel may be breached leading to air intrusion in the core and consequent oxidation of relatively cold fuel cladding. Another example is structural failure of dry storage and transportation casks, which may result in air intrusion and consequent interaction with spent fuel rods. In spent fuel pool accident arising from loss of pool water inventory, spent fuel rods can be exposed to an air environment. Knowledge of air oxidation kinetics of cladding at relatively low temperatures is needed in assessing safety and determining the margin for clad integrity in all these cases. Prior data on cladding oxidation in air environment was based on a very limited set of experiments not directly applicable to the low temperature range of interest for the above cases. Recognizing this, the NRC Office of Regulatory Research (RES) initiated an experimental research program in July 2002 at the Argonne National Laboratory. The objective of the program was to obtain experimental data on air oxidation kinetics of Zircaloy-4, Zirlo, and M5 cladding, which are representatives of current and/or projected cladding inventory in operating reactors and in spent fuel discharged after a medium or high level of fuel burnup.

Experiments were conducted with unirradiated specimens of Zircaloy-4, Zirlo, and M5 cladding in which the specimens were subjected to isothermal air oxidation at different temperatures and for different duration of time. One series of experiments investigated the effect of a pre-existing layer of oxide on further oxide layer growth during air oxidation of cladding. The pre-existing layers simulated steam oxidation of cladding during in-reactor operation and in that sense unirradiated samples were prototypic of irradiated cladding. Another series of experiments investigated air oxidation kinetics of bare cladding, which provided a data set for comparison with the previous tests. Additionally, experiments were performed to investigate the kinetics of air oxidation in a nitrogen-rich environment. This simulated the effect of nitriding on cladding in a situation where the air is mostly depleted of oxygen. The effect of pre-existing hydrides, formed on the cladding surface during in-reactor operation and relevant, in particular, for high burnup operation, is being investigated under a follow-on program at the Argonne National Laboratory. This latter study will be reported separately.

The results showed that the correlations developed for the air oxidation of Zircaloy-4, Zirlo, and M5 cladding in the temperature range of 300 to 900°C are in fair agreement with those used previously for the spent fuel pool accident risk study. The results also showed that within the temperature range of interest, the pre-existing oxide layer has no discernible beneficial or deleterious effect on further clad oxidation in air environment.

Farouk Eltawila, Director
Division of Systems Analysis and Regulatory Effectiveness

Acknowledgments

This work is sponsored by the Office of Nuclear Regulatory Research, U.S. Nuclear Regulatory Commission, under Job Codes Y6707 and Y6512; Program Manager: S. Basu. Zircaloy-4 and M5 cladding tubes were supplied by Framatome ANP, Lynchburg, VA; and cladding tubes of Zirlo were supplied by Westinghouse, Pittsburgh, PA. D. L. Rink and L. Cairo assisted in the metallography of the air-oxidized specimens and in the oxide thickness measurements.

1 Introduction

The kinetics of cladding oxidation in air environment is important in many safety-related studies. For example, in a pressurized thermal shock event, the reactor pressure vessel may be breached leading to air intrusion in the core and consequent oxidation of relatively cold fuel cladding. Another example is structural failure of dry storage and transportation cask, which may result in air intrusion and consequent interaction with spent fuel rods. In both cases, knowledge of air oxidation kinetics of cladding at relatively low temperatures is essential in assessing and determining the margin for clad integrity.

Zirconium-based alloys are prone to oxidize fairly easily because of their affinity for oxygen and inherent thermodynamic stability of the zirconium oxide that forms when the alloys are exposed to steam and air environments at elevated temperatures. High temperature oxidation of zirconium and Zirconium alloys in oxygen, air, and steam has been the subject of extensive research due to their use as cladding materials in nuclear reactors (Cubiciotti, 1950; Gulbransen and Andrew, 1957; Pemsler, 1962, 1964; Mackay, 1963; Hussey and Smeltzer, 1964; Wallwork et al., 1964; Kidson, 1966; Com-Nougue et al., 1969; Pawel, 1979; Pawel and Campbell, 1980). Over the years, several studies have been conducted to evaluate the kinetics of oxidation of Zircaloy-4 in steam environments, but most of the studies were conducted at temperatures $>700^{\circ}\text{C}$ on bare alloys and for short time periods to predict the cladding behavior under loss-of-coolant situations (Leistikow et al., 1978, 1980; Leistikow and Borg, 1987; Moalem and Olander, 1991; Rosa and Smeltzer, 1980; Powers et al., 1994).

The objective of this program is to obtain experimental data on the air oxidation kinetics of unirradiated Zircaloy-4, Zirlo, and M5 cladding with an oxide layer that is representative of the current inventory of spent fuel discharged after a medium or high level of fuel burnup. The expected oxide thickness on the cladding stored in spent fuel pool is in the range of 25-30 μm after service in medium burnup conditions and can be as high as 100 μm after high burnup service. It is proposed that the protective capacity of the oxide against further oxidation is dictated by the crystal structure of the oxide, and a tetragonal oxide is much more protective than the monoclinic oxide (Godlewski 1994). It is also suggested in the literature that only 5-10 μm layer of the oxide adjacent to the metal is tetragonal in structure and may be protective over the service exposure of the cladding. Preliminary examination of air-oxidized specimens using X-rays from Advanced Photon Source at Argonne National Laboratory showed presence of little, if any, tetragonal oxide in the oxide scale. The aim of this study is to preoxidize the bare cladding in a steam environment to achieve an oxide thickness of 25-30 μm to simulate the oxide layer on the cladding in spent fuel pool.

The air oxidation tests are performed on the steam-preoxidized cladding at temperatures representative of cladding heatup in the event of a partial or full draining of spent fuel pool coolant. Air oxidation tests are performed on the steam-preoxidized cladding of all three alloys over a wide temperature range of 300-900 $^{\circ}\text{C}$, but the emphasis in the program is the low temperature regime of 300-600 $^{\circ}\text{C}$.

This report describes the work performed at Argonne National Laboratory on oxidation tests conducted on Zircaloy-4, Zirlo, and M5 materials in steam and in air environments. The tests for air oxidation included both bare and steam-preoxidized materials. Limited tests were also conducted to evaluate the effect of oxygen-deficient high-nitrogen environment on the oxidation rate for Zircaloy-4. In addition, tests were conducted to evaluate the effect of internal pressure on the air oxidation rate of steam-preoxidized Zircaloy-4 at 600-900 $^{\circ}\text{C}$. The weight-change and oxide-thickness data from the study were analyzed to develop oxidation rate correlations, which were then compared with the correlations that are currently used in the accident analysis codes.

2 Experimental Procedure

This section of the report discusses the size and composition of the test materials, type and geometry of the specimens used in various tests, facilities and approach for steam preoxidation and air oxidation of the specimens, and test apparatus and procedure used for the isothermal oxidation tests under internal pressure. This section also presents the test matrices used for the conduct of various types of tests.

2.1 Materials

The Zircaloy-4 material used in the study was produced by Sandvik Special Metals Corp. and was supplied by Framatome ANP, Lynchburg, VA. The material was identified by Ingot #234719Q and Lot #9DHK83. The material had room-temperature UTS (ultimate tensile strength) and 0.2% yield strength of 105,000 and 80,000 psi (724 and 552 MPa), respectively. The material had a tensile elongation of 22% in a 2-in. (51 mm) specimen. The material had a grain size of ASTM 10 and 10.5 in the longitudinal and transverse directions, respectively. The tube material was supplied with a surface finish of SiC belt polish with 400 grit on the OD surface and with etched surface on the ID. The tubes had dimensions of 0.376 ± 0.0020 in. OD (9.45 ± 0.05 mm), 0.328 ± 0.0015 in. ID (8.33 ± 0.038 mm), and a minimum wall thickness of 0.022 in. (0.59 mm). The chemical composition is listed in Table 2.1 for the ingot and final tube versions of the material, analyzed as per the ASTM A-1409 and ASTM-1019 test methods.

The Zirlo material used in the study was supplied by Westinghouse. The material, supplied in the form of tubes, had dimensions of 0.374 ± 0.0020 in. OD (9.45 ± 0.05 mm), 0.328 ± 0.0015 in. ID (8.33 ± 0.038 mm), and an average wall thickness of 0.023 in. (0.58 mm). The chemical composition was determined by both Westinghouse and by ANL, and the values are listed in Table 2.2.

Table 2.1. Chemical composition of Zircaloy-4 used in the study

Element ¹	Ingot analysis ²	Final tube analysis ³
Sn (wt.%)	1.28	1.28, 1.28
Fe (wt.%)	0.22	0.25, 0.26
Cr (wt.%)	0.12	0.15, 0.14
Si (wt.%)	0.01	<0.01, <0.01
Zr (wt.%)	Balance	Balance
Hf (wt ppm)	72	<100, <100
C (wt ppm)	144	300, 220
O (wt ppm)	1250	1000, 1200
H (wt ppm)	3	8.7, 4.4
N (wt ppm)	25	50, 50
Nb (wt ppm)	<50	<100, <100
Ni (wt ppm)	40	<100, <100
Ta (wt ppm)	<100	<100, <100
W (wt ppm)	<50	400, 200
Ca (wt ppm)	<10	-
Al (wt ppm)	54	-

¹Units of measure in parentheses; ²Supplied by Framatome ANP; ³Duplicate analysis done by ANL.

Table 2.2. Chemical composition of Zirlo used in the study

Element ¹	Westinghouse analysis	ANL analysis ²
Sn (wt.%)	0.99	0.73, 0.74
Fe (wt.%)	0.11	0.11, 0.12
Nb (wt.%)	0.98	0.96, 0.88
Cr (wt.%)	NR ³	<0.01, <0.01
Si (wt.%)	0.005	<0.005, <0.005
Zr (wt.%)	Balance	Balance
Hf (wt ppm)	40	200, 200
C (wt ppm)	135	180, 90
O (wt ppm)	1100	1200, 1300
H (wt ppm)	NR	3.5, 5.7
N (wt ppm)	46	34, 36
Ni (wt ppm)	NR	<100, <100
Ta (wt ppm)	NR	<50, <50
W (wt ppm)	NR	<100, <100

¹Units of measure in parentheses; ²Duplicate analysis; ³NR = Not reported.

Table 2.3. Chemical composition of M5 used in the study

Element ¹	Final tube analysis ²
Sn (wt.%)	0.02
Fe (wt.%)	0.04-0.06
Cr (wt.%)	<0.01
Si (wt.%)	<0.01
Nb (wt.%)	1.01, 1.02
Zr (wt.%)	Balance
Hf (wt ppm)	<100
C (wt ppm)	90-130
O (wt ppm)	1300, 1500
H (wt ppm)	6.0, 6.2
N (wt ppm)	50, 60
Ni (wt ppm)	<100
Ta (wt ppm)	<100
W (wt ppm)	<100
S (wt ppm)	20, 30
Pb (wt ppm)	<100

¹Units of measure in parentheses; ²Duplicate analysis done by ANL

The M5 material used in the study was supplied by Framatome ANP. The material, supplied in the form of tubes, had nominal dimensions of 0.430 in. OD (10.92 mm), 0.380 in. ID (9.65 mm), and an average wall thickness

of 0.025 in. (0.635 mm). The material had a final annealing treatment at a temperature between 550 and 600°C. The chemical composition, analyzed by ANL, is listed in Table 2.3.

2.2 Specimen Geometry

Three types of specimens, namely, rings ≈ 6.5 mm in length and capsules 75 mm and 150 mm in length, were used in the present study. Figure 2.1 shows a photograph of the three types. Ring specimens were used to establish the time and temperature for the steam preoxidation of tube specimens to obtain an oxide thickness $\approx 25\text{--}30$ μm . Zircaloy-4, Zirlo, and M5 capsule specimens 75 mm in length were fabricated, and the capsules were back filled with argon gas and welded shut in a glove box. The capsule specimens were welded by e-beam on one side, whereas the other side was welded shut with the TIG welding technique. The end caps were fabricated from Zircadyne 702 (Zr-702) material. These specimens were used for air oxidation study in the initially bare and steam-preoxidized conditions.

Zircaloy-4 tube specimens 150 mm in length were fabricated for use in air oxidation tests with internal pressure. The approach we have used after experimenting and evaluating several options was as follows. Either side of the 150-mm-long tube specimen of Zircaloy-4 was welded with ≈ 25 -mm-long sleeve of Zr-702 alloy. A disk of Zr-702 alloy was welded using the e-beam technique on one side of the tube, and the other end was welded with another disk using the TIG welding technique in an argon glove box (see Figure 2.2). The specimens sealed on both

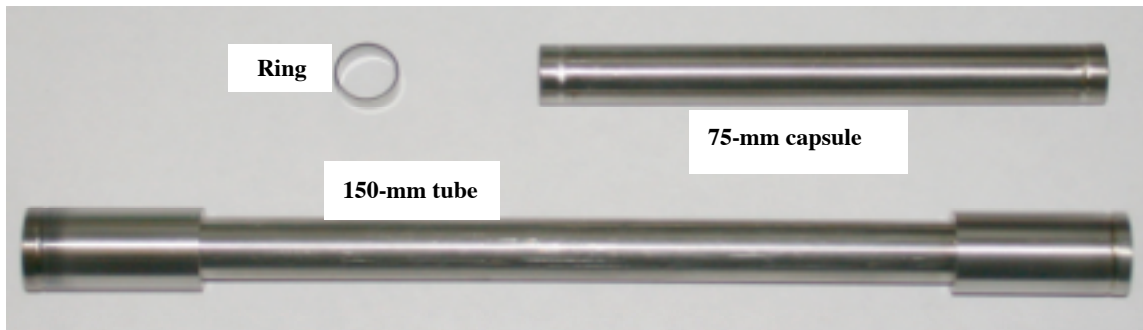


Figure 2.1. Ring, 75-mm capsule and 150-mm tube specimens used for various tests in the study.

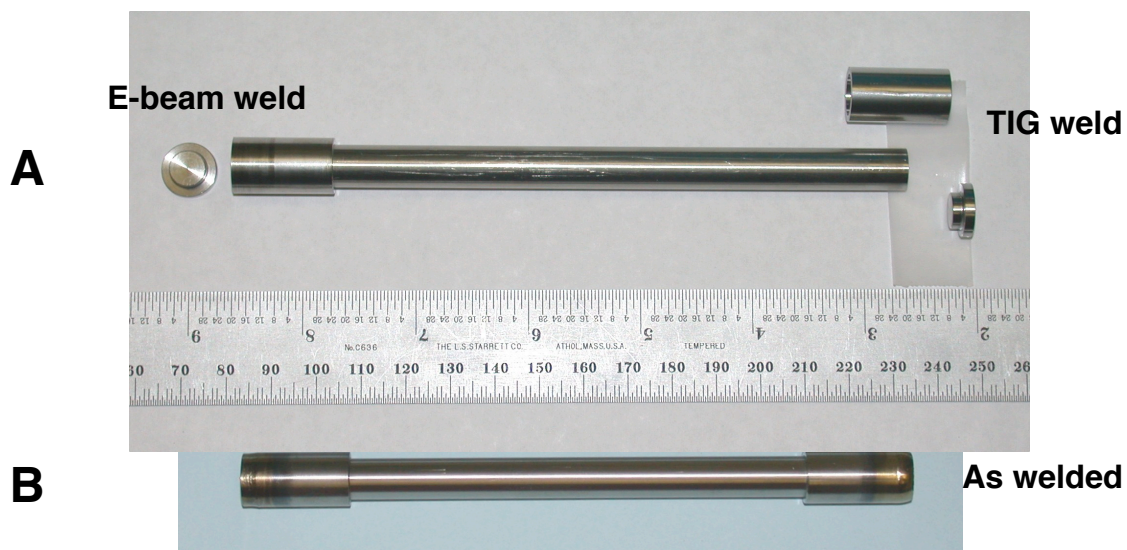


Figure 2.2. Steps involved in the fabrication of tube specimens for air oxidation tests on steam-preoxidized Zircaloy-4 with internal pressure.

sides by this procedure were exposed in an assembly to a steam environment for 140 h at 550°C to develop an oxide of $\approx 30 \mu\text{m}$ thickness. The sleeve regions of the steam-exposed specimens were ground to remove the oxide layer and make these regions conducting for direct-current heating of the specimens during air oxidation tests. The specimen ends were drilled to enable insertion of a thermocouple from one side and to pressurize the specimen from the other side.

2.3 Steam Exposure of Capsule Specimens

Several facilities with retort chambers were used to conduct the tests in air and steam environments. Two tubular resistance-heated furnaces were used to expose ring and capsule specimens of Zircaloy-4, Zirlo, and M5 for steam oxidation. Figure 2.3 shows one of the facilities used for steam oxidation. The system consists of a resistance-heated furnace with a constant temperature zone of ≈ 20 cm, and the reaction chamber was made of high-purity alumina. The steam for the experiment was generated by pumping distilled water from a water source and converting it to steam in the preheat portion of the furnace, ahead of the specimen exposure location. The exhaust steam from the chamber was condensed in a steam condenser. The flow rate was 6 cc/h of water. A mass balance on the water flow showed that almost all the input water was collected as the effluent, indicating that the steam consumption was negligible during the oxidation of specimens. Argon gas was used to disperse the steam in the reaction chamber.

Figure 2.4 shows the 75-mm-long Zircaloy-4 capsule specimens before/after oxidation and a test assembly with oxidized specimens. In the specimens shown in Figure 2.4, the e-beam and TIG welds are on the right and left sides of the specimens, respectively. Figure 2.5 shows an assembly with capsule specimens of Zircaloy-4 after 140 h oxidation in steam at 550°C. The specimens were exposed in such a way that the flow of steam was from right to left. Figure 2.6 shows an assembly of Zirlo specimens before and after steam oxidation for 140 h at 550°C.

2.4 Air Exposure

Four resistance-heated furnaces were used for oxidation of steam-preoxidized and bare Zircaloy-4, zirlo, and M5 capsule specimens in air. The capsules were retrieved periodically to measure the weight changes and determine the oxide thickness by optical metallography. The test matrix used for the air oxidation of steam-preoxidized Zircaloy-4 specimens is shown in Table 2.4. Table 2.5 lists the exposure times for air oxidation of bare specimens of Zircaloy-4 at 300-600°C. Table 2.6 lists the exposure times for air oxidation of bare and steam-preoxidized specimens of Zircaloy-4 at 700-900°C. For the tests listed in Tables 2.5 and 2.6, a single specimen was used at each temperature and for each pretreatment; weight gain during oxidation was determined as a function of exposure time by retrieving the samples periodically.

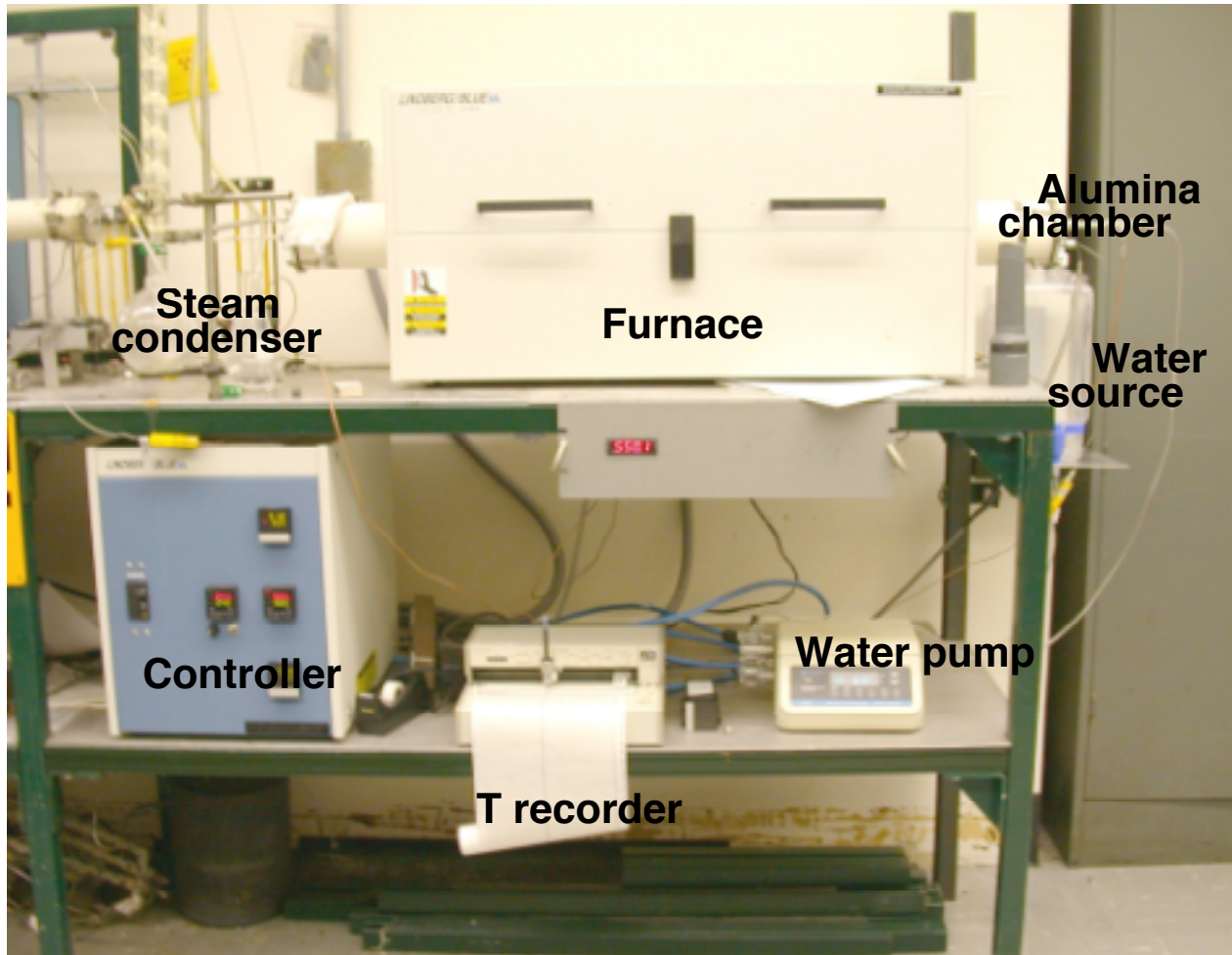


Figure 2.3. Test facility used for steam preoxidation of Zircaloy-4, Zirlo, and M5 specimens.

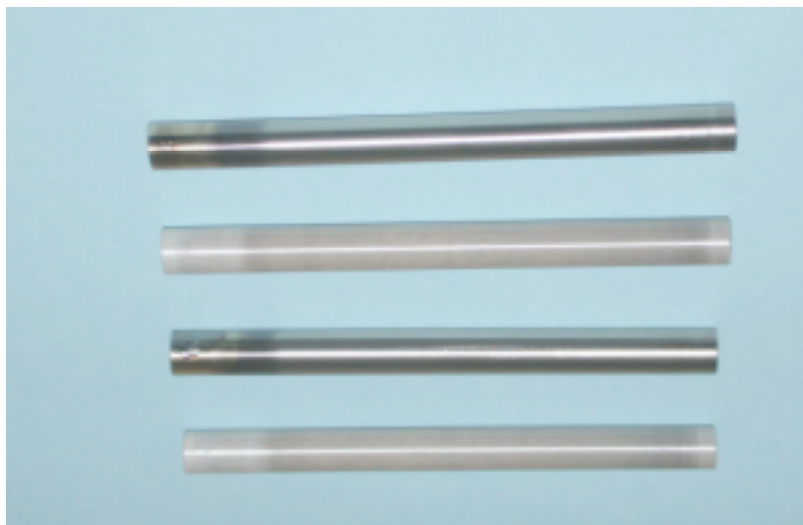


Figure 2.4. Specimens of Zircaloy-4 (75-mm long) before and after oxidation in steam. Dark gray color: as fabricated; light white color: after 140-h exposure in steam at 550°C.

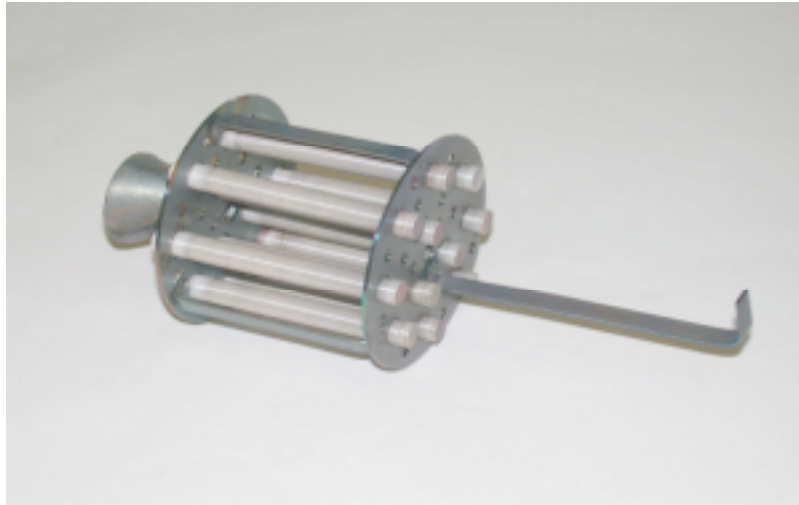


Figure 2.5. Specimen assembly with 75-mm-long capsule specimens of Zircaloy-4 after 140 h oxidation in steam at 550°C.

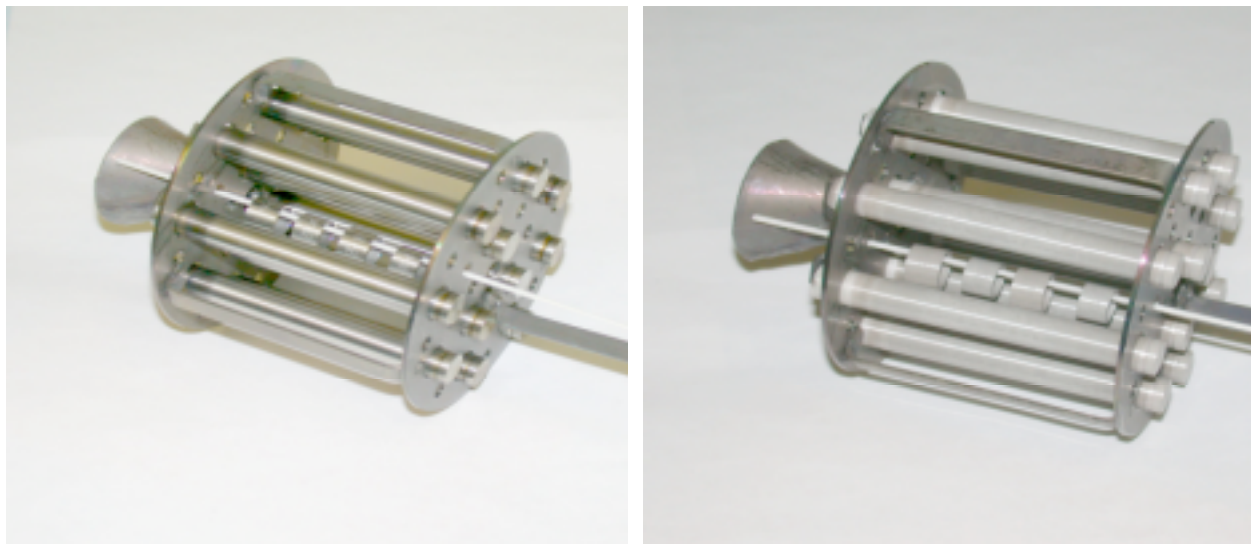


Figure 2.6. Capsule specimens (75-mm long) and rings of Zirlo before and after oxidation in steam for 140 h at 550°C.

Table 2.4. Test matrix for oxidation of steam-preoxidized Zircaloy-4 in air at 300-600°C

Temperature (°C)		Exposure time (h)		
300	97	305	600	1260
400	74	161	305	600
500	50	97	257	402
600	40	84	155	299

Table 2.5. Test matrix for oxidation of bare Zircaloy-4 in air at 300-600°C

Temperature (°C)	Exposure time (h)
300	102, 294, 613, 1037
400	75, 149, 287, 600
500	50, 97, 234, 401
600	43, 85, 154, 300

Table 2.6. Exposure times for air oxidation of steam-preoxidized and bare Zircaloy-4 in air at 700-900°C

Temperature (°C)	Exposure time (h)
700	2, 4, 6, 8, 10, 12, 16, 20, 24
800	1, 2, 4, 6, 8, 10, 14, 18, 22
900	0.5, 1, 1.5, 2, 2.5

Table 2.7. Test matrix for oxidation of steam-preoxidized Zirlo in air at 300-600°C

Temperature (°C)	Exposure time (h)			
300	101	300	602	1013
400	73	150	300	602
500	50	100	261	429
600	40	80	151	304

Table 2.8. Test matrix for oxidation of bare Zirlo in air at 300-600°C

Temperature (°C)	Exposure time (h)
300	101, 301, 605, 1000
400	75, 150, 299, 604
500	53, 104, 180, 252, 412
600	40, 80, 152, 313

Table 2.9. Exposure times for air oxidation of steam-preoxidized and bare Zirlo capsules in air at 700-900°C

Temperature (°C)	Exposure time (h)
700	2, 4, 6, 8, 10, 12, 16, 20, 24
800	1, 2, 4, 6, 8, 10, 14, 18, 22
900	0.5, 1, 1.5, 2, 2.5

Table 2.10. Test matrix for oxidation of steam-preoxidized M5 in air at 300-600°C

Temperature (°C)	Exposure time (h)			
300	98	336	599	1003
400	73	167	300	600
500	51	100	246	407
600	41	86	161	305

Table 2.11. Test matrix for oxidation of bare M5 in air at 300-600°C

Temperature (°C)	Exposure time (h)
300	98, 312, 601, 1008
400	73, 147, 315, 643
500	51, 100, 245, 412, 507, 580
600	41, 81, 156, 300

Table 2.12. Exposure times for air oxidation of steam-preoxidized and bare M5 capsules in air at 700-900°C

Temperature (°C)	Exposure time (h)
700	1, 2, 3, 5, 8, 12.3, 16.3, 20.3, 24.6, 46.2
800	1, 2, 3, 4, 6, 8.3, 10.3
900	0.5, 1.2, 1.7

The test matrix used for the air oxidation of steam-preoxidized Zirlo specimens is shown in Table 2.7. One capsule was retrieved after each exposure time to measure the weight change and determine the oxide thickness by optical metallography. Table 2.8 lists the exposure times for air oxidation of bare specimens of Zirlo at 300-600°C. Table 2.9 lists the exposure times for air oxidation of bare and steam-preoxidized specimens of Zirlo at 700-900°C. For the tests listed in Table 2.8 and 2.9, a single specimen was used at each temperature; weight gain during oxidation was determined as a function of exposure time by retrieving the samples periodically.

The test matrix used for the air oxidation of steam-preoxidized M5 specimens is shown in Table 2.10. One capsule was retrieved after each exposure time to measure the weight change and determine the oxide thickness by optical metallography. Table 2.11 lists the exposure times for air oxidation of bare specimens of M5 at 300-600°C. Table 2.12 lists the exposure times for air oxidation of bare and steam-preoxidized specimens of M5 at 700-900°C. For the tests listed in Table 2.11 and 2.12, a single specimen was used at each temperature; weight gain during oxidation was determined as a function of exposure time by retrieving the samples periodically.

For the steam-preoxidized specimens of all three materials that were exposed in air at 300-600°C, the specimens after each exposure time were cut, mounted, polished, and analyzed by SEM to determine the total oxide thickness and that developed during the air exposure step. The specimens oxidized in air at 700-900°C were cut at the completion of the exposures, mounted, polished for oxide-thickness measurements. Oxide thickness was measured in the four quadrants around the capsule specimen, and the values were averaged to establish the scale thickness.

2.5 Oxidation Tests with Internal Pressure

2.5.1 Steam Exposure

The objective of this subtask is to evaluate and quantify the effect of internal pressure in a steam-preoxidized cladding tube on the subsequent oxidation in air at elevated temperatures. These tests will generate data on the effect of pressure, if any, on the air oxidation of cladding tubes. This type of test also involves gathering of data on the pressure-temperature correlation for air oxidation by varying the internal pressure at holding temperatures in the range of 600 to 900°C for a prolonged period. Under these conditions, cladding burst and air oxidation on the inner and outer surfaces are predicted to occur.

Zircaloy-4 tube specimens 150-mm in length were fabricated for use in air oxidation tests with internal pressure. The specimen fabrication procedure is described in Section 2.2. The specimens were exposed in an assembly to a steam environment for 140 h at 550°C to develop an oxide of $\approx 25 \mu\text{m}$ thickness. Figure 2.7 shows an assembly with several tube specimens after oxidation in steam at 550°C. The sleeve regions of the steam-exposed specimens were ground to remove the oxide layer and make these regions conducting for direct-current heating of the specimens during air oxidation tests. The specimen ends were drilled to enable insertion of a thermocouple from one side and to pressurize the specimen from the other side. Figure 2.8 shows a Zircaloy-4 specimen after steam oxidation, grinding of sleeves, and drilling of ends. This specimen is ready for air oxidation test under internal pressure. The steam-oxidized specimens were tested in air with an internal pressure of argon at several temperatures according to the test matrix given in Table 2.13.

2.5.2 Air Exposure

Two approaches were used for the air oxidation of steam-preoxidized specimens with internal pressure. In the first, transient cladding heatup was simulated to evaluate creep failure, rapid ballooning and burst at high temperatures. Figure 2.9 is a photograph of the overall system. The system consists of five sub-assemblies: a gas pressure supply system (GPS), an electric DC power supply (DCPS), Zircaloy tube support fixture (TSF),

temperature and pressure control console (TPC), and a computer data acquisition system (DAS). The DCPS supplies direct-current electric power to heat the Zircaloy tube specimen to the desired test temperature. It is operated in the programmable constant-current mode, and electric current is supplied to the Zircaloy test specimen-electrode assembly in the TSF module by two parallel pair of 4/0 gage insulated weld cable. The TSF module (see Fig. 2.10) is a rectangular steel structure used to support the Zircaloy tube specimen-electrode assembly, thermocouple monitoring assembly, helium gas pressure manifold system, and protective containment shroud. The thermocouple monitoring assembly consists of a pair of phenolic terminal barrier strips and adjustable-position alumina support insulators mounted to the phenolic platen on each side of the test specimen. Each terminal barrier strip has three sets of Type-S thermocouple-compensated barrier lugs. The barrier lugs connect a 0.005 - 0.010 in. (0.127 - 0.254 mm) Type-S platinum thermocouple wire, which is welded to the test specimen, to the compensated extension wires. Several oxidation tests were conducted using this approach, but we found that isothermal air



Figure 2.7. 150-mm-long specimens of Zircaloy-4 specimens after oxidation in steam for 140 h at 550°C.



Figure 2.8. Zircaloy-4 specimen after steam oxidation, sleeve grinding, and end drilling. This specimen is ready for air oxidation test under internal pressure.

Table 2.13. Test matrix for air oxidation of steam-preoxidized Zircaloy-4 with internal pressure

Temperature (°C)	Initial internal pressure [MPa (psi)]	
600	2.76 (400)	1.38 (200)
700	2.76 (400)	1.38 (200)
800	1.21 (175)	0.69 (100)
900	0.69 (100)	0.35 (50)



Figure 2.9. Experimental setup for air oxidation studies on Zircaloy cladding tubes with internal pressure.

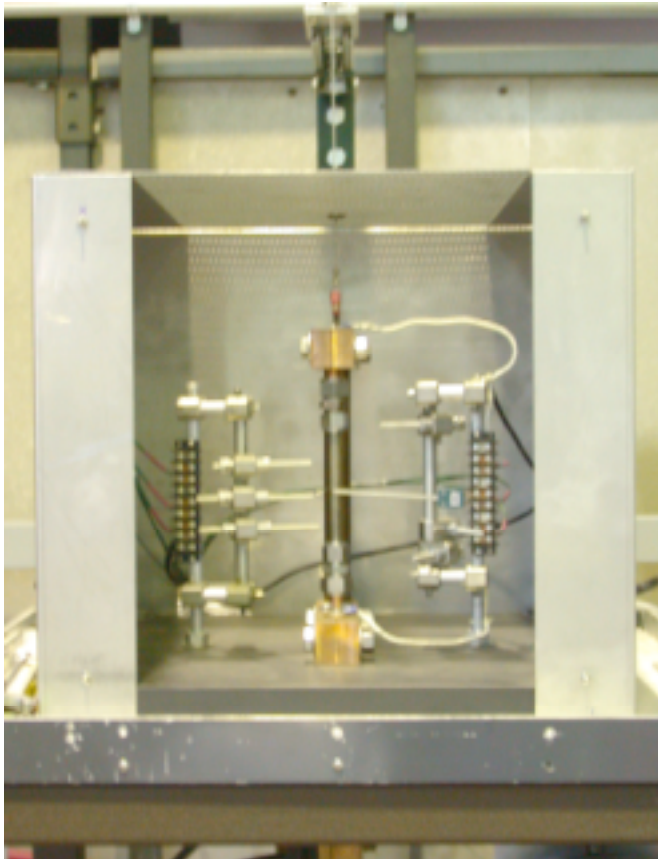


Figure 2.10. Steam-preoxidized Zircaloy-4 specimen assembled in the pressure test facility for air oxidation study.

oxidation using the direct electrical heating approach is not viable. Problems were encountered in maintaining uniform temperature (along the axial direction) and controlling the temperature at the desired value for the long periods of time needed for oxidation rate measurements.

In the second approach, we assembled a steam-preoxidized specimen with pressure fittings, which was exposed in a radiant furnace (see Figures 2.11 and 2.12); such a procedure enabled achieving uniform temperature for the entire specimen during high-temperature exposure. The specimen was pressurized with argon gas via a gas line run from the specimen to the gas supply outside the furnace. In such a setup, the temperature of the specimen and internal pressure were monitored continuously. Also determined were rupture pressure at temperature, time to rupture, internal volume change during the test, and change in tube length during the test.

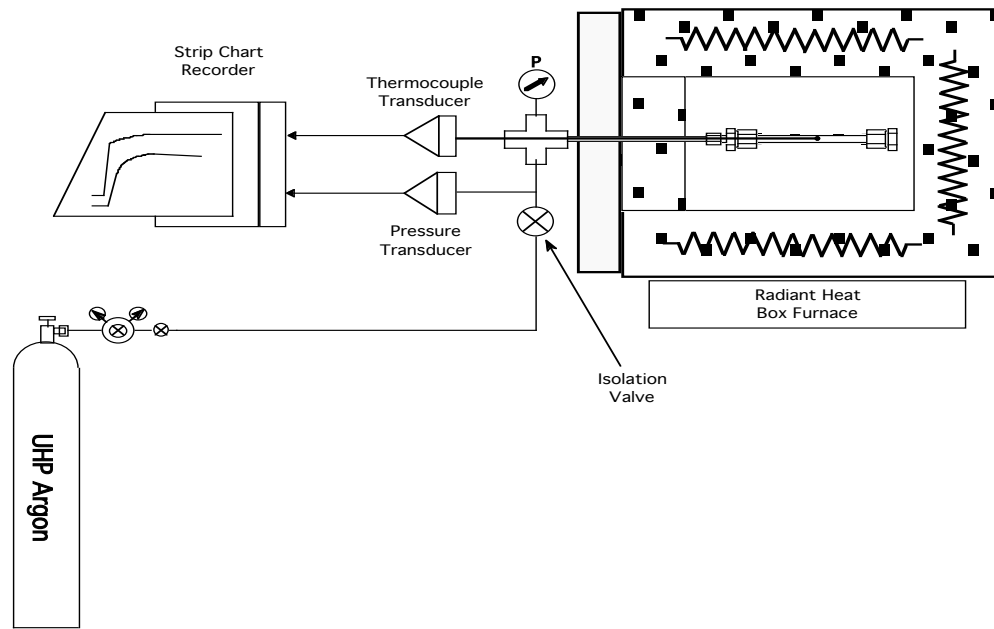


Figure 2.11. Schematic of a test facility for isothermal long-term air oxidation testing under internal pressure.

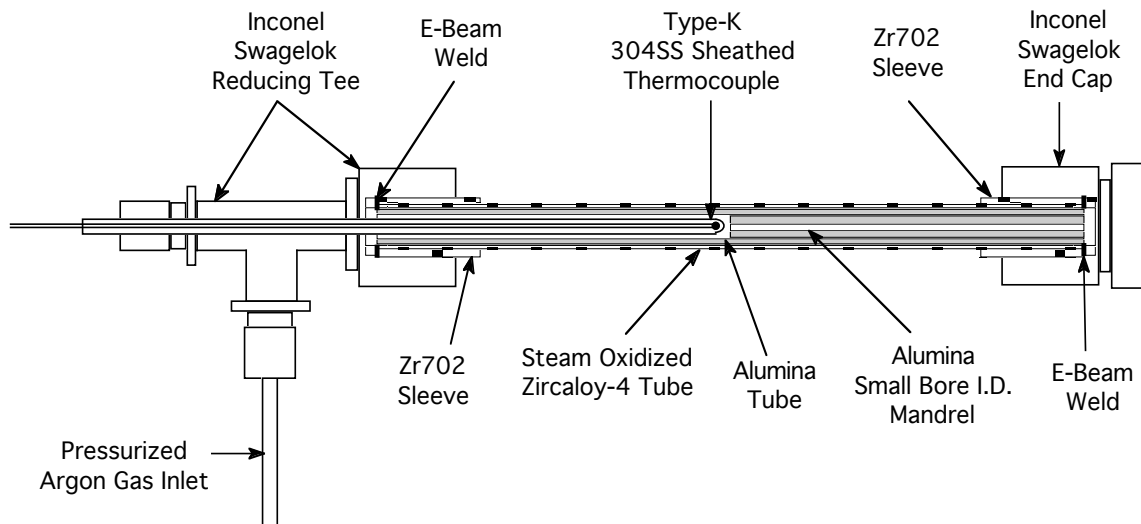


Figure 2.12. Magnified view of the specimen assembly used in air oxidation testing with internal pressure.

3 Results for Zircaloy-4

3.1 Preoxidation in Steam

The oxidation of Zircaloy-4 cladding in steam simulated the amount of oxidation that is representative of the current inventory of spent fuel discharged after medium fuel burnup. A layer thickness in the range of 25-30 μm is desired after steam oxidation. To establish the time and temperature conditions necessary to achieve such a thickness, several 6.5-mm-long ring specimens of the cladding were oxidized in a steam environment at temperatures of 400, 500, 550, and 600°C for several exposure periods. After exposure, the specimens were retrieved, and the weight changes were determined. In addition, the exposed rings were mounted and polished, and oxide thickness was determined by optical metallography.

Figure 3.1 shows the normalized weight change data for the ring specimens as a function of square root of exposure time after oxidation in steam at several temperatures. Figures 3.2-3.5 show the scanning electron photomicrographs of the cross sections of specimens oxidized in steam for various times at 594, 550, 500, and 400°C, respectively. Several conclusions were derived from an analysis of these photomicrographs:

- The oxide thickness was much less than the desired range of 25-30 μm for the specimens after exposure at 400 and 500°C for the longest times (600 and 297 h, respectively) used in the present study.
- The oxide scale developed on specimens exposed at 594°C had a tendency to crack, indicating an inherent weakness in the protective capacity of the oxide layer against further oxidation in air.
- The oxide scale developed at 550°C exhibited an acceptable growth rate to achieve the desired thickness of 25-30 μm within a relatively short and acceptable exposure time, and the oxide developed seemed to be crack free with adequate adherence to the substrate.

Figure 3.6 shows the measured ZrO_2 thickness for several of the ring specimens oxidized in a steam environment. Based on these test data, an exposure time of 140 h at 550°C was selected for oxidation of 75-mm long capsule specimens to achieve an oxide thickness in the range of 25-30 μm .

Zircaloy-4 capsule specimens (75-mm in length, back filled with argon gas and welded shut) were preoxidized in a steam environment to obtain $\approx 30\text{-}\mu\text{m}$ thick oxide. Figure 3.7 shows the weight change data for capsule specimens of Zircaloy-4 after steam oxidation for 140 h at 550°C. The weight change for the 22 Zircaloy-4 specimens ranged between 0.042 and 0.048 mg/mm^2 .

The oxide thickness for various capsule specimens, calculated from the weight change data, was in agreement with data developed on ring specimens. Figure 3.8 shows a plot of oxide thickness on the O.D. side of the capsule specimens, along with those developed on ring specimens. The oxide thickness for the 22 Zircaloy-4 specimens ranged between 28.5 and 32.8 μm . Note that the oxide thickness for the 22 capsules, shown in Figure 3.8, was calculated using the weight change measurements. Oxide thickness was not measured by optical metallography since the samples were needed for subsequent oxidation studies in air at different temperatures. Figure 3.9 shows the temperature dependence of the rate constant derived from the data on steam oxidation of Zircaloy-4. The equations for steam oxidation kinetics in the temperature range of 300-600°C are as follows:

$$\text{Rate constant (in } \text{kg}^2/\text{m}^4\text{-s)} = 505 \exp(-22005/\text{TK}) \text{ for pre-breakaway} \quad (3.1)$$

$$\text{Rate constant (in } \text{kg}^2/\text{m}^4\text{-s)} = 3.7 \times 10^4 \exp(-27860/\text{TK}) \text{ for post-breakaway} \quad (3.2)$$

where TK is temperature in Kelvin units.

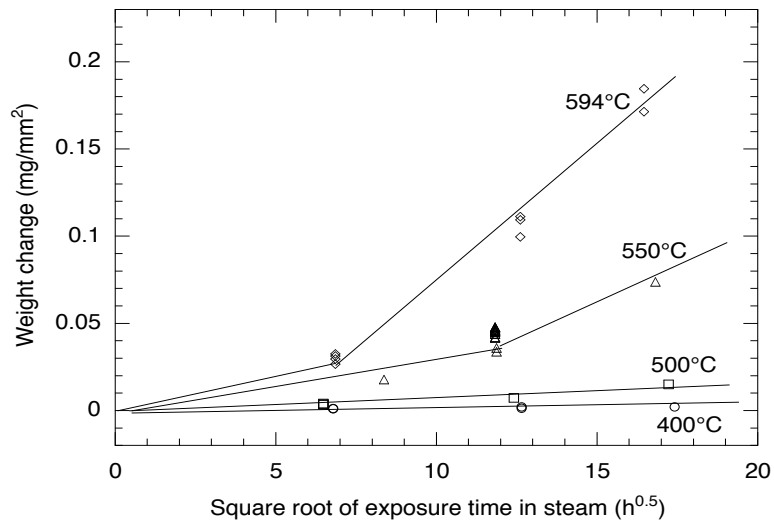


Figure 3.1. Weight change during oxidation of Zircaloy-4 in a steam environment.

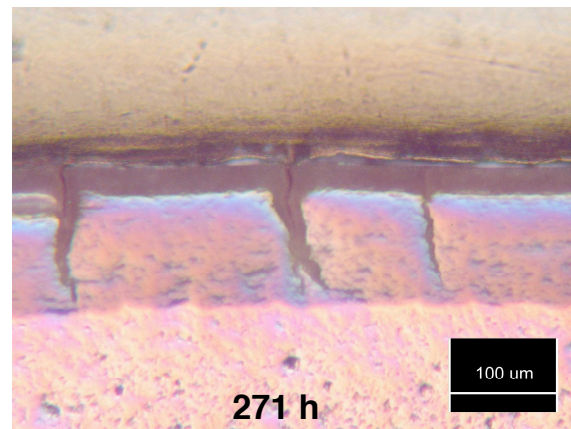
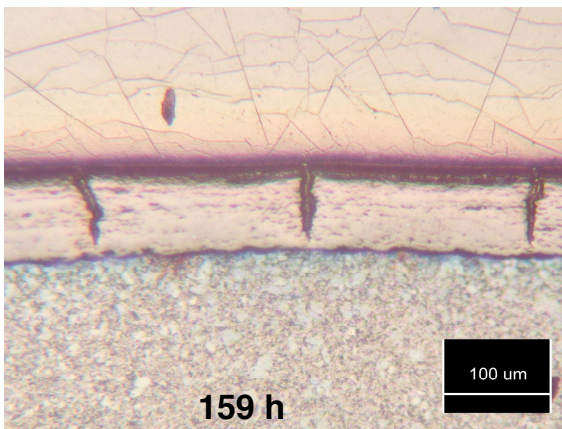
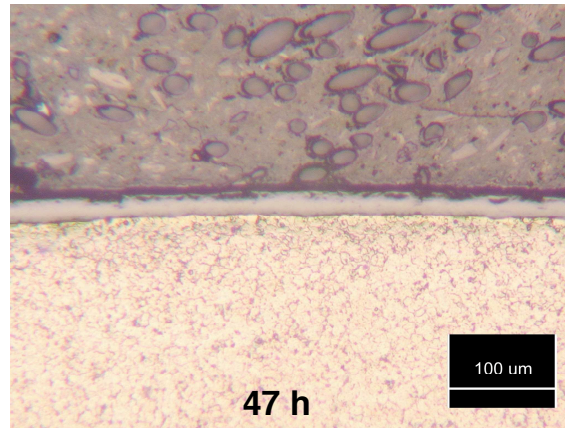


Figure 3.2. SEM photomicrographs of cross sections of Zircaloy-4 ring specimens after oxidation in steam for different times at 594°C.

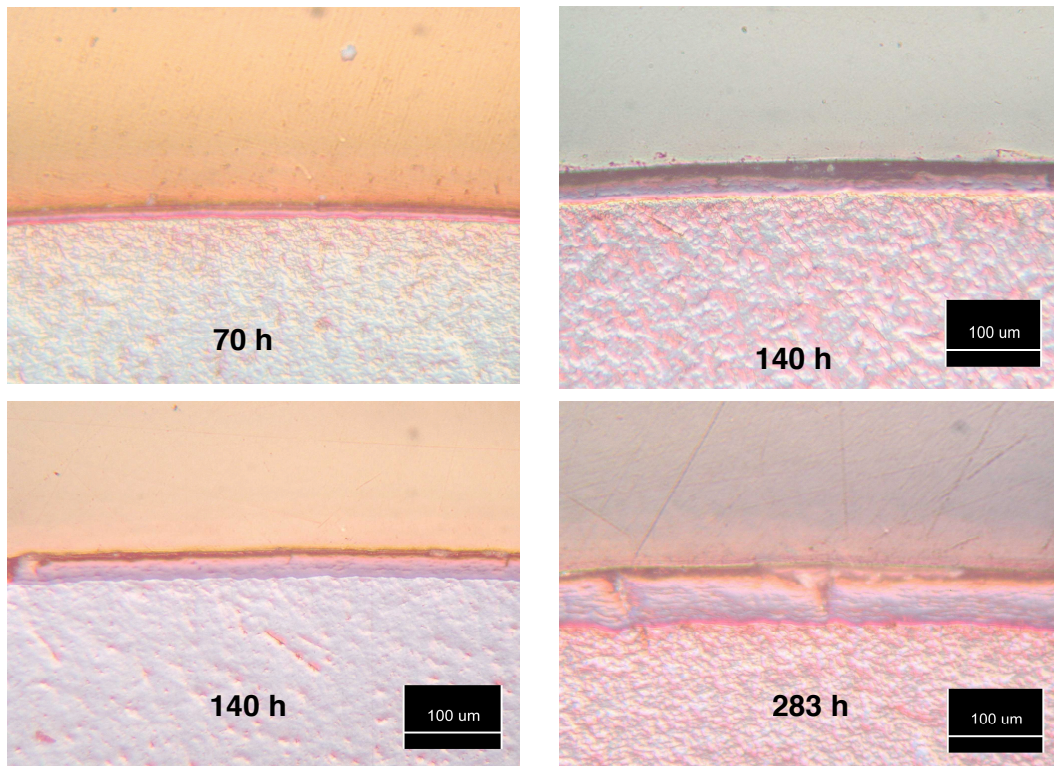


Figure 3.3. SEM photomicrographs of cross sections of Zircaloy-4 ring specimens after oxidation in steam for different times at 550°C.

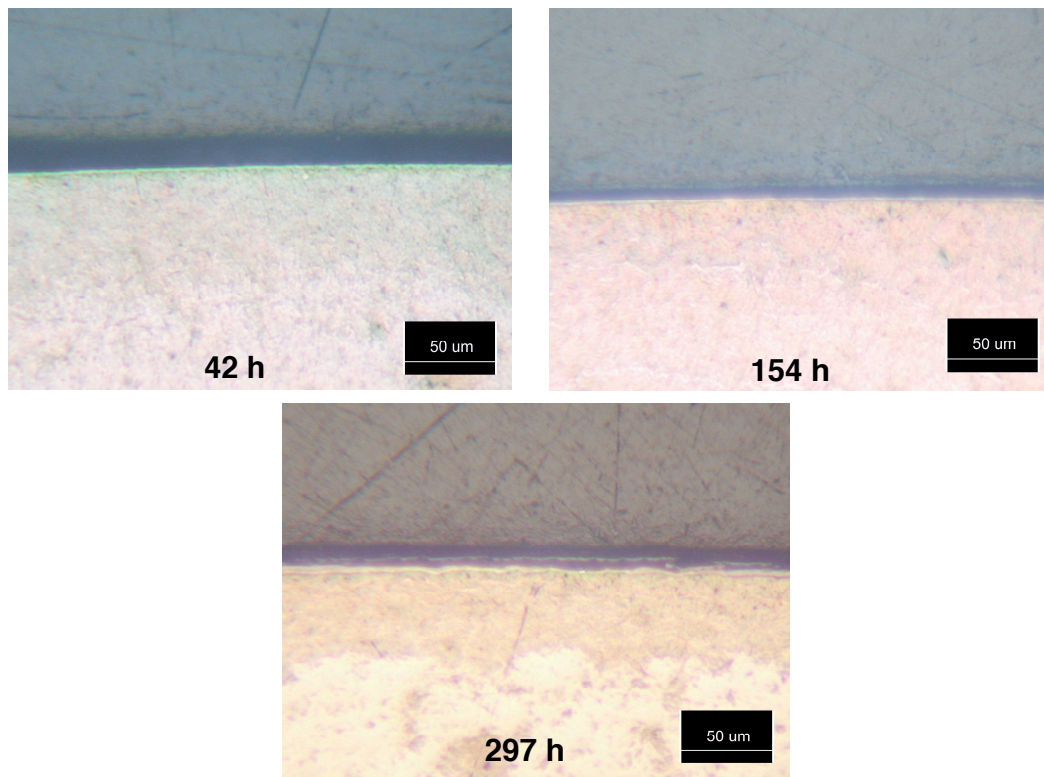


Figure 3.4. SEM photomicrographs of cross sections of Zircaloy-4 ring specimens after oxidation in steam for different times at 500°C.

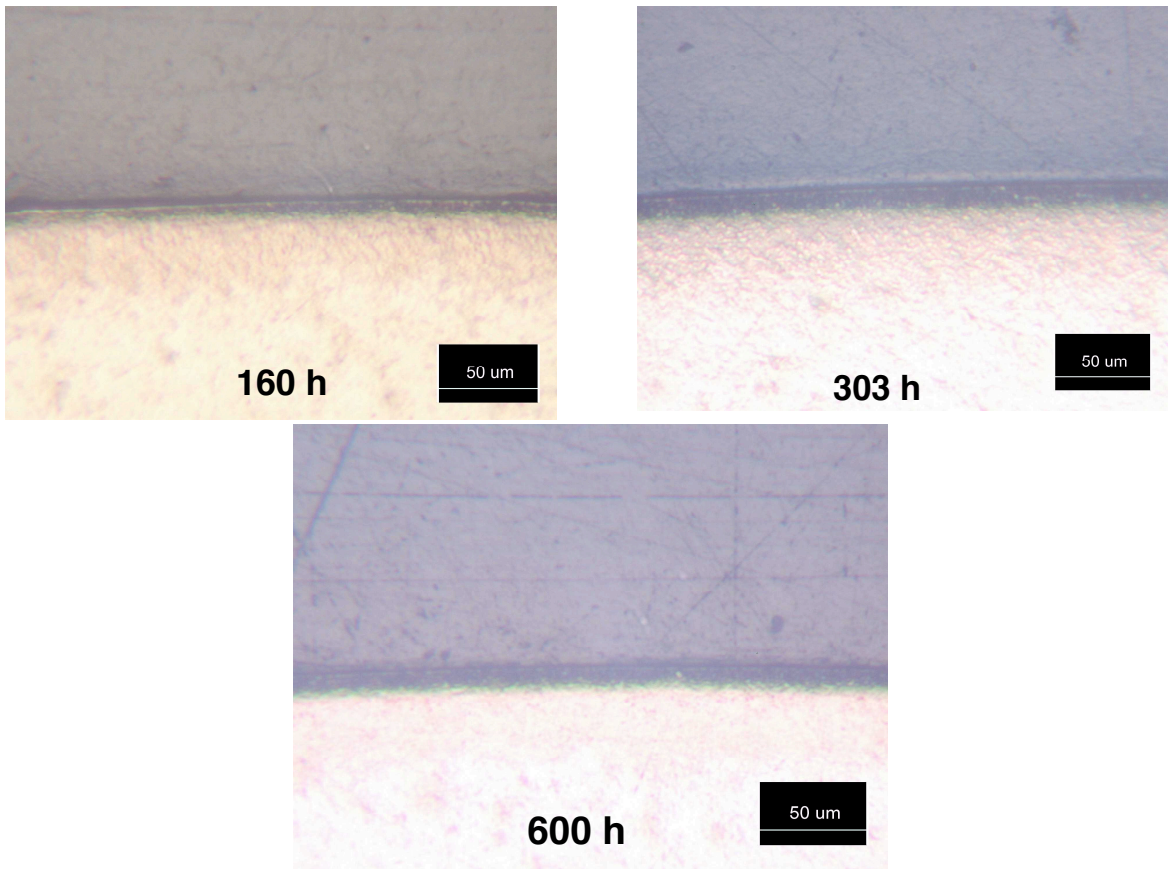


Figure 3.5. SEM photomicrographs of cross sections of Zircaloy-4 ring specimens after oxidation in steam for different times at 400°C.

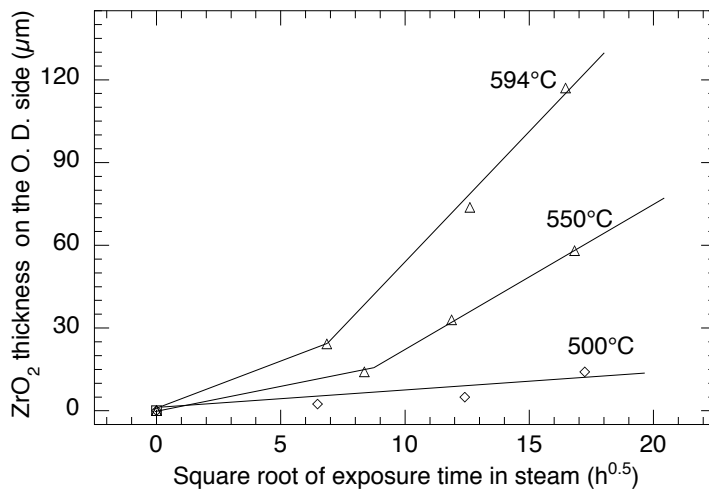


Figure 3.6. Variation in oxide thickness as a function of exposure time during steam oxidation of Zircaloy-4 ring specimens.

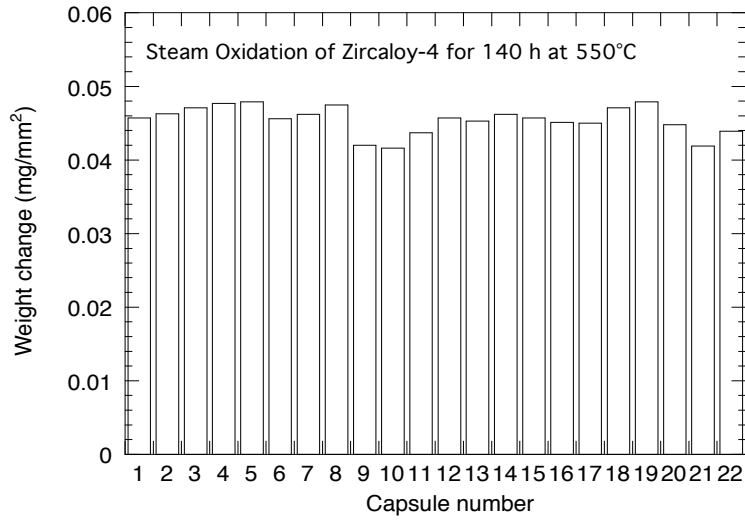


Figure 3.7. Weight change during steam oxidation of Zircaloy-4 capsule specimens for 140 h at 550°C.

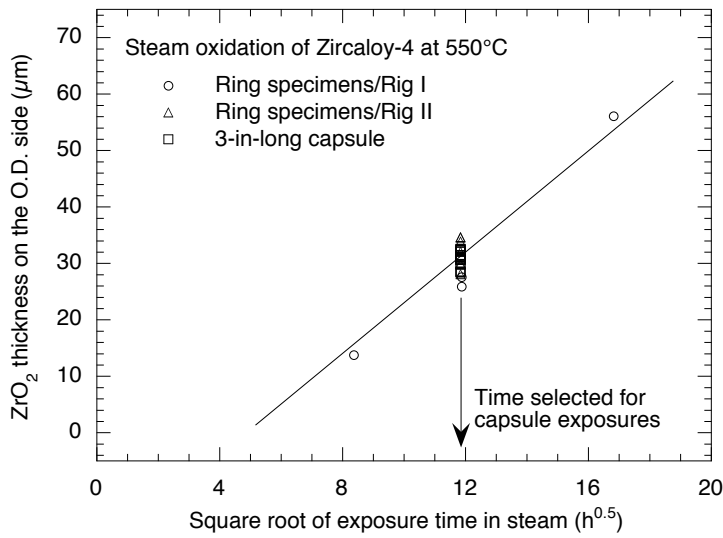


Figure 3.8. Oxide thickness developed on ring and capsule specimens of Zircaloy-4 after oxidation in steam at 550°C.

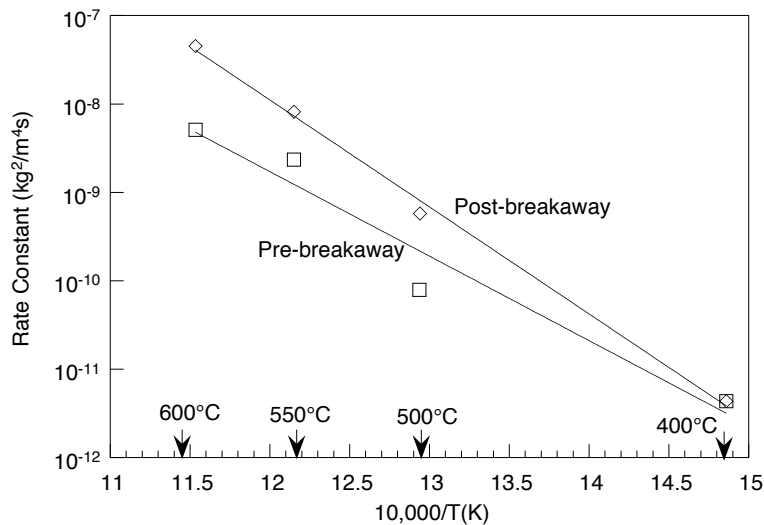


Figure 3.9. Temperature dependence of the rate constant for the steam oxidation of Zircaloy-4.

3.2 Air Oxidation of Steam-Preoxidized Capsules

3.2.1 300-600°C

Figure 3.10 shows weight change data for the 75-mm long capsules of steam-preoxidized Zircaloy-4 after various oxidation times in air at temperatures of 300, 400, 500, and 600°C. It is evident from Figure 3.10 that the oxidation process exhibits a breakaway trend (see data for 500 and 600°C) even though the specimens were preoxidized in steam. The data obtained up to 1260 h at 300°C did not show a breakaway trend. Figures 3.11-3.14 show the SEM photomicrographs of cross sections of steam-preoxidized specimens after oxidation in air for different times at 600, 500, 400, and 300°C, respectively. Several conclusions were drawn from these photomicrographs:

- Though the initial oxide scale, developed by 140-h exposure in steam at 550°C, was adherent and crack free, the oxide tended to crack when exposed in air for 40 h at 600°C.
- The thickness of the oxide developed during air exposure increased significantly with time and the transverse cracks persisted over the entire thickness of the scale, as evidenced by the micrograph of the specimen air exposed for 155 and 299 h at 600°C.
- The growth rate for oxide at 500°C in air was much less and the scales exhibited virtually no cracks even after an exposure time of 402 h at 500°C.
- The oxidation rates in air for steam-preoxidized specimens were minimal to negligible at 400 and 300°C after exposure times of 600 and 1260 h, respectively.

Figure 3.15 shows oxide thickness measured for the 75-mm-long capsules of steam-preoxidized Zircaloy-4 after various oxidation times in high-purity air at temperatures of 300, 400, 500, and 600°C. The thickness values are for the oxide that grew during air oxidation only and do not include the $\approx 30\text{-}\mu\text{m}$ -thick oxide that developed during steam preoxidation. The thickness results showed good agreement with data on weight change. Figure 3.16 shows a composite plot of weight change data for different conditions, including both steam preoxidation and subsequent oxidation in air. Note that steam preoxidation was performed for 140 h at 550°C, whereas the exposures in air were conducted at 300 to 600°C for times up to ≈ 1000 h.

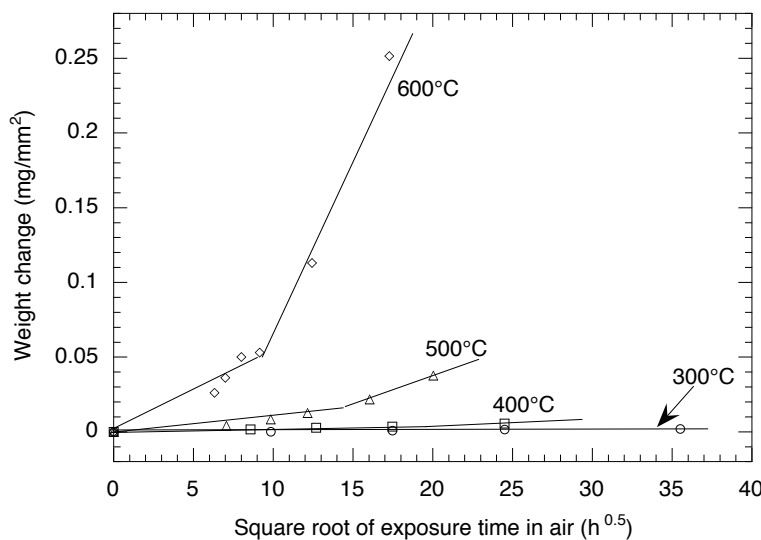


Figure 3.10. Weight change during air oxidation of steam-preoxidized Zircaloy-4 capsule specimens at several temperatures.

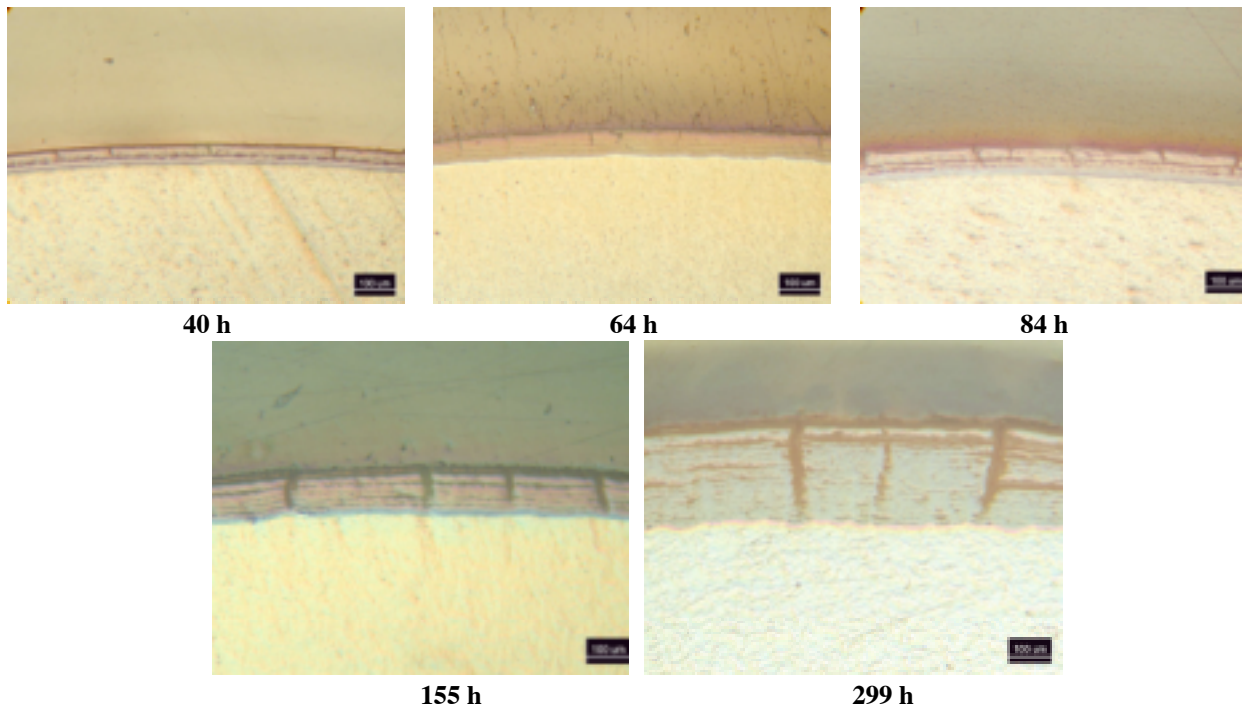


Figure 3.11. SEM photomicrographs of cross sections of steam-preoxidized Zircaloy-4 capsule specimens after oxidation in air for different times at 600°C.

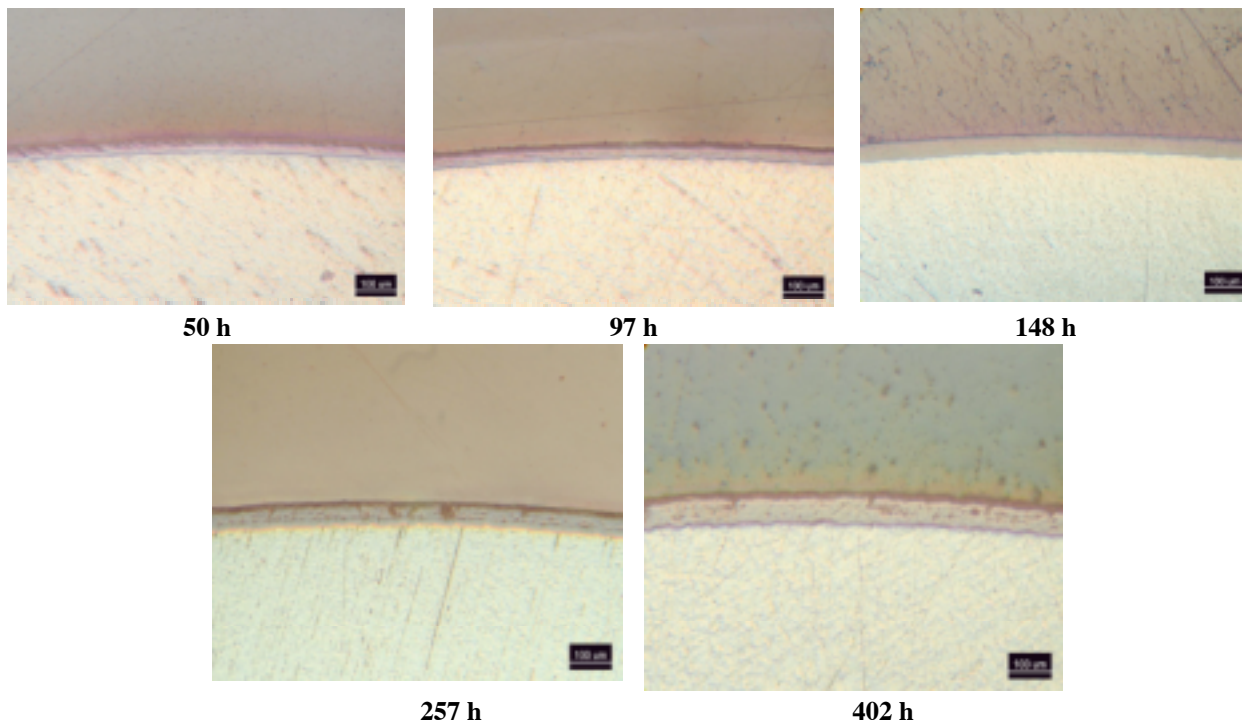


Figure 3.12. SEM photomicrographs of cross sections of steam-preoxidized Zircaloy-4 capsule specimens after oxidation in air for different times at 500°C.

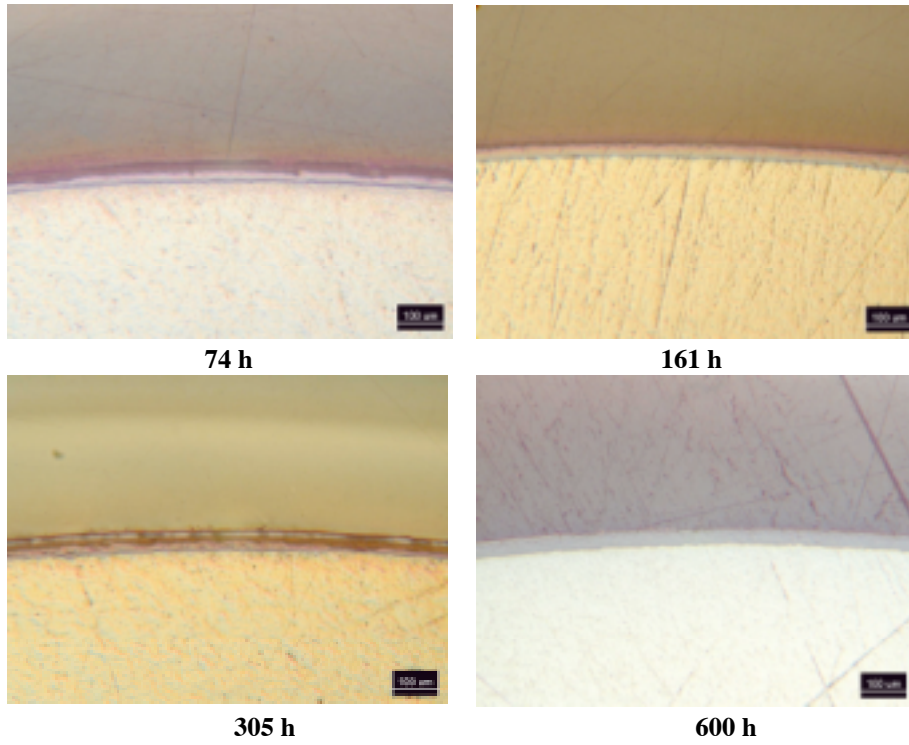


Figure 3.13. SEM photomicrographs of cross sections of steam-preoxidized Zircaloy-4 capsule specimens after oxidation in air for different times at 400°C.

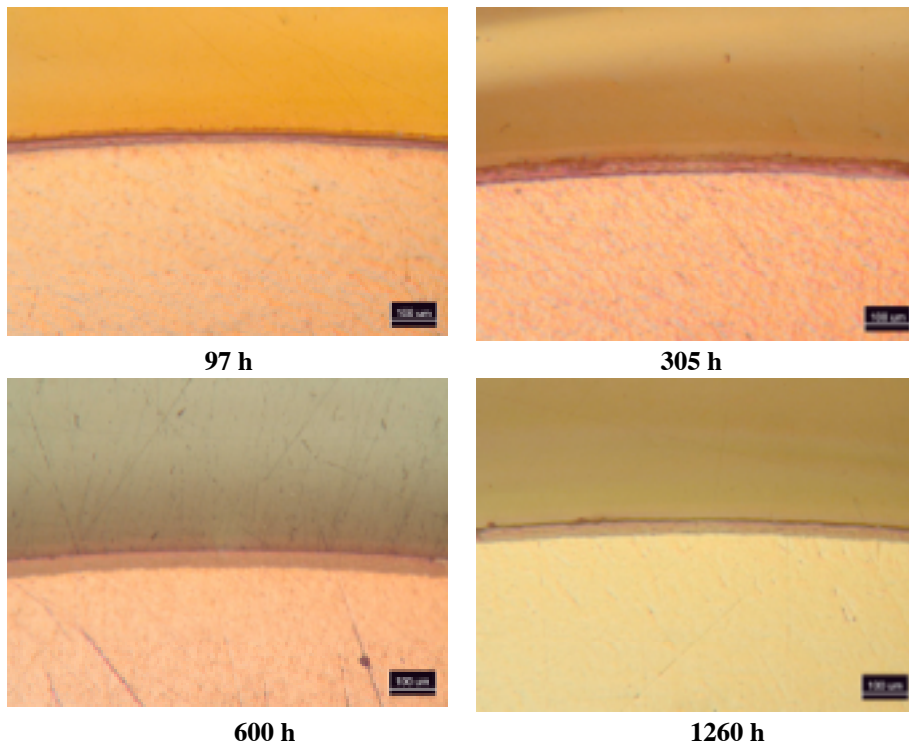


Figure 3.14. SEM photomicrographs of cross sections of steam-preoxidized Zircaloy-4 capsule specimens after oxidation in air for different times at 300°C.

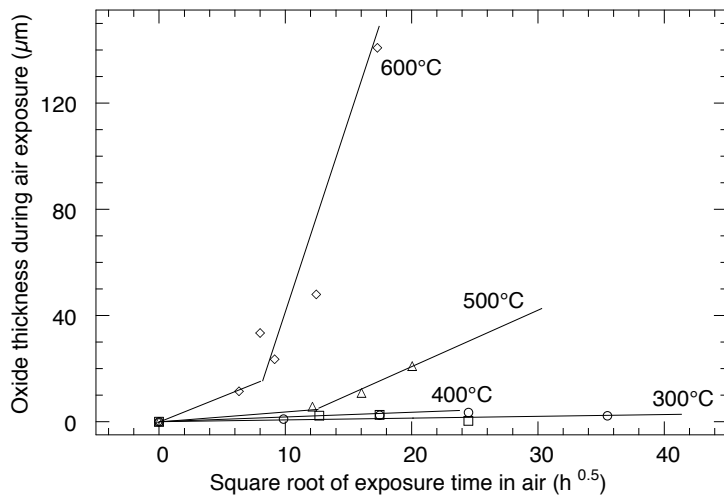


Figure 3.15. Oxide thickness for air oxidation of steam-preoxidized Zircaloy-4 capsule specimens at several temperatures.

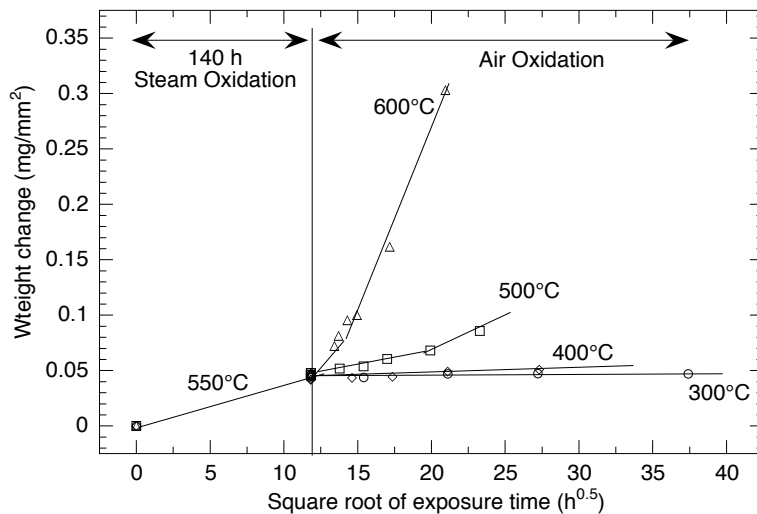


Figure 3.16. Weight change during air oxidation of steam-preoxidized Zircaloy-4 capsule specimens at several temperatures.

3.2.2 700-900°C

Table 2.6 lists the exposure times used for evaluating the air oxidation characteristics of steam-preoxidized Zircaloy-4 at 700, 800, and 900°C. A single specimen was used at each temperature. The weight change as a function of exposure time was obtained by periodic retrieval and weighing of the specimen. The exposures were terminated when the oxidation became substantial and/or when the specimen deformed significantly. Oxide thickness was measured on the specimens, if possible, after the final exposure at each temperature. Figure 3.17 shows the weight change data as a function of square root of time at the three temperatures.

Significant swelling of the oxide was observed for specimens exposed at 700-900°C. Oxide thickness was calculated from the weight change data as a function of time at the three exposure temperatures. Figure 3.18 shows the oxide thickness as a function of square root of time. The calculated oxide thickness after 34.5-h exposure in air at 700°C was 156.8 μm , and the total (in steam and in air) calculated thickness was 186.4 μm . This compares with a measured value of 207.3 μm after 34.5-h exposure at 700°C. The calculated oxide thickness (not shown in Fig. 3.18) after 14-h exposure in air at 800°C was 591.8 μm , and the total (in steam and in air) calculated value was 632.8 μm .

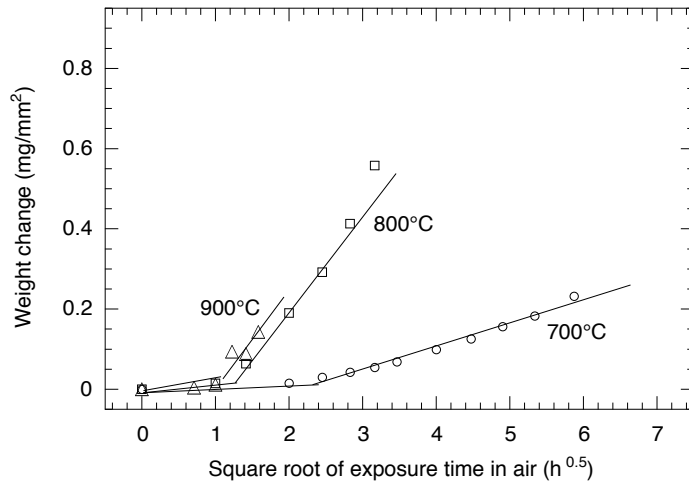


Figure 3.17. Weight change during oxidation of steam-preoxidized Zircaloy-4 capsule specimens at 700, 800, and 900°C.

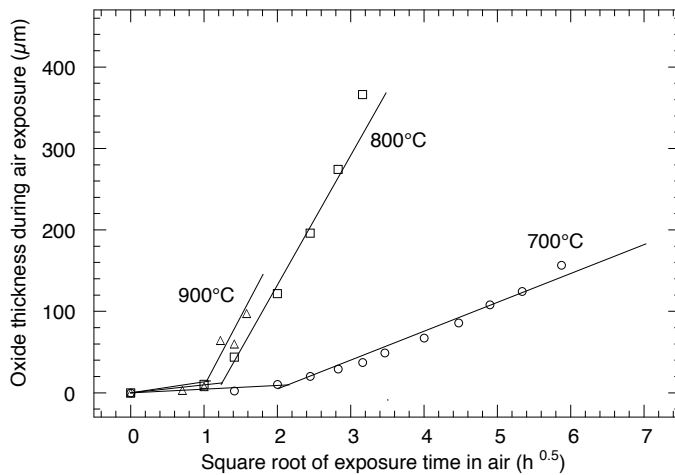


Figure 3.18. Oxide thickness calculated from the weight change data for air oxidation of steam-preoxidized Zircaloy-4 capsule specimens at 700, 800, and 900°C.

This compares with a measured value of 580.4 μm after 14-h exposure at 800°C. The calculated oxide thickness after 2.5-h exposure in air at 900°C was 97.4 μm , and the total (in steam and in air) calculated thickness was 123.8 μm . No measurement was made on the specimen exposed at 900°C since the specimen fractured into pieces.

3.2.3 Oxygen Analysis

Several air-oxidized specimens of Zircaloy-4 were analyzed for oxygen concentration, and the values were compared with those calculated from the weight change data, assuming all of the weight change in the specimen is due to oxygen ingress. The sample was reacted with carbon by rapidly heating it to over 2700°C in a helium-purged graphite crucible. The evolved carbon monoxide was carried by helium to a copper oxide furnace, where carbon monoxide converted to carbon dioxide. The concentration of carbon dioxide was measured by an infrared cell and reported in terms of oxygen concentration. In Table 3.1, the oxygen concentration values that were calculated from the weight change data are compared with the analyzed values for specimens air oxidized at 300-600°C. In several cases, the specimens were analyzed more than once, as shown in the table. In general, the calculated and measured values agree well for all the specimens tested, except when the oxide was thick and/or had a tendency to spall (e.g., specimen exposed for 154.7 h at 600°C).

Table 3.1. A comparison of the oxygen concentration values calculated from the weight change data with the measured values for steam-preoxidized Zircaloy-4 specimens after air oxidation

Air exposure temperature (°C)	Air exposure time (h)	Calculated oxygen content (wt.%)	Analyzed oxygen content (wt.%)
300	97.0	0.874	1.00
300	305.2	0.937	0.86, 1.03
300	600.0	0.944	1.01, 1.04
300	1260.0	0.932	0.87, 0.89
400	73.7	0.864	0.90
400	161.0	0.888	0.98
400	305.2	0.979	1.09, 1.09
400	600.0	1.013	1.24, 1.25
500	50.0	1.032	1.09
500	97.0	1.078	1.18
500	257.2	1.353	1.46
500	401.5	1.690	1.72, 1.76
600	40.0	1.434	0.62, 0.93, 1.25
600	83.7	1.992	2.20
600	154.7	3.221	3.51
600	298.7	6.027	-

3.3 Air Oxidation of Bare Alloy

3.3.1 300-600°C

Table 2.5 lists the exposure times used for evaluating the air oxidation characteristics of bare Zircaloy-4 at 300, 400, 500, and 600°C. A single specimen was used at each temperature, and weight-change data as a function of exposure time were obtained by periodic retrieval and weighing of the specimen. Exposures were, in general, complementary to those conducted on air oxidation of steam-preoxidized specimens. Oxide thickness was measured on the specimens after the final time of exposure at each temperature. Figure 3.19 shows the weight change data as a function of square root of time at the four temperatures.

Oxide thickness was calculated from the weight change data as a function of time at the four exposure temperatures. Figure 3.20 shows oxide thickness as a function of square root of time. The calculated oxide thickness after 300-h exposure in air at 600°C was 231.0 μm . This compares with a measured value of 197.0 μm . The calculated oxide thickness after 401-h exposure in air at 500°C was 21.6 μm , and the measured thickness was 21.4 μm . The calculated values after 599.7 h at 400°C and 1036.8 h at 300°C were 3.4 and 1.1 μm , respectively. No measurement was made on the specimens exposed at 300 and 400°C, since they were negligibly small.

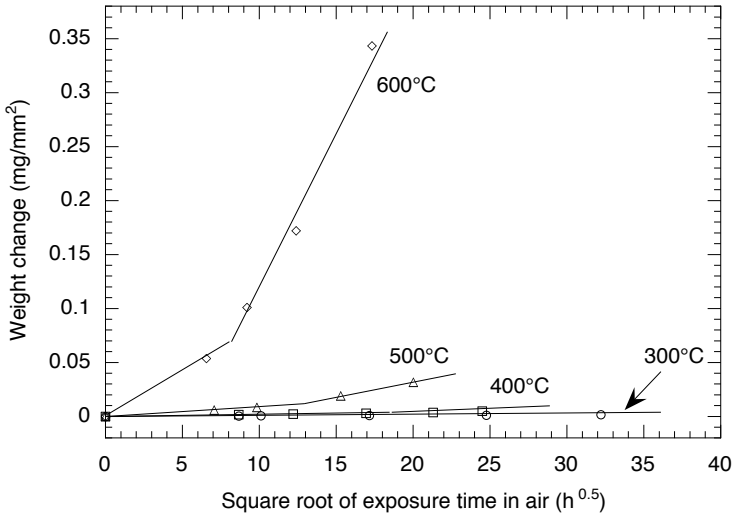


Figure 3.19. Weight change during oxidation of bare Zircaloy-4 capsule specimens at 300, 400, 500, and 600°C.

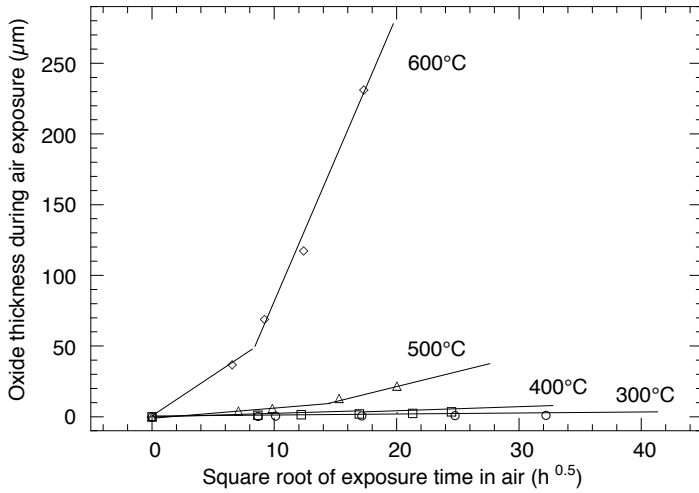


Figure 3.20. Oxide thickness calculated from the weight change data for air oxidation of bare Zircaloy-4 capsule specimens at 300, 400, 500, and 600°C.

3.3.2 700-900°C

Table 2.6 lists the exposure times used for evaluating the air oxidation characteristics of bare Zircaloy-4 at 700, 800, and 900°C. A single specimen was used at each temperature, and weight change as a function of exposure time was obtained by periodic retrieval and weighing of the specimen. The exposures were terminated when the oxidation became substantial and/or when the specimen deformed significantly. Oxide thickness was measured on the specimens, if possible, after the final time of exposure at each temperature. Figure 3.21 shows the weight change data as a function of square root of time at the three temperatures.

Oxide thickness was calculated from the weight change data as a function of time at the three exposure temperatures. Figure 3.22 shows oxide thickness as a function of square root of time. The calculated oxide thickness after 34.5-h exposure in air at 700°C was 172.1 µm. This compares with a measured value of 179.1 µm. The calculated oxide thickness after 14-h exposure in air at 800°C was 364.2 µm. No measurement was made on the specimen exposed at 800°C since the specimen disintegrated into pieces. The calculated total oxide thickness after 2.5-h exposure in air at 900°C was 148.6 µm. No measurement was made on the specimen exposed at 900°C since it fractured into pieces.

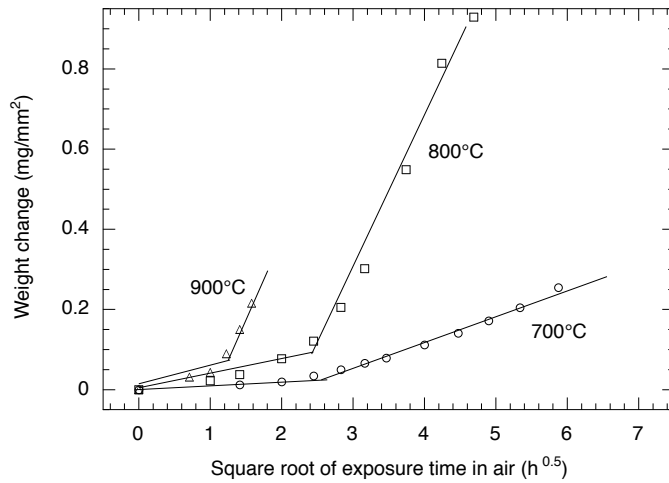


Figure 3.21. Weight change during oxidation of bare Zircaloy-4 capsule specimens at 700, 800, and 900°C.

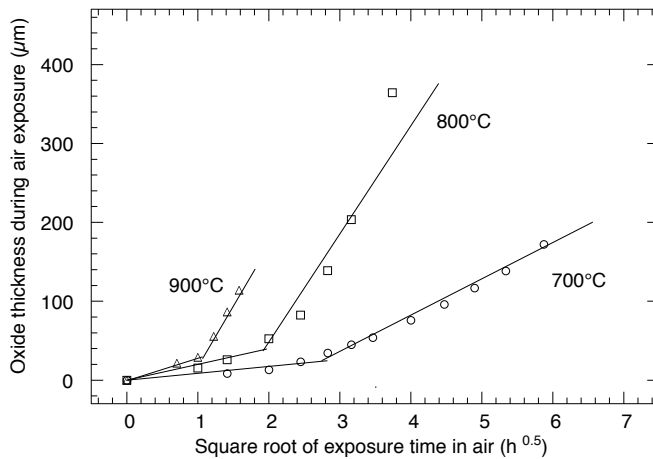


Figure 3.22. Oxide thickness calculated from the weight change data for air oxidation of bare Zircaloy-4 capsule specimens at 700, 800, and 900°C.

3.4 Oxidation in Low-Oxygen Environment

To evaluate the role, if any, of the oxygen-deficient and nitrogen-enriched gas mixture in the oxidation of Zircaloy-4, tests were conducted in a 2.5 vol.% O₂-N₂ gas mixture at 400 and 600°C. Oxidation experiments of steam-preoxidized cladding were performed in the low-O₂ environment at 400°C for ≈600 h and at 600°C for ≈300 h. The specimens were periodically retrieved from the furnace, the weight changes were measured, and the specimens were re-exposed for continued oxidation.

Figure 3.23 shows weight change data for the 75-mm-long capsules of steam-preoxidized Zircaloy-4 after various oxidation times in low-O₂ environment at 400 and 600°C. Also shown in the figure are the oxidation data obtained in air for steam-preoxidized Zircaloy-4, the details of which were presented in earlier reports. At 600°C, the weight change data indicate that the rates are somewhat lower in the low-O₂ environment when compared with those in air. The rates are almost the same in both environments at 400°C. Table 3.2 lists the calculated rates for the oxidation of steam-preoxidized Zircaloy-4 in air and low-O₂ environments.

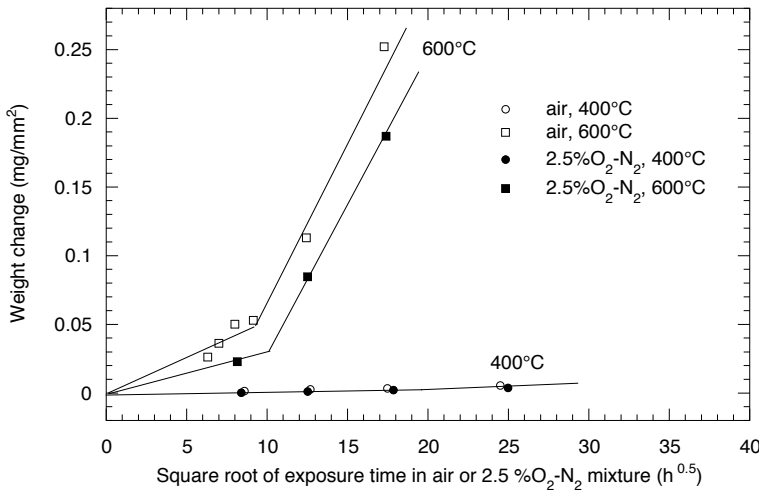


Figure 3.23. Weight change during oxidation of steam-preoxidized Zircaloy-4 capsule specimens in air and in 2.5 vol.% O₂-N₂ gas mixture at 400 and 600°C.

Table 3.2. Oxidation rates for steam-preoxidized¹ Zircaloy-4 in air and in low-O₂ environments

Temperature (°C)	Oxidation rate (kg ² /m ⁴ ·s) of steam-preoxidized Zircaloy-4			
	In air, pre-breakaway	In air, post-breakaway	In 2.5 vol% O ₂ -N ₂ , pre-breakaway	In 2.5 vol% O ₂ -N ₂ , post-breakaway
400	4.3 x 10 ⁻¹²	6.4 x 10 ⁻¹¹	NB ²	7.1 x 10 ⁻¹²
600	8.4 x 10 ⁻⁹	7.2 x 10 ⁻⁸	2.7 x 10 ⁻⁹	5.1 x 10 ⁻⁸

¹Steam preoxidation condition: 140 h at 550°C; oxide thickness ≈30 μm.

²No breakaway observed during the exposure time used in the present study.

3.5 Effect of Internal Pressure on Air Oxidation

In the early part of the program, several oxidations were conducted in air with internally pressurized, steam-preoxidized Zircaloy-4 specimens using the direct electrical heating apparatus. Since the test approach was not adequate to maintain isothermal conditions in the entire length of the specimen during the test, results from only two of the experiments are presented to describe the information obtained. Two air oxidation tests (designated as Tests 4 and 5) were conducted with steam preoxidized specimens at 600°C. In both tests, an alumina rod (simulating fuel pellets) was inserted into the specimen and held concentric to the tube diameter in order to minimize the gas volume and maintain a gap between the cladding tube and the alumina rod. An alumina-sheathed Type S (0.375-mm Pt/Pt-Rh) thermocouple was inserted from the top into the specimen and spot welded onto its inner surface approximately at the middle. The specimen was pressurized to 400 psi at room temperature with UHP Ar gas, and the pressurized specimen was isolated from the Ar gas supply by closing a valve in the vicinity of the specimen.

In Test 4, the oxide was removed locally from the specimen surface at the center and at a distance of ≈25 mm on either side from the center of the specimen so that external (0.25-mm Type S) thermocouples could be spot welded onto the bare metal. A fourth thermocouple physically touched the oxide on the OD at the center of the specimen. The thermocouple, spot welded on the ID side of the specimen, was used for monitoring and controlling the temperature of the specimen at 600°C.

Figure 3.24 shows the experimental setup in which the steam-preoxidized specimen was assembled for Test 4. The temperature measurements made during this test indicated hot spots at two locations away from the center. Even though the radiant ID and the OD spot-welded thermocouples read 600°C, the other two external



Figure 3.24. Steam-preoxidized Zircaloy-4 specimen setup with an internal Ar pressure of 400 psi in Test 4.



Figure 3.25. Steam-preoxidized Zircaloy-4 specimen with an internal Ar pressure of 400 psi after 22 h elapsed time and at the end of Test 4 at ≈ 40 h.

thermocouples showed temperatures as high as 725°C. The thermocouple touching the oxide generally indicated ≈200°C lower. The lack of uniformity in temperature in the axial direction and the presence of hot spots seemed inherent in the electrically heated test procedure. As the exposure progressed, the cladding deformation concentrated in the hot spot region, as shown in the specimen photographs (see Figure 3.25) after 22 h elapsed time and at the end of the test at ≈40 h. The specimen exhibited significant ballooning in the hot spot region and developed at least two pin-hole leaks with eventual loss of pressure. The test was terminated after ≈40 h, and the specimen was sliced at several locations to examine the oxidation performance (see Figure 3.26). Figure 3.27 shows a microphotograph of a steam-preoxidized Zircaloy-4 specimen after air oxidation with internal argon pressure of 400 psi in Test 4, showing a region with an elongated fissure crack.

Test 5 was conducted in a setup similar to Test 4 with one exception. Five external thermocouples (equally spaced axially at 12.5 mm interval) were used, and all the thermocouples were attached on the oxide with alumina cement, to ensure that hot spots are not forming on the surface by local removal of the oxide (as in Test 4). Similar to Test 4, one thermocouple spot welded on the ID side of the specimen was used for monitoring and controlling the temperature of the specimen at 600°C. Figure 3.28 shows the specimens after elapsed times of 17 and 34 h. Figure 3.29 shows the specimen after the termination of the test at 47 h, which was necessitated by the lack of adhesion of the ID and OD thermocouples (due to bulging of the alloy) and by the inability to monitor and control the temperature of the specimen. Even in this test, the specimen exhibited some ballooning (but no failure), indicating the presence of local hot spots that enabled accelerated deformation of the cladding.

Tests 4 and 5 showed that isothermal air oxidation by means of direct electrical heating is not viable, especially for maintaining a uniform temperature (along the axial direction) and controlling the temperature at the desired value for the long periods of time needed for measurement of oxidation rates.

Alternatively, we used a modified procedure in which steam-preoxidized specimens with pressure fittings were exposed in a radiant furnace; such a procedure resulted in achieving uniform temperature for the entire specimen during high-temperature exposure. The specimen was pressurized with argon gas via a gas line run from the specimen to the gas supply outside the furnace. In such a setup, the temperature of the specimen and internal pressure were monitored continuously during tests at 600, 700, 800, and 900°C. Table 3.3 lists the test conditions used for various tests along with test data such as maximum pressure at temperature (P_{max}), rupture pressure at temperature (P_r), initial pressure (P_o), time to rupture, internal volume change during the test, and tube length change during the test. It is evident from the data that at 600°C and 400 psig, the tube ruptures in 43 h. The rupture times are even shorter at higher temperatures. To obtain prolonged oxidation time in air, the initial pressure within the specimen was reduced. Even with the decreased pressure, the increment in time to rupture was minimal, especially at 800 and 900°C. Figures 3.30-3.33 show steam-preoxidized Zircaloy-4 specimens after testing in air at 600-900°C with various internal pressures. The photographs indicate that ballooning of the specimens in the center region and associated accelerated oxidation lead to a pin-hole mode of failure at all temperatures. The extent of ballooning is dependent on the exposure time at temperature, which in turn is dependent on the magnitude of the internal pressure.

The tested specimens were cut at several locations to establish the oxide thickness in the undeformed or minimally deformed region (generally far away from the failure zone) and in the vicinity of the ballooned failure zone. The cut sections of the tubes were mounted and polished for metallographic examination of the cross sections. In addition, the pin-hole failure in each tested specimen was examined on the tube surface and in tube cross section by using scanning electron microscopy. Figures 3.34-3.37 show SEM photomicrographs of cross sections of various specimens in a region far away from the rupture area. The oxide thickness near the failure area was, in general, much thicker, even though the entire specimen was at constant temperature. The cause for such an accelerated



Figure 3.26. Steam-preoxidized Zircaloy-4 specimen after air oxidation with internal Ar pressure of 400 psi in Test 4.

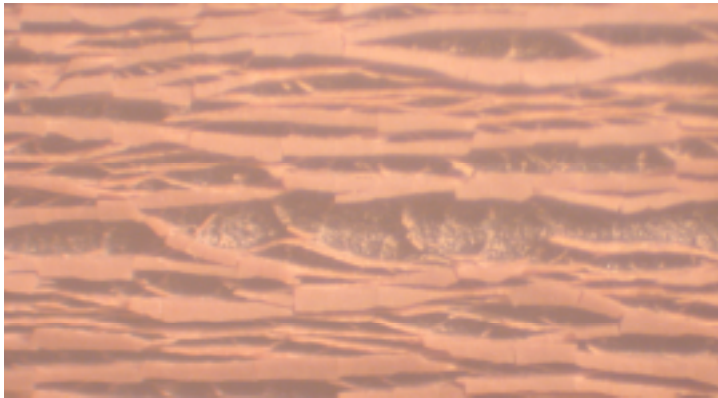


Figure 3.27. Micrograph of a steam-preoxidized Zircaloy-4 specimen after air oxidation with internal Ar pressure of 400 psi in Test 4, showing a region with an elongated-fissure crack.

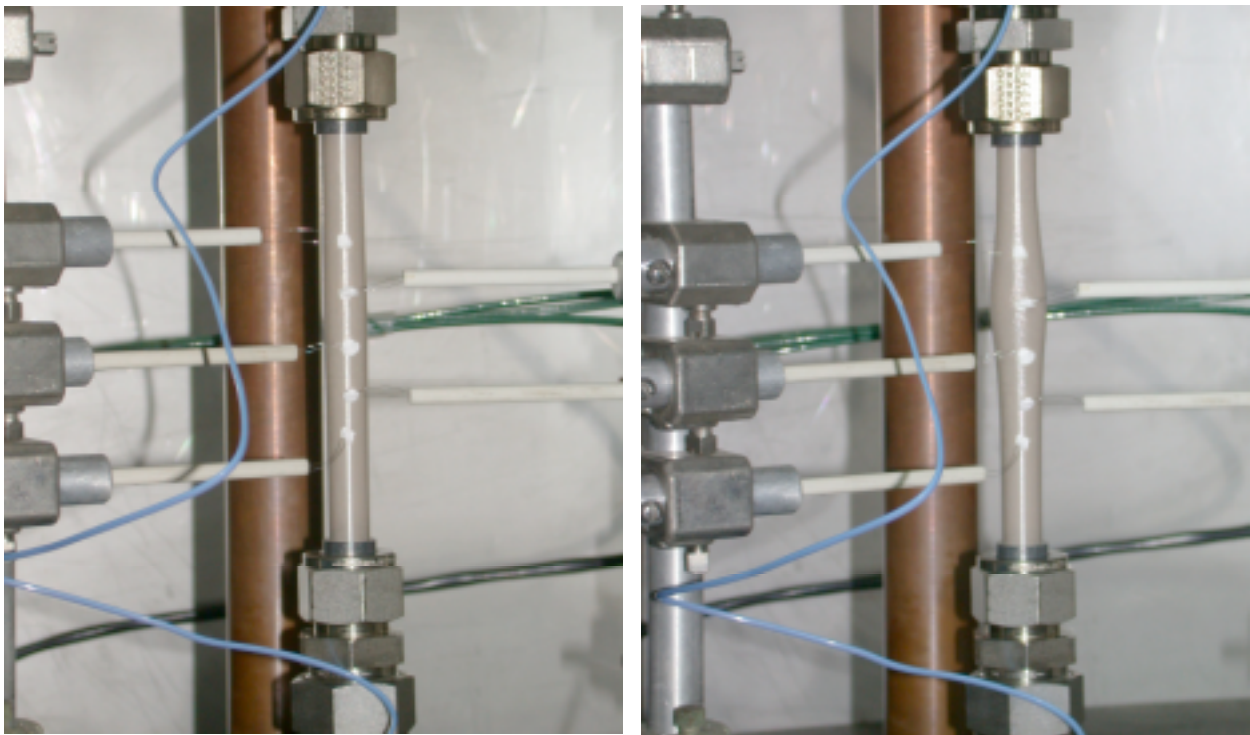


Figure 3.28. Steam-preoxidized Zircaloy-4 specimen with an internal Ar pressure of 400 psi after elapsed times of (left) 17 and (right) 34 h in Test 5.



Figure 3.29. Steam-preoxidized Zircaloy-4 specimen with internal Ar pressure of 400 psi after oxidation in air for 47 h (end of test) in Test 5.

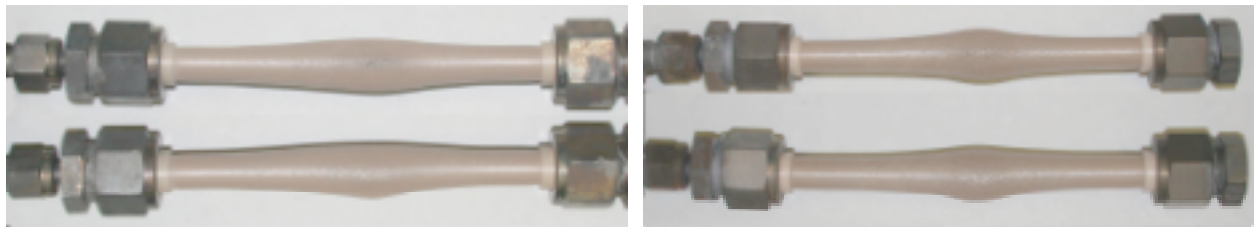


Figure 3.30. Zircaloy-4 specimens (in two orientations) tested with internal pressure of (left) 400 and (right) 200 psig at 600°C.



Figure 3.31. Zircaloy-4 specimens tested with internal pressure of (left) 400 and (right) 200 psig at 700°C.



Figure 3.32. Zircaloy-4 specimens tested with internal pressure of (left) 175 and (right) 100 psig at 800°C.

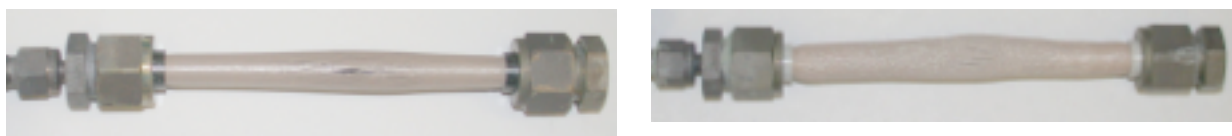


Figure 3.33. Zircaloy-4 specimens tested with internal pressure of (left) 100 and (right) 50 psig at 900°C.

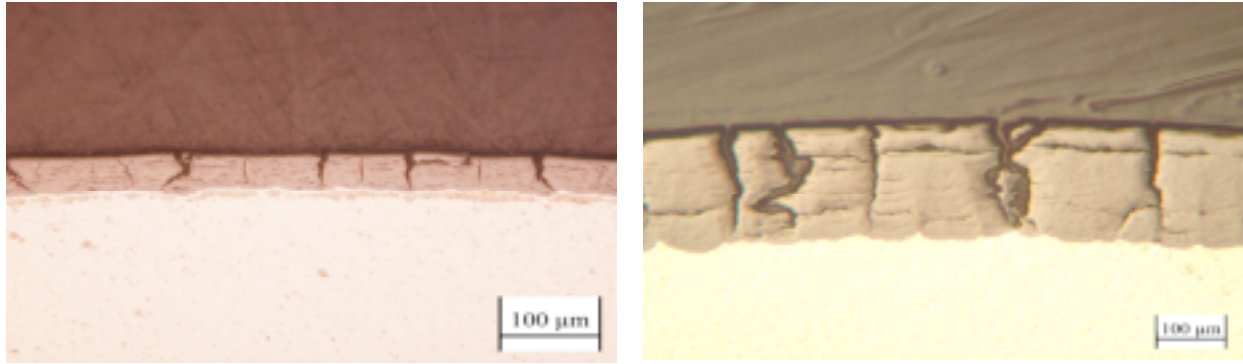


Figure 3.34. Microphotographs of oxide developed on Zircaloy-4 specimens tested with internal pressure of (left) 400 and (right) 200 psig at 600°C.

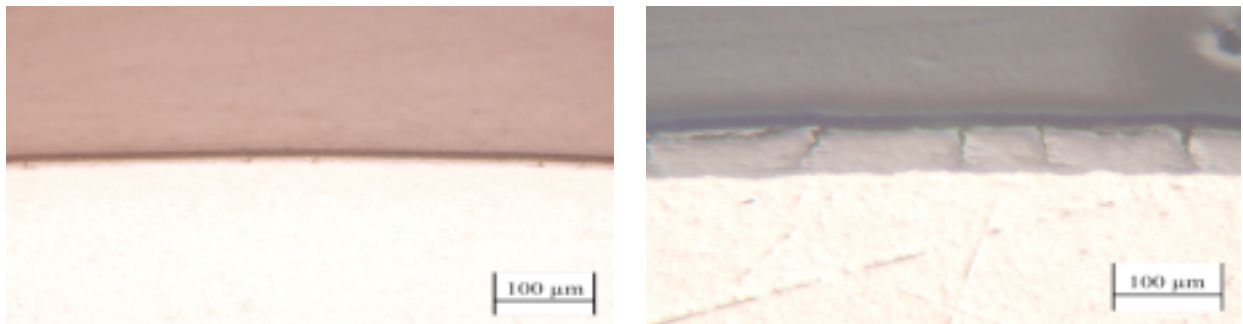


Figure 3.35. Microphotographs of oxide developed on Zircaloy-4 specimens tested with internal pressure of (left) 400 and (right) 200 psig at 700°C.

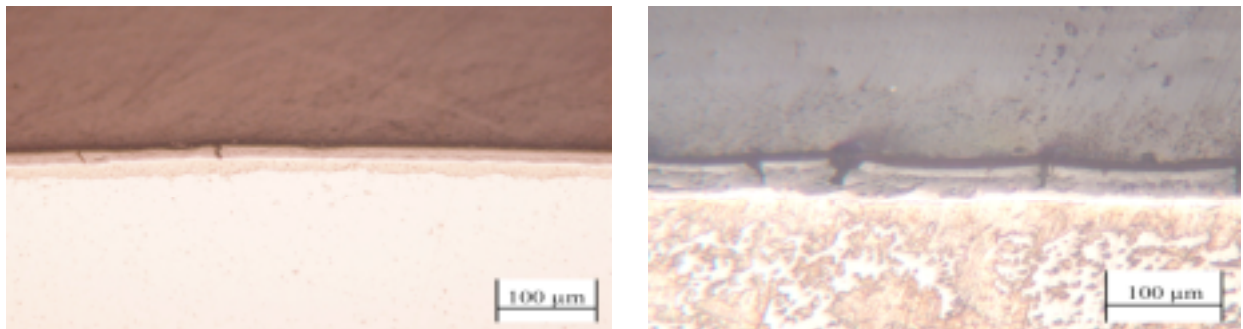


Figure 3.36. Microphotographs of oxide developed on Zircaloy-4 specimens tested with internal pressure of (left) 175 and (right) 100 psig at 800°C.

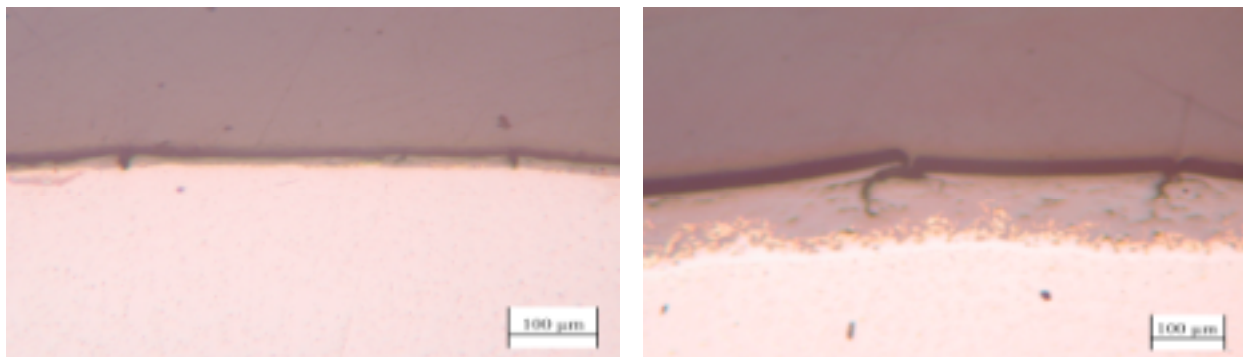


Figure 3.37. Microphotographs of oxide developed on Zircaloy-4 specimens tested with internal pressure of (left) 100 and (right) 50 psig at 900°C.

oxidation is deformation in the ballooning region, which resulted in significant microcracking in the oxide scale and led to additional paths for the air to reach the virgin metal for further oxidation. Figures 3.38-3.40 show the SEM photomicrographs of oxide scale morphology and thickness in the failure region and far away from that region, for tests conducted at several temperatures and pressures. Figures 3.41 and 3.42 show the SEM photomicrographs of the failure region on the surface of the tube and in cross section for the tests conducted at 600°C, 400 and 200 psig internal pressure. Circles in Figure 3.41 indicate the failure locations, whereas Figure 3.42 shows complete oxidation of the cladding tube and oxide separation at the failure location. Similar photomicrographs are shown in Figures 3.43-3.48 for specimens tested at 700, 800, and 900°C at various internal pressures.

Figures 3.49-3.52 show the variation in pressure and temperature for air oxidation tests conducted with internally pressurized steam-preoxidized Zircaloy-4 specimens at nominal temperatures of 600, 700, 800, and 900°C, respectively. Data in Figure 3.49 for specimen Z4T-8, tested at 600°C with internal pressures of 400 psig, indicate that the pressure initially increases from 400 to 490 psig within a short time and starts to decrease until the specimen exhibits ballooning and pin-hole failure after 43 h. The temperature of the specimen was maintained at 600°C through the entire exposure. Data for specimen Z4T-14, conducted at 200 psig, shows a pressure increase to 240 psig during the initial period, which gradually decreases to below 200 psig prior to pin-hole failure. Similar information is presented in Figures 3.50-3.52 for tests conducted at 700, 800, and 900°C, respectively.

Oxide thickness was measured on the specimens tested at various conditions, and the results are compared with air oxidation data developed on steam-preoxidized specimens with initial pressure of 14.7 psia at 600-900°C. Table 3.4 lists the calculated initial oxide thickness (after steam preoxidation, based on weight change measurements) and final measured oxide thickness after air oxidation tests. Figure 3.53 shows the oxide thickness data for specimens tested with and without internal pressure at 600 and 700°C. The data indicate that the oxide thickness is somewhat larger in the tests conducted with high internal pressure than that obtained in the absence of it. The increase is attributed to microcracks in the oxide (and associated oxidation) that results from increased deformation in the specimen due to pressurization. The oxidation times (before failure) were too small at 800 and 900°C to make a valid comparison of the oxidation rates to evaluate the effect of internal pressure.

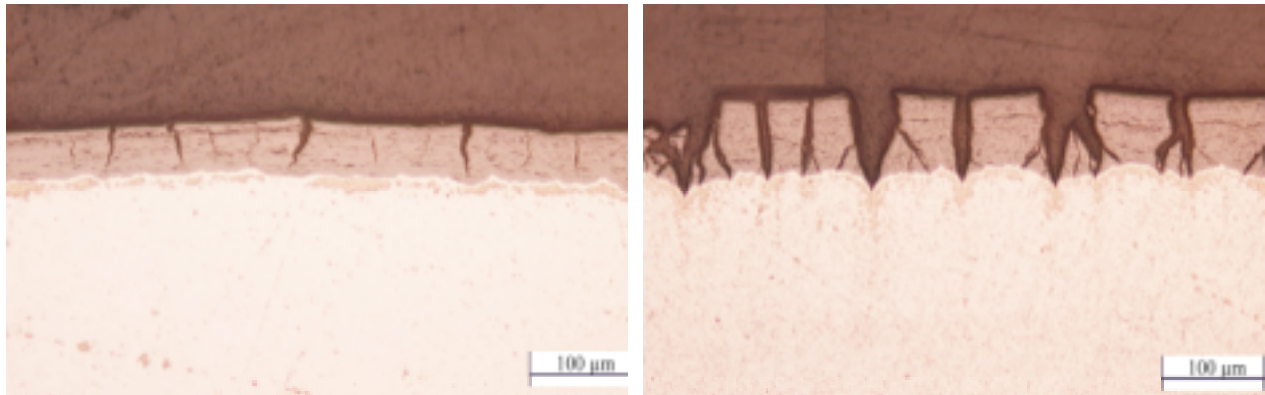


Figure 3.38. SEM photomicrographs of the cross sections of a steam-preoxidized Zircaloy-4 specimen with an internal pressure of 400 psi, after 43-h oxidation in air at 600°C. Left: far away from rupture area; right: in the failure area, 180° (opposite side) from the failure.

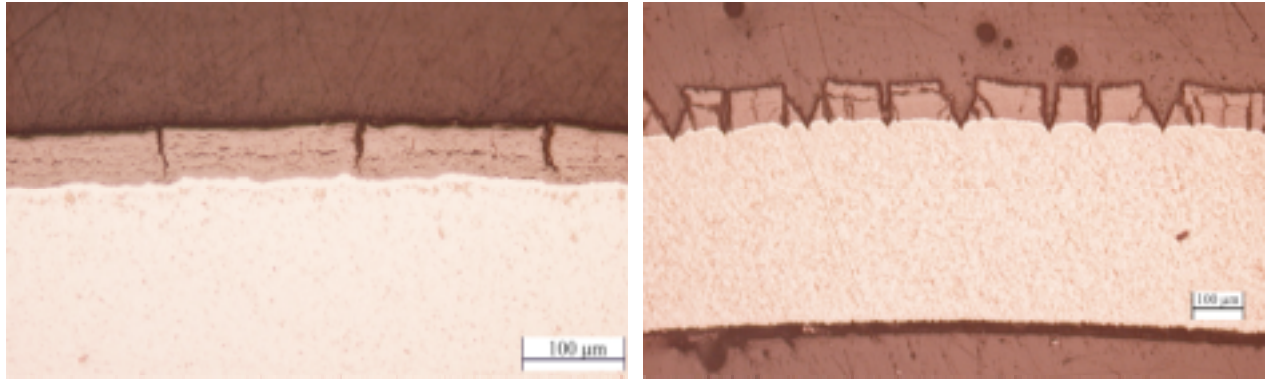


Figure 3.39. SEM photomicrographs of the cross sections of a steam-preoxidized Zircaloy-4 specimen with an internal pressure of 200 psi, after 5.9-h oxidation in air at 700°C. Left: far away from failure area; right: in the rupture area, 180° (opposite side) from the failure.

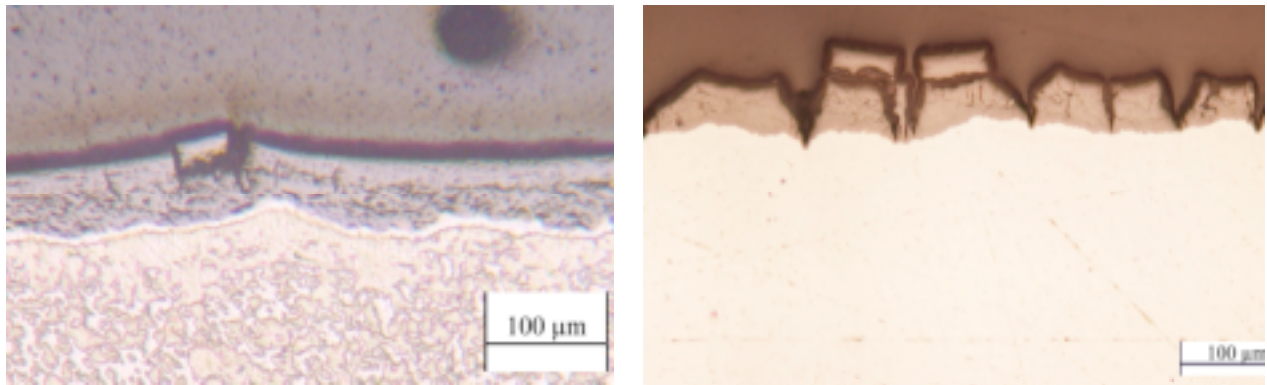


Figure 3.40. SEM photomicrographs of the cross sections of a steam-preoxidized Zircaloy-4 specimen with an internal pressure of 100 psi, after 1.18-h oxidation in air at 800°C. Left: far away from failure area; right: in the rupture area, 180° (opposite side) from the failure.

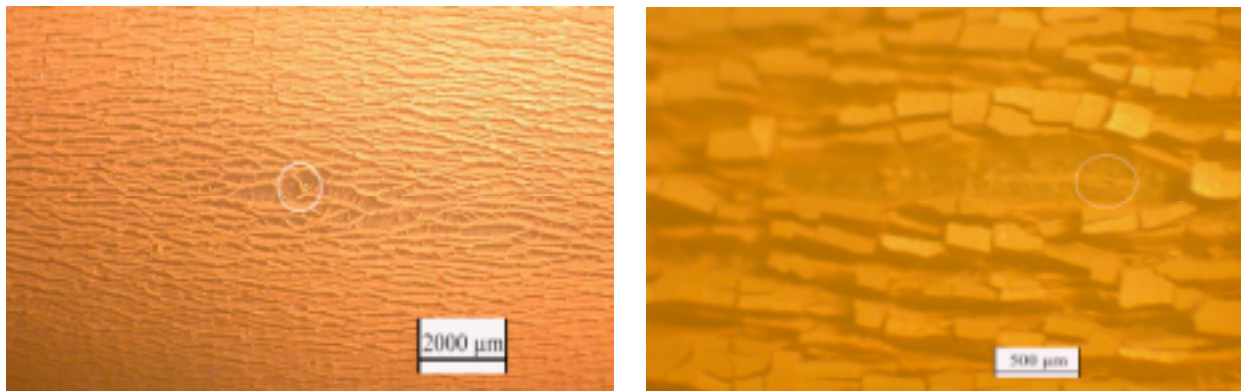


Figure 3.41. Microphotographs indicating failure region in Zircaloy-4 specimens tested with internal pressure of (left) 400 and (right) 200 psig at 600°C.

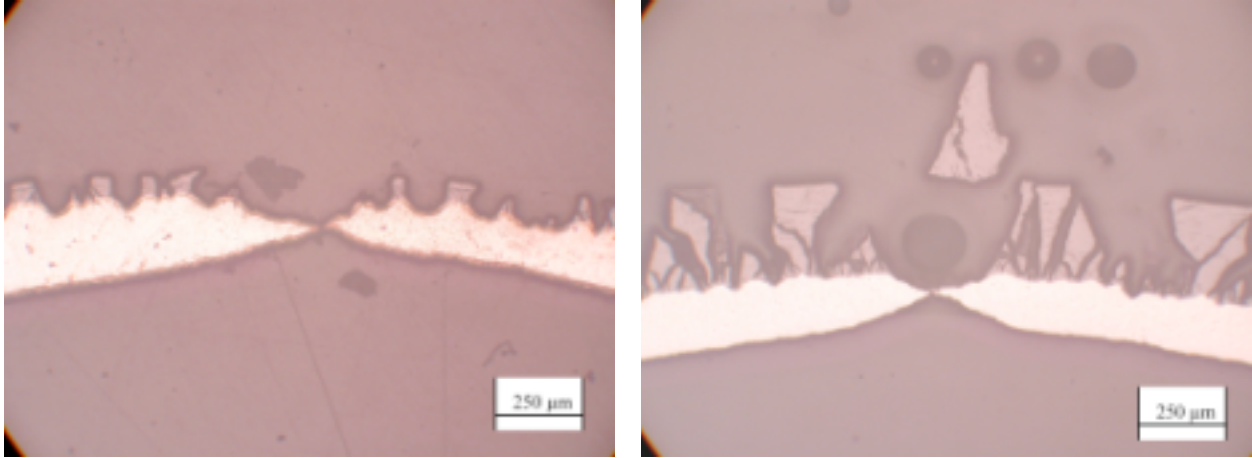


Figure 3.42. Microphotographs indicating oxide fracture leading to failure in Zircaloy-4 specimens tested with internal pressure of (left) 400 and (right) 200 psig at 600°C.

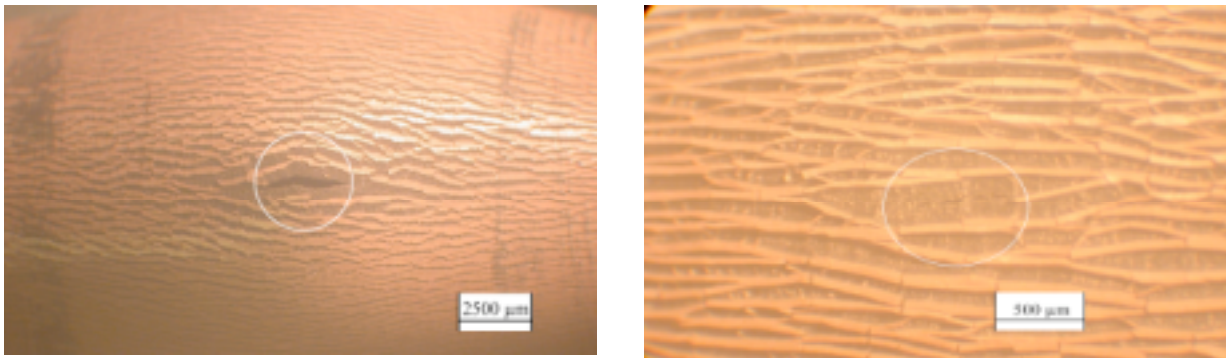


Figure 3.43. Microphotographs indicating failure region in Zircaloy-4 specimens tested with internal pressure of (left) 400 and (right) 200 psig at 700°C.

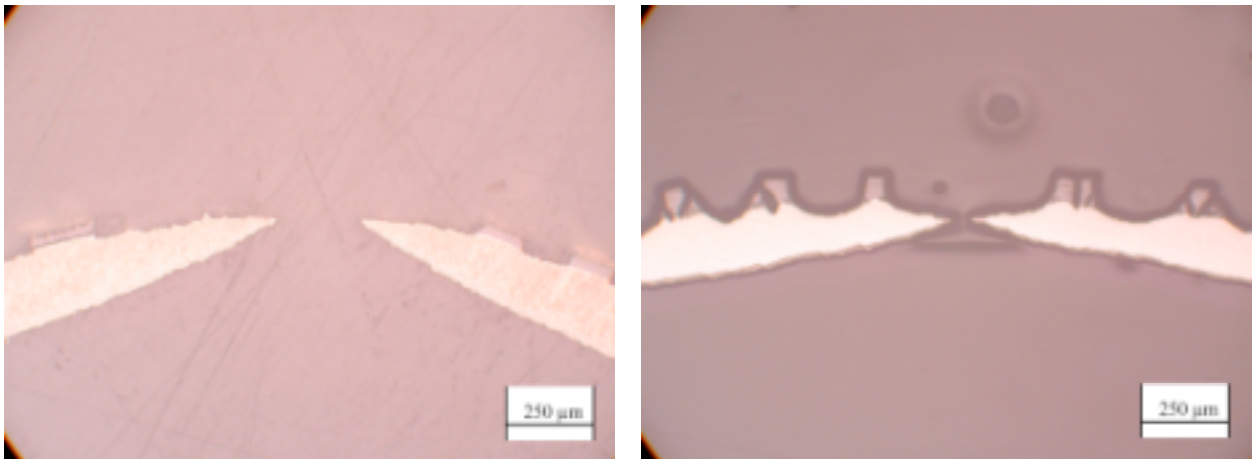


Figure 3.44. Microphotographs indicating oxide fracture leading to failure in Zircaloy-4 specimens tested with internal pressure of (left) 400 and (right) 200 psig at 700°C.

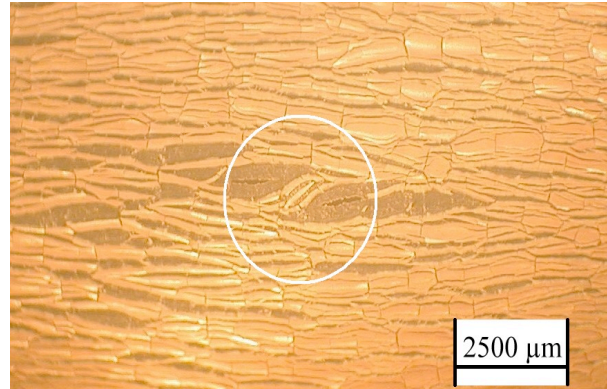


Figure 3.45. Microphotographs indicating failure region in Zircaloy-4 specimens tested with internal pressure of (left) 175 and (right) 100 psig at 800°C.

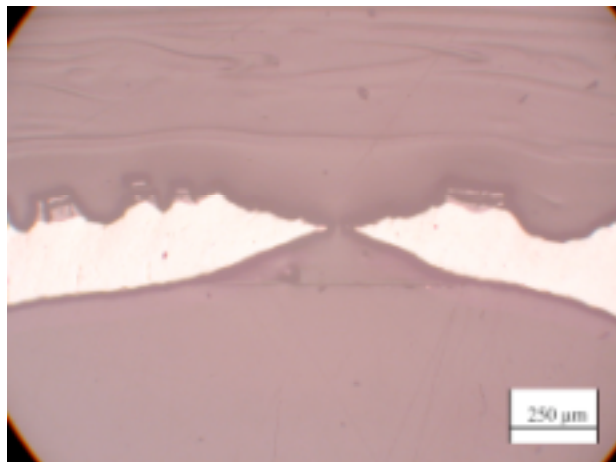
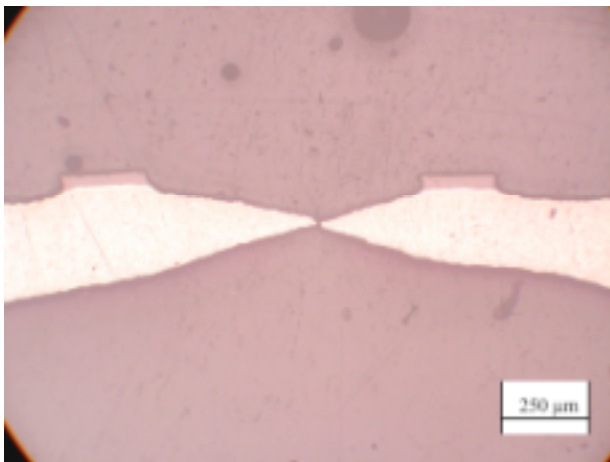


Figure 3.46. Microphotographs indicating oxide fracture leading to failure in Zircaloy-4 specimens tested with internal pressure of (left) 175 and (right) 100 psig at 800°C.

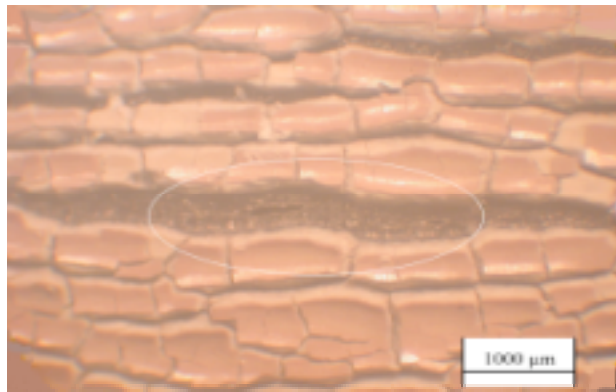


Figure 3.47. Microphotographs indicating failure region in Zircaloy-4 specimens tested with internal pressure of (left) 100 and (right) 50 psig at 900°C.

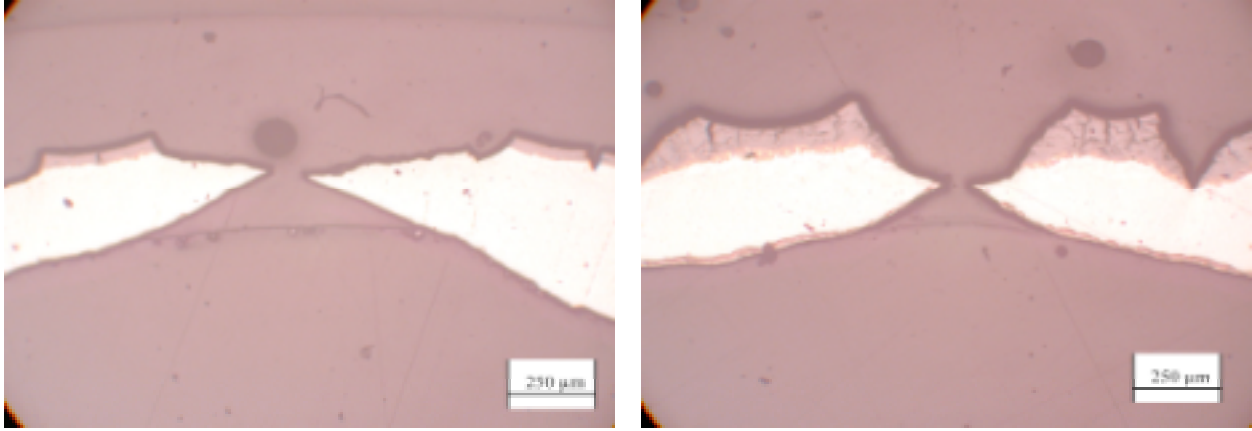


Figure 3.48. Microphotographs indicating oxide fracture leading to failure in Zircaloy-4 specimens tested with internal pressure of (left) 100 and (right) 50 psig at 900°C.

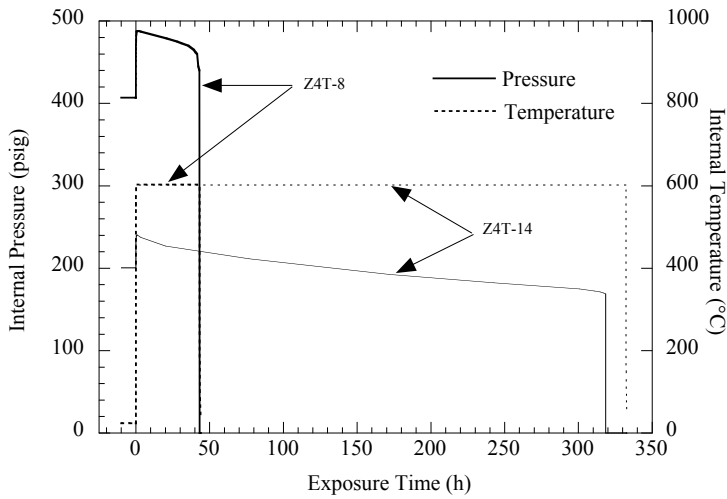


Figure 3.49. Variation in pressure and temperature for air oxidation tests conducted at 600°C on steam-preoxidized Zircaloy-4 with initial internal pressures of 400 and 200 psig.

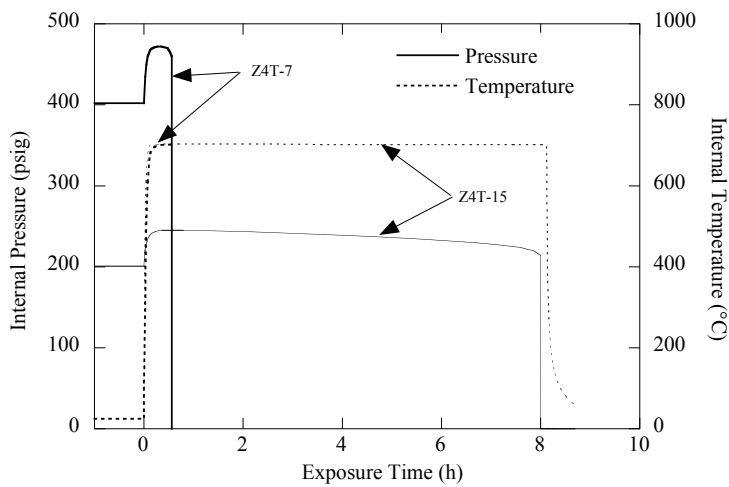


Figure 3.50. Variation in pressure and temperature for air oxidation tests conducted at 700°C on steam-preoxidized Zircaloy-4 with initial internal pressures of 400 and 200 psig.

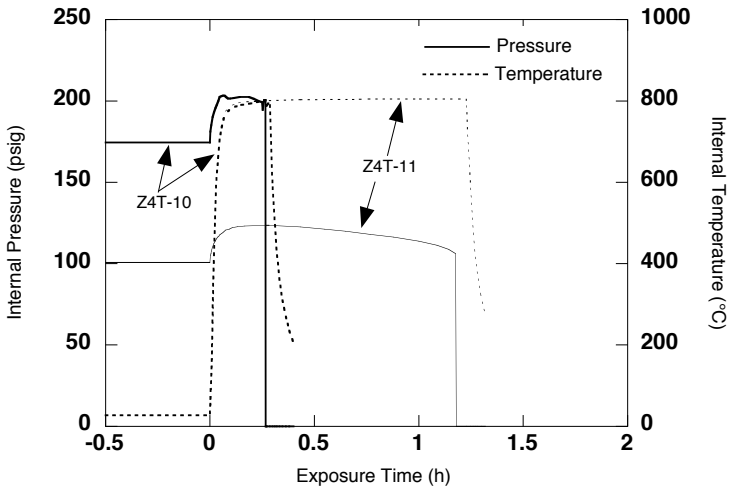


Figure 3.51. Variation in pressure and temperature for air oxidation tests conducted at 800°C on steam-preoxidized Zircaloy-4 with initial internal pressures of 175 and 100 psig.

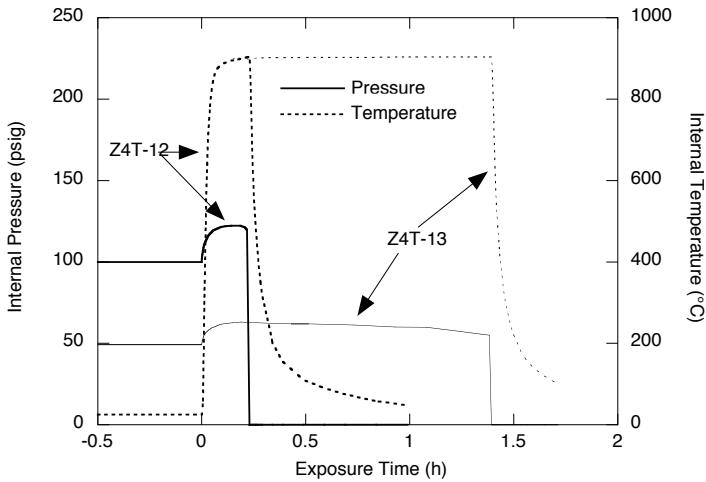


Figure 3.52. Variation in pressure and temperature for air oxidation tests conducted at 900°C on steam-preoxidized Zircaloy-4 with initial internal pressures of 100 and 50 psig.

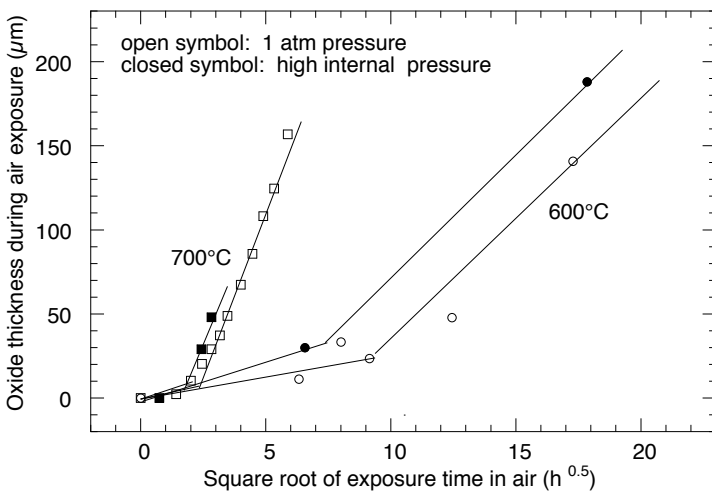


Figure 3.53. Oxide thickness data obtained for steam-preoxidized Zircaloy-4 specimens that were air oxidized with and without internal pressure at 600 and 700°C. The values for 700°C/1-atm condition were calculated from weight change data, whereas values for other conditions were obtained by metallography.

Table 3.3. Air oxidation test data on steam-preoxidized Zircaloy-4 with internal pressure

Specimen #	Air exposure temperature (°C)	Internal test pressure at RT, Po (psig)	Maximum pressure at temperature, Pmax (psig)	Rupture pressure at temperature, Pr (psig)	Time to rupture (h)	Internal volume change (%)	Exposed length change (%)	Pr/Pmax	Pmax/Po	Pr/Po
Z4T-6 ¹	600	400	465	-	-	-	-	-	-	-
Z4T-8 ²	600	400	488	440	43.0	56.5	0.67	0.90	1.22	1.10
Z4T-14	600	200	240	169	318.5	69.2	5.32	0.70	1.20	0.84
Z4T-7 ²	700	400	472	460	0.56	26.8	0.36	0.98	1.18	1.15
Z4T-9 ³	700	200	233	200	5.90	71.1	4.01	0.86	1.17	1.00
Z4T-15	700	200	245	214	7.99	84.1	0.80	0.87	1.23	1.07
Z4T-10 ²	800	175	203	200	0.27	52.8	0.89	0.99	1.16	1.14
Z4T-11 ⁴	800	100	123	106	1.18	139.2	2.79	0.86	1.23	1.06
Z4T-12	900	100	122	120	0.22	35.6	0.72	0.98	1.22	1.20
Z4T-13	900	50	63	55	1.38	83.9	9.26	0.87	1.26	1.10

¹The specimen tube leaked at the fitting, no rupture, test terminated.

²The specimen ruptured at the center of tube.

³The specimen ruptured at the center of tube; since the fitting leaked at the start of the test at high temperature, the specimen assembly was cooled and retightened, and the test was continued.

⁴The specimen tube ruptured near the plug end of the tube.

Table 3.4. Oxide thickness data developed during air oxidation of steam-preoxidized Zircaloy-4 with internal pressure

Specimen #	Air exposure temperature (°C)	Internal test pressure at RT, Po (psig)	Oxide thickness (μm)		Description of failure
			Calculated initial OD	Measured final OD	
Z4T-6 ¹	600	400	18	81	Bad test - no rupture, tube gradually leaked at fitting to 0 psig @78 h
Z4T-8	600	400	19	49	Pin hole leak failure at center of tube
Z4T-14	600	200	18	206	Pin hole leak failure at center of tube
Z4T-7	700	400	19	18	Pin hole leak failure at center of tube
Z4T-9 ²	700	200	20	49	Bad test - failure at center of tube, but fitting leaked and had to restart twice
Z4T-15	700	200	17	65	Pin hole leak failure at center of tube
Z4T-10	800	175	20	21	Pin hole leak failure at center of tube
Z4T-11	800	100	17	59	Pin hole leak failure off-center, towards plug end of tube
Z4T-12	900	100	18	24	Pin hole leak failure at center of tube
Z4T-13	900	50	19	96	Pin hole leak failure at center of tube

¹The specimen tube leaked at the fitting, no rupture, test terminated.

²Since the fitting leaked at the start of the test at high temperature, the specimen assembly was cooled, retightened, and the test was continued.

4 Results for Zirlo

4.1 Preoxidation in Steam

The Zirlo cladding in steam tests simulate an amount of cladding oxidation that is representative of medium fuel burnup. A thickness in the range of 25-30 μm was desired after steam oxidation. To establish the time and temperature conditions necessary to obtain such a thickness, we experimented with ring specimens of Zircaloy-4. In those tests, several 6.5-mm-long ring specimens of the Zircaloy-4 cladding specimens were exposed in a steam environment at temperatures of 400, 500, 550, and 600°C for different exposure periods. The specimens were retrieved at several exposure times, and weight changes were determined. In addition, the exposed rings were mounted and polished, and oxide thickness was determined by optical metallography. Based on the data developed on Zircaloy-4 specimens, steam exposure conditions of 550°C and 140 h were selected for the development of the needed preoxidation layer. We used the same conditions for the development of the preoxidation layer in Zirlo material.

Twenty-one Zirlo capsules were preoxidized in a steam environment to obtain $\approx 30\text{-}\mu\text{m}$ -thick oxide. Figure 4.1 shows the weight change data for several capsule specimens of Zirlo after steam oxidation for 140 h at 550°C. The weight change for the twenty-one Zirlo specimens ranged between 0.038 and 0.044 mg/mm^2 . A comparison of the results for Zirlo with those for Zircaloy-4 indicated that weight gain for Zirlo was $\approx 10\%$ less than that for Zircaloy-4 for the same exposure conditions in a steam environment. Figure 4.2 shows the calculated oxide thickness for various capsule specimens of Zirlo after steam oxidation for 140 h at 550°C. The oxide thickness for the twenty one Zirlo specimens ranged between 26.0 and 30.0 μm .

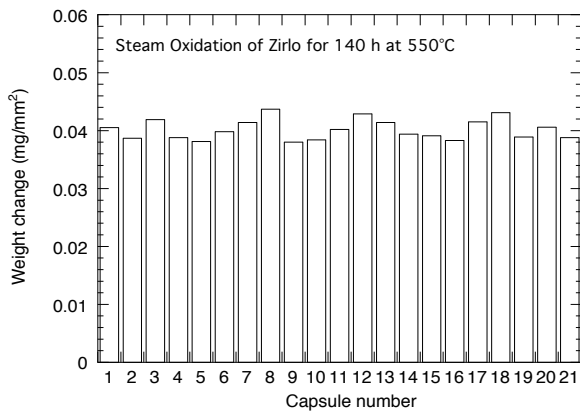


Figure 4.1. Weight change during steam oxidation of Zirlo capsule specimens for 140 h at 550°C.

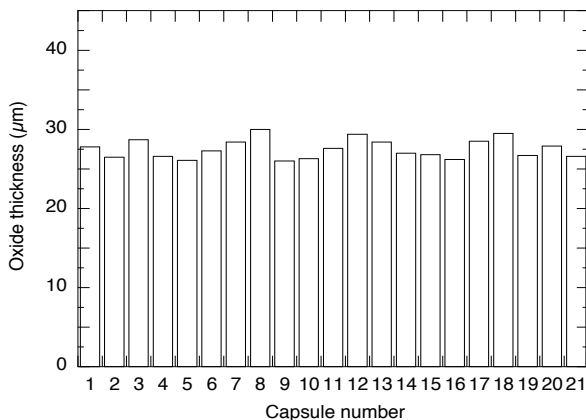


Figure 4.2. Calculated oxide thickness for Zirlo capsule specimens oxidized in steam for 140 h at 550°C.

4.2 Air Oxidation of Steam-Preoxidized Capsules

4.2.1 300-600°C

The steam-preoxidized Zirlo capsules were oxidized in air at 300, 400, 500, and 600°C for times shown in Table 2.7. The exposed specimens were sectioned and mounted for metallographic examination and oxide thickness measurements. Figure 4.3 shows the weight change data obtained during air oxidation of the steam-preoxidized Zirlo specimens. It is evident from Fig. 4.3 that the oxidation process exhibits a breakaway trend (see data for 500 and 600°C) even though the specimens were preoxidized in steam. The data obtained up to 1013 h at 300°C did not show a breakaway trend.

In general, the kinetics of oxidation of Zirlo specimens were derived from weight change data by plotting the weight change against square root of exposure time and fitting the data by two lines to depict before and after breakaway. The slopes of both fitted lines were used to develop rate constants for the oxidation process. A comparison of the data for Zirlo with those reported earlier for Zircaloy-4 showed that the post-breakaway rates are somewhat lower for Zirlo at $T \leq 500^\circ\text{C}$; however, the rate is higher for Zirlo than for Zircaloy-4 at 600°C. Table 4.1 lists the rates, calculated based on the weight change data, for oxidation in air for both Zircaloy-4 and Zirlo alloys that were initially in the steam-preoxidized condition.

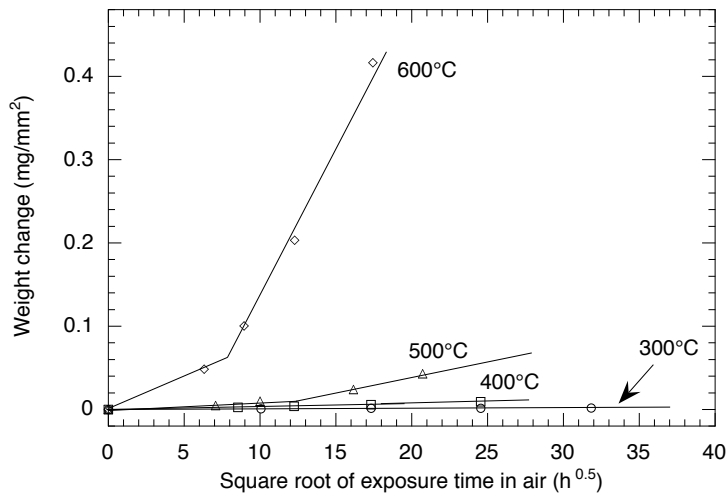


Figure 4.3. Weight change during air oxidation of steam-preoxidized Zirlo capsule specimens.

Table 4.1. Oxidation rates (based on weight change) in air for steam-preoxidized Zirlo and Zircaloy-4 specimens

Specimen Treatment	Pre or Post breakaway	Oxidation rate ($\text{kg}^2/\text{m}^4 \cdot \text{s}$) at temperature			
		600°C	500°C	400°C	300°C
Air oxidation of steam-preoxidized Zirlo ¹	Pre-breakaway	1.8×10^{-8}	1.1×10^{-10}	2.6×10^{-11}	1.4×10^{-12}
	Post-breakaway	1.9×10^{-7}	8.2×10^{-10}	4.6×10^{-11}	NB ²
Air oxidation of steam-preoxidized Zircaloy-4 ¹	Pre-breakaway	8.4×10^{-9}	2.8×10^{-10}	4.3×10^{-12}	5.7×10^{-12}
	Post-breakaway	7.2×10^{-8}	1.9×10^{-9}	6.4×10^{-11}	NB ²

¹Steam preoxidation condition: 140 h at 550°C; oxide thickness ≈ 30 and $27 \mu\text{m}$ for Zircaloy-4 and Zirlo, respectively.

²NB = No breakaway observed during the exposure times used in the present study.

Figures 4.4-4.7 show the SEM photomicrographs of cross sections of steam-preoxidized specimens after oxidation in air for different times at 600, 500, 400, and 300°C, respectively. Several conclusions were drawn from these photomicrographs:

- Though the initial oxide scale, developed by 140-h exposure in steam at 550°C, was adherent and crack free, the oxide tended to crack in air within 40 h (the shortest time of exposure in the present study) at 600°C.
- The thickness of the oxide developed during air exposure increased significantly with time, and the transverse cracks persisted over the entire thickness of the scale, as evidenced by the micrograph of the specimen exposed to air for times ≥ 80 h at 600°C. The radial cracks were connected by bridging cracks that were parallel to the alloy surface.
- The growth rate for oxide at 500°C in air was much less, and the scales exhibited radial cracks that traveled part way from the external surface, especially for exposure times of 261 and 429 h at 500°C.
- The oxidation rates in air for steam-preoxidized specimens were minimal to negligible at 400 and 300°C after exposure times of 602 and 1013 h, respectively.

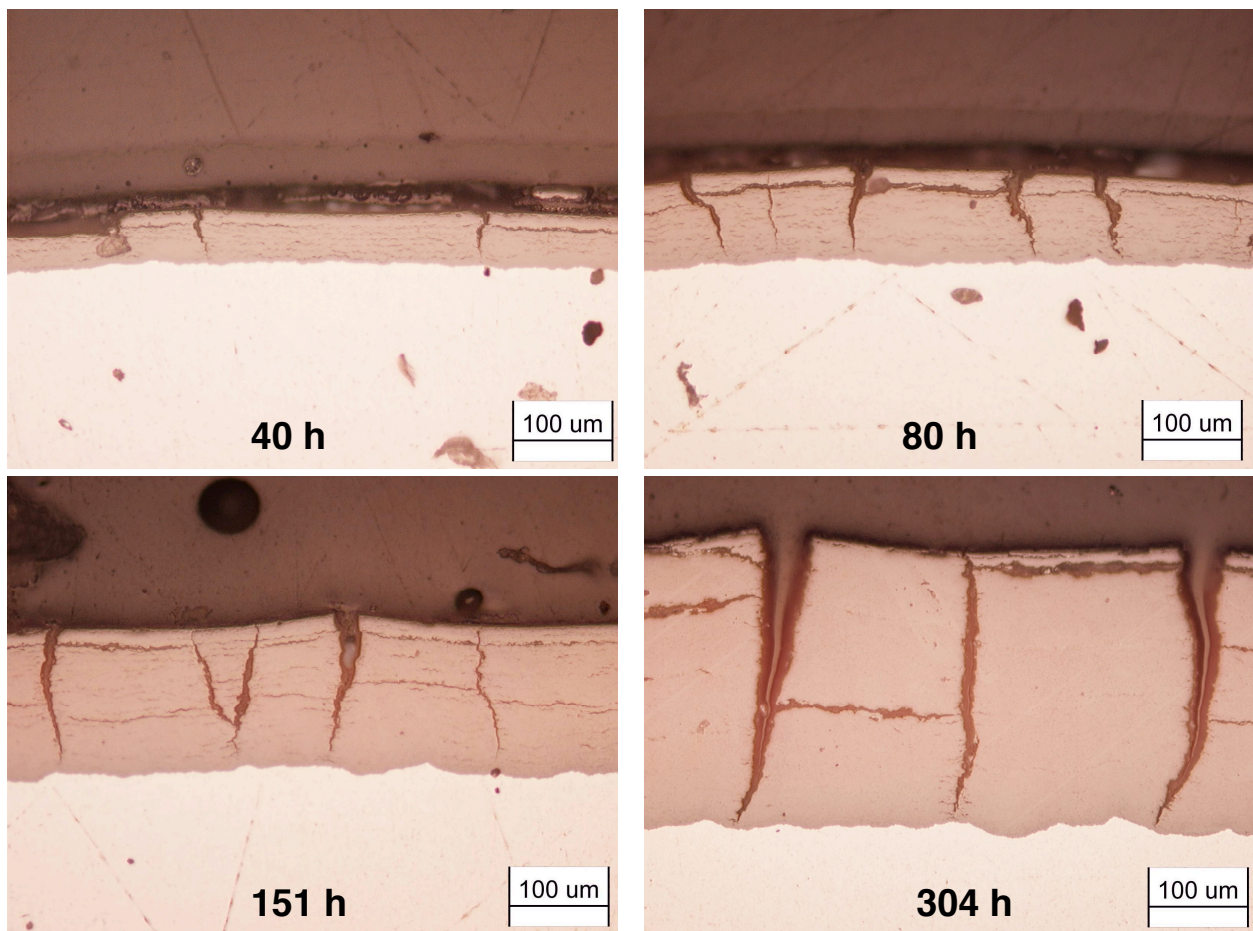


Figure 4.4. SEM photomicrographs of cross sections of steam-preoxidized Zirlo after oxidation in air for 40, 80, 151, and 304 h at 600°C.

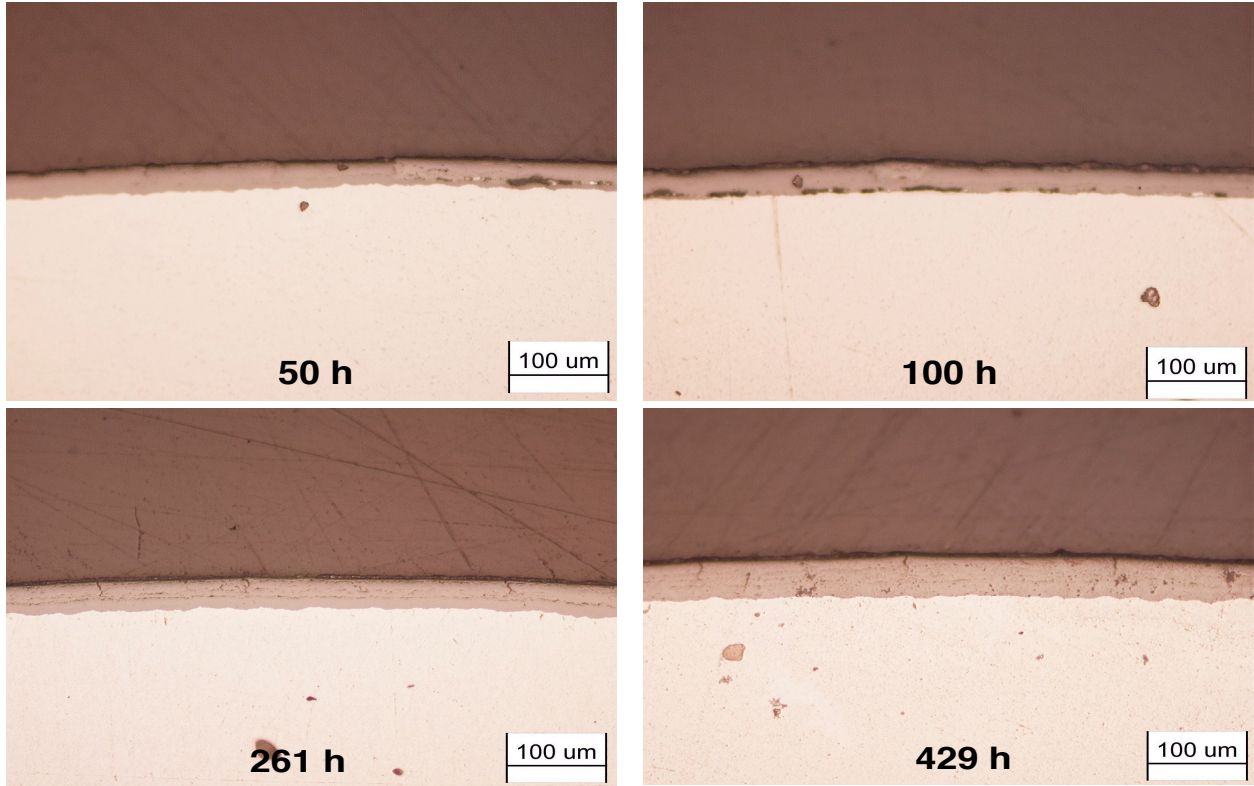


Figure 4.5. SEM photomicrographs of cross sections of steam-preoxidized Zirlo after oxidation in air for 50, 100, 261, and 429 h at 500°C.

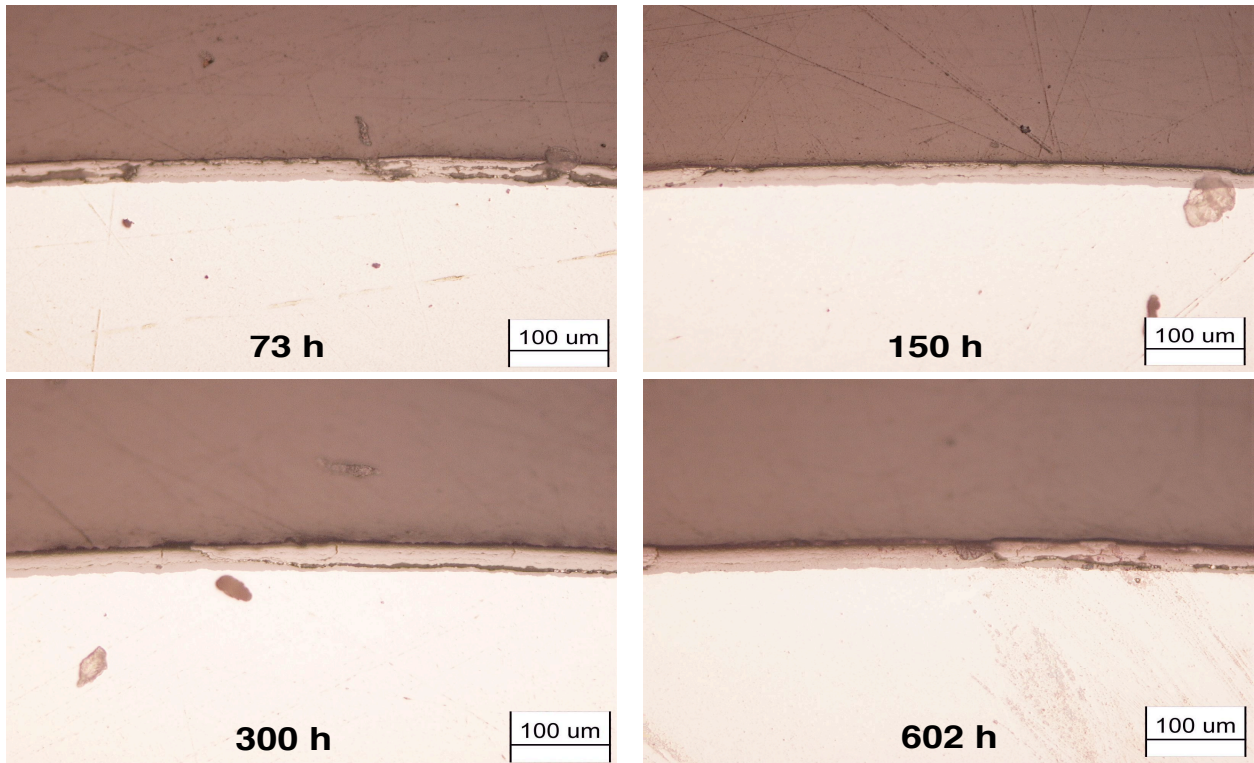


Figure 4.6. SEM photomicrographs of cross sections of steam-preoxidized Zirlo after oxidation in air for 73, 150, 300, and 602 h at 400°C.

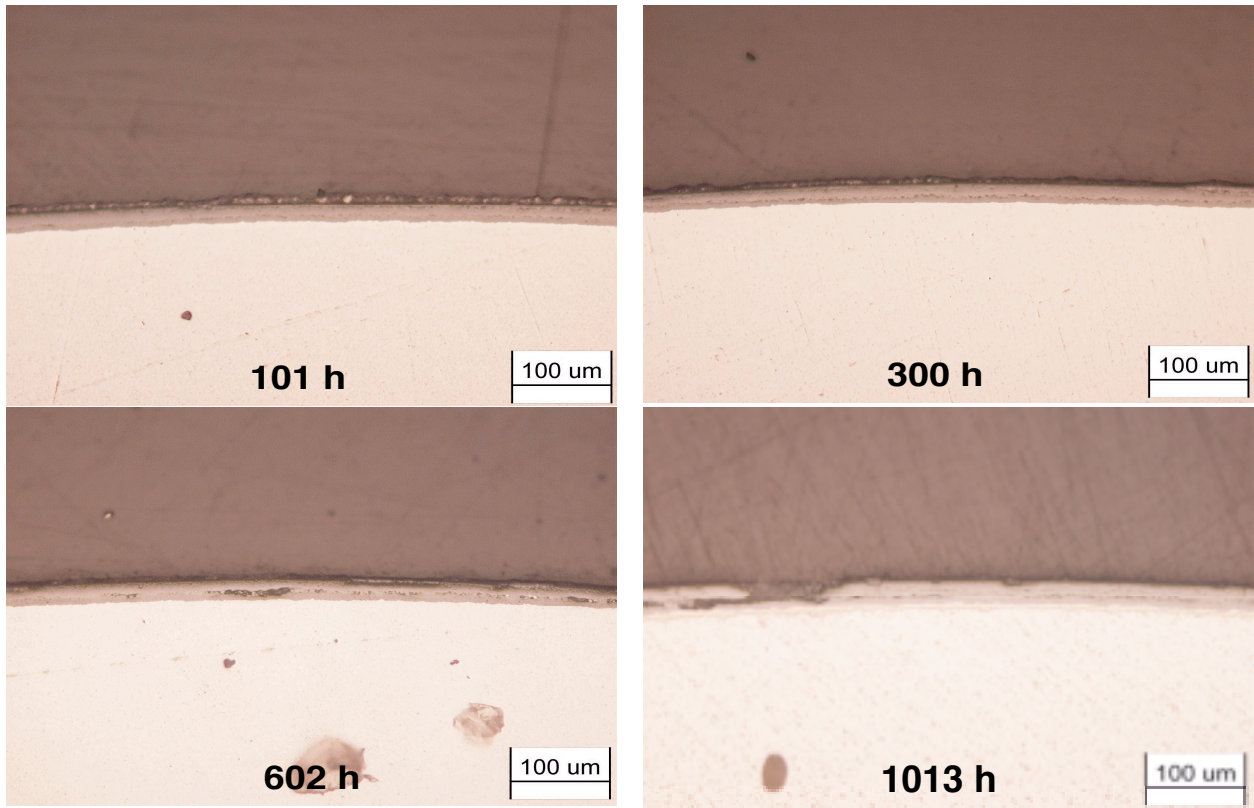


Figure 4.7. SEM photomicrographs of cross sections of steam-preoxidized Zirlo after oxidation in air for 101, 300, 602, and 1013 h at 300°C.

Figure 4.8 shows oxide thicknesses that were measured in the 75-mm-long capsules of steam-preoxidized Zirlo after various oxidation times in air at temperatures of 300, 400, 500, and 600°C. These thickness values are for the oxide that grew during air oxidation only and do not include the $\approx 30\text{-}\mu\text{m}$ -thick oxide that was developed during steam preoxidation. The thickness results showed good agreement with the data on weight change.

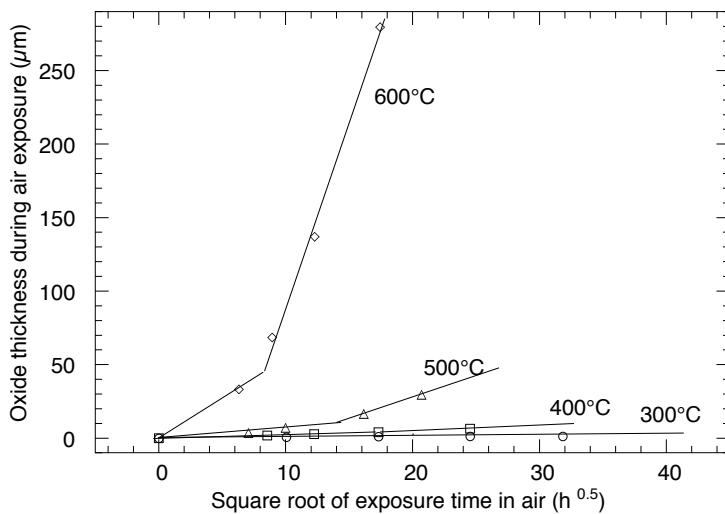


Figure 4.8. Oxide thickness for air oxidation of steam-preoxidized Zirlo capsule specimens at several temperatures.

4.2.2 700-900°C

Table 2.9 lists the exposure times used for evaluating the air oxidation characteristics of steam-preoxidized Zirlo at 700, 800, and 900°C. A single specimen was used at each temperature, and the weight change as a function of exposure time was obtained by periodic retrieval and weighing of the specimen. The exposures were terminated when the oxidation became substantial and/or when the specimen deformed significantly. Oxide thickness was measured on the specimens, if possible, after the final time of exposure at each temperature. Figure 4.9 shows the weight change data as a function of square root of time at the three temperatures.

Oxide thickness was calculated from the weight change data as a function of square root of time at the three exposure temperatures. Figure 4.10 shows a plot of the oxide thickness as a function of square root of time. The calculated oxide thickness after 34.5-h exposure in air at 700°C was 218.6 μm , and the total (in steam plus in air) calculated thickness was 249.3 μm . This compares with a measured value of 252.2 μm after 34.5-h exposure at 700°C. The calculated oxide thickness after 10-h exposure in air at 800°C was 428.6 μm , and the total (in steam plus in air) calculated thickness was 466.6 μm . This compares with a measured value of 397.0 μm after 10-h exposure at 800°C; the discrepancy between the measured and calculated values is primarily due to excessive spallation of the scale at 800°C. The calculated oxide thickness after 2.5-h exposure in air at 900°C was 358.8 μm , and the total (in steam plus in air) calculated thickness was 391.8 μm . This compares with a measured value of 372.0 μm for the total thickness after 2.5-h exposure at 900°C.

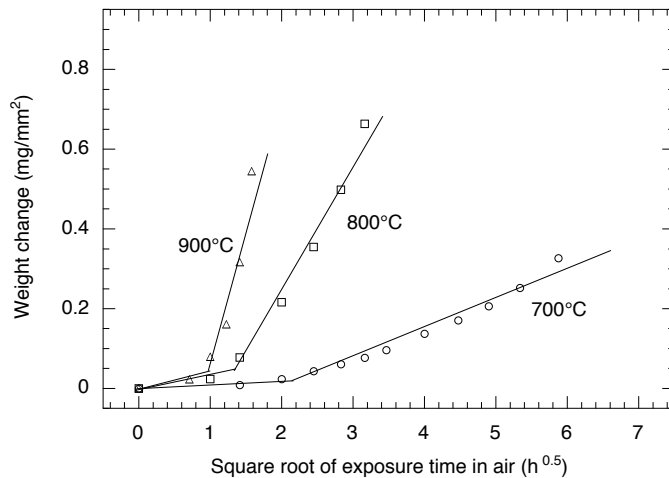


Figure 4.9. Weight change during air oxidation of steam-preoxidized Zirlo capsule specimens at 700, 800, and 900°C.

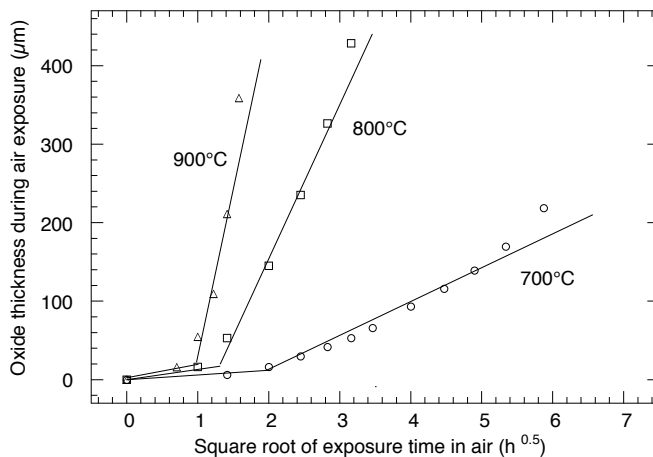


Figure 4.10. Oxide thickness calculated from the weight change data for air oxidation of steam-preoxidized Zirlo capsule specimens at 700, 800, and 900°C.

4.2.3 Oxygen Analysis

Several air-oxidized specimens of Zirlo were analyzed for oxygen and nitrogen concentrations. The oxygen values were compared with those calculated from the weight change data, assuming all of the weight change in the specimen is due to oxygen ingress. The sample is reacted with carbon by rapidly heating it to over 2700°C in a helium-purged graphite crucible. The evolved carbon monoxide is carried by helium to a copper oxide furnace, where carbon monoxide is converted to carbon dioxide. The concentration of carbon dioxide is measured by an infrared cell and reported in terms of oxygen concentration. The nitrogen gas that evolved on combustion is measured by a thermal conductivity detector.

Table 4.2 shows the oxygen concentration values that were calculated from the weight change data along with the analyzed values for Zirlo specimens air oxidized at 300-600°C. The specimens were analyzed three times. In general, agreement between the calculated and measured values was good for all the specimens tested, except when the oxide was thick and/or had a tendency to spall (e.g., specimens exposed for 429 h at 500°C and 151 and 304 h at 600°C).

Table 4.2. A comparison of the oxygen concentration values calculated from the weight change data with the measured values for steam-preoxidized Zirlo specimens after air oxidation

Air exposure temperature (°C)	Air exposure time (h)	Calculated oxygen content (wt.%)	Analyzed oxygen content (wt.%)	Analyzed nitrogen content (wt.%)
300	101.0	0.864	0.79, 0.80, 0.84	0.030, 0.038, 0.042
300	300.0	0.901	0.75, 0.81, 0.87	0.048, 0.054, 0.061
300	602.0	0.959	0.85, 0.90, 0.94	0.071, 0.079, 0.079
300	1013.0	0.837	0.72, 0.88, 0.96	0.095, 0.100, 0.120
400	73.0	0.864	0.83, 0.89, 1.04	0.11, 0.12, 0.14
400	150.0	0.929	0.68, 0.87, 0.89	0.085, 0.090, 0.091
400	300.0	1.021	0.97, 1.01, 1.04	0.093, 0.110, 0.100
400	602.0	1.061	0.86, 0.95, 1.20	0.098, 0.110, 0.091
500	50.0	0.925	0.69, 0.77, 0.85	0.082, 0.083, 0.093
500	100.0	1.032	0.58, 0.69, 0.73	0.078, 0.079, 0.089
500	261.0	1.322	0.71, 1.2, 1.3	0.090, 0.14, 0.15
500	429.0	1.769	1.0, 1.3, 1.4	0.12, 0.14, 0.15
600	40.0	1.923	1.5, 2.0, 2.1	0.20, 0.20, 0.21
600	80.0	2.904	2.6, 2.6, 2.7	0.26, 0.29, 0.30
600	151.0	4.958	3.3, 3.5, 3.7	0.28, 0.33, 0.38
600	304.0	8.892	3.0, 3.9, 3.9	0.47, 0.49, 0.53

4.3 Air Oxidation of Bare Alloy

4.3.1 300-600°C

Table 2.8 lists the exposure times used for evaluating the air oxidation characteristics of bare Zirlo at 300, 400, 500, and 600°C. A single specimen was used at each temperature, and weight-change data as a function of

exposure time were obtained by periodic retrieval and weighing of the specimen. Exposures were, in general, complementary to those conducted on air oxidation of steam-preoxidized specimens. Oxide thickness was measured on the specimens after the final time of exposure at each temperature. Figure 4.11 shows the weight change data as a function of square root of time at the four temperatures.

Oxide thickness was calculated from the weight change data as a function of time at the four exposure temperatures. Figure 4.12 shows oxide thickness as a function of square root of time. The calculated oxide thickness after 313-h exposure in air at 600°C was 228.0 μm. This compares with a measured value of 219.4 μm. The calculated oxide thickness was 20.4 μm and the measured value was 21.7 μm, after 412-h exposure in air at 500°C. The calculated values after 604 h at 400°C and 1036.8 h at 300°C were 2.5 and 1.0 μm, respectively. The specimens exposed at 300 and 400°C were not examined since the oxide thickness in them were negligibly small.

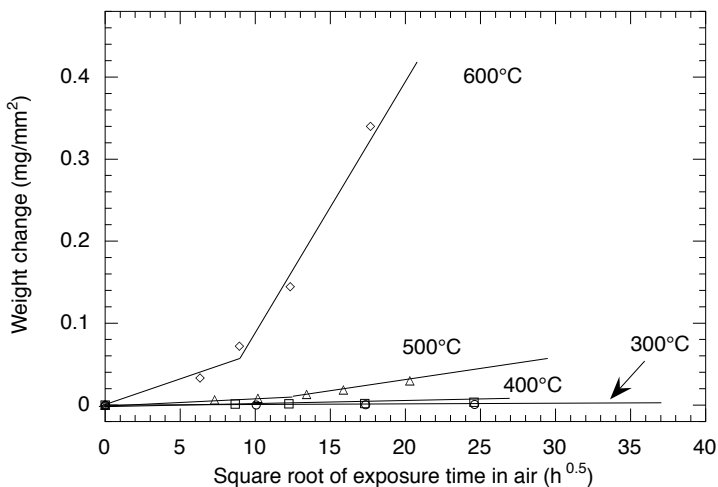


Figure 4.11. Weight change during oxidation of bare Zirlo capsule specimens at 300, 400, 500, and 600°C.

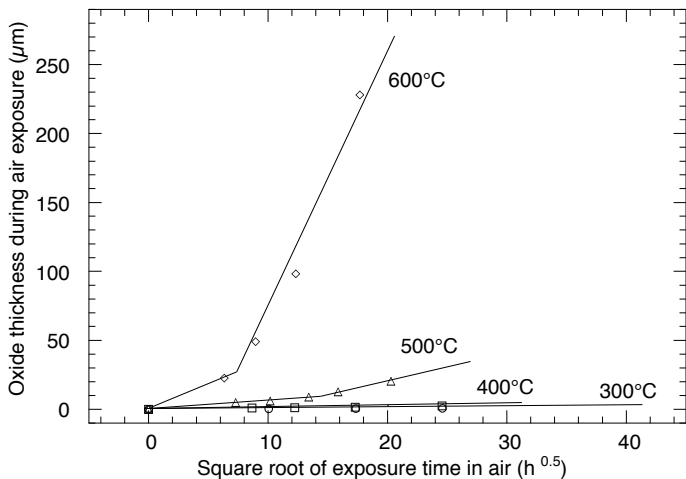


Figure 4.12. Oxide thickness calculated from the weight change data for air oxidation of bare Zirlo capsule specimens at 300, 400, 500, and 600°C.

4.3.2 700-900°C

Table 2.9 lists the exposure times used for evaluating the air oxidation characteristics of bare Zirlo at 700, 800, and 900°C. A single specimen was used at each temperature, and the weight change as a function of exposure time was obtained by periodic retrieval and weighing of the specimen. The exposures were terminated when the oxidation became substantial and/or when the specimen deformed significantly. Oxide thickness was measured on

the specimens, if possible, after the final time of exposure at each temperature. Figure 4.13 shows the weight change data as a function of square root of time at the three temperatures.

Oxide thickness was calculated from the weight change data as a function of time at the three exposure temperatures. Figure 4.14 shows a plot of the oxide thickness as a function of square root of time. The calculated oxide thickness after 34.5-h exposure in air at 700°C was 226.0 μm . This compares with a measured value of 237.0 μm . The calculated oxide thickness after 10-h exposure in air at 800°C was 390 μm . The specimen exposed at 800°C was not examined since it disintegrated into pieces when the exposure was continued to 14 h. The calculated oxide thickness after 2.5-h exposure in air at 900°C was 220.8 μm . Even though significant spallation of oxide was noted, an oxide thickness of 183.0 μm was measured.

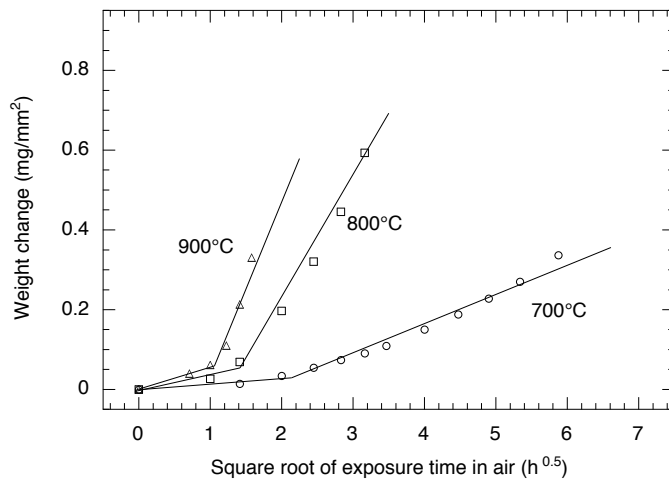


Figure 4.13. Weight change during oxidation of bare Zirlo capsule specimens at 700, 800, and 900°C.

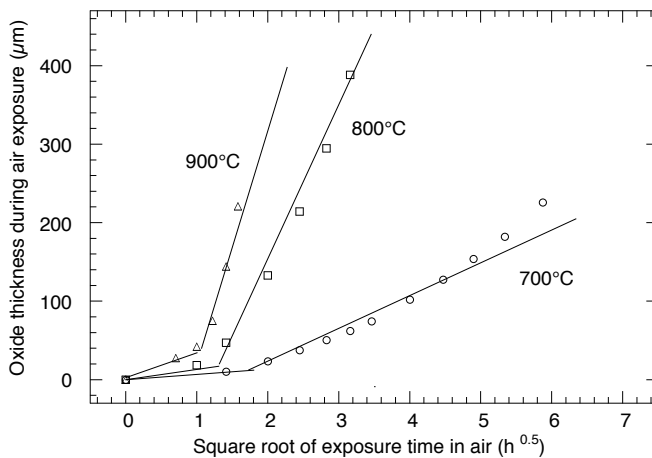


Figure 4.14. Oxide thickness calculated from the weight change data for air oxidation of bare Zirlo capsule specimens at 700, 800, and 900°C.

5 Results for M5

5.1 Preoxidation in Steam

The M5 cladding in steam tests simulate an amount of cladding oxidation that is representative of medium-to-high fuel burnup. An oxide thickness of $\approx 25 \mu\text{m}$ was desired after steam oxidation. To establish the time and temperature conditions necessary to obtain such a thickness, we experimented with ring specimens of M5. In those tests, several 6.5-mm-long ring specimens of the M5 cladding specimens were exposed in a steam environment at temperatures of 550°C for different exposure periods. The specimens were retrieved at several exposure times, and weight changes were determined. In addition, the exposed rings were mounted and polished, and oxide thickness was determined by optical metallography. Figure 5.1 shows the SEM photomicrographs of cross sections of ring specimens of M5 after exposure for various times at 550°C . Based on the data developed on M5 ring specimens, steam exposure conditions of 550°C and 427 h were selected for the development of the needed $\approx 25 \mu\text{m}$ preoxidation layer. Note that the exposure time selected for preoxidation of M5 is ≈ 3 times that used for Zircaloy-4 and Zirlo alloys.

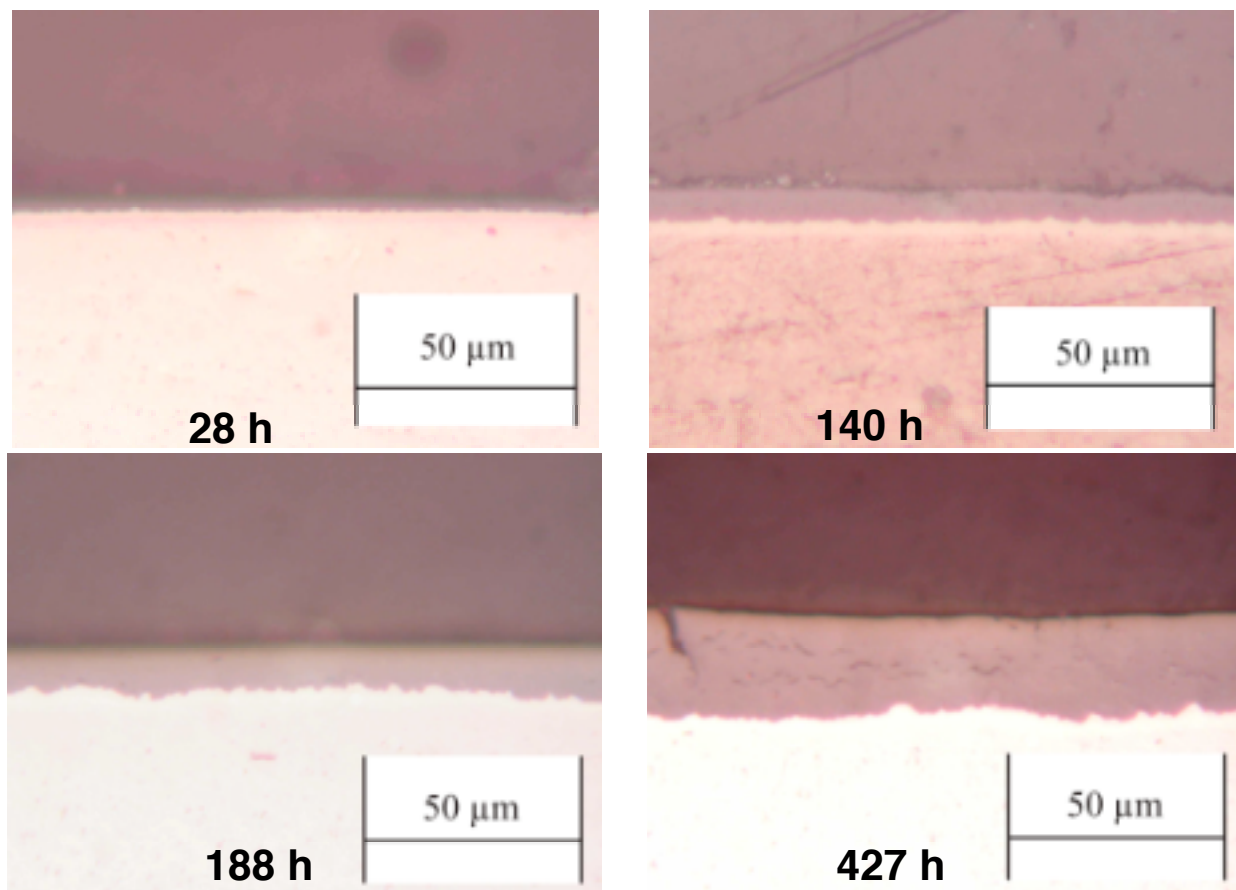


Figure 5.1. SEM photomicrographs of cross sections of M5 after oxidation in steam for 28, 140, 188, and 427 h at 550°C .

Nineteen M5 capsules were preoxidized in a steam environment to obtain $\approx 25\text{-}\mu\text{m}$ -thick oxide. Figure 5.2 shows the weight change data for several capsule specimens of M5 after steam oxidation for 427 h at 550°C . Since the end caps (made of Zircadyne 702) and the heat affected zones at the two ends of the capsule specimen oxidized much more than the M5 itself, it was necessary to correct the measured weight changes for the capsule specimen to

obtain the true oxidation rate for M5. Oxidation data correlating normalized weight gain versus exposure time at 550°C was obtained for Zircadyne 702 ring specimens and the information was used to make a correction to the M5 capsule weight change. The weight change for the nineteen M5 specimens ranged between 0.03 and 0.046 mg/mm². Figure 5.3 shows the calculated oxide thickness for various capsule specimens of M5 after steam oxidation for 427 h at 550°C. The oxide thickness for the nineteen M5 capsules ranged between 21.3 and 25.3 μm.

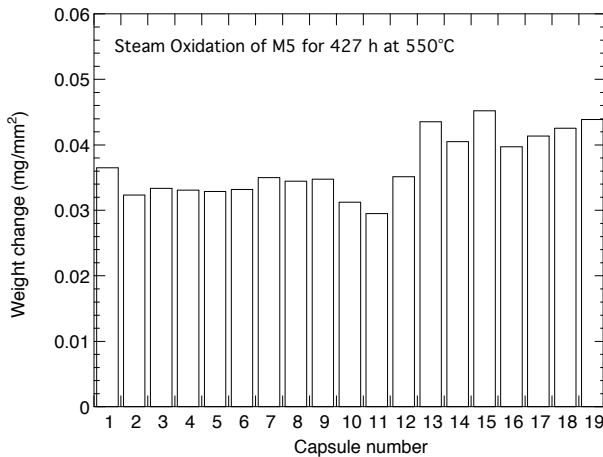


Figure 5.2. Weight change during steam oxidation of M5 capsule specimens for 427 h at 550°C.

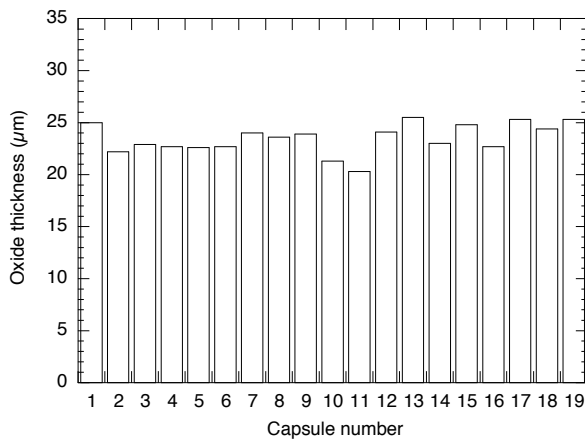


Figure 5.3. Calculated oxide thickness for M5 capsule specimens oxidized in steam for 427 h at 550°C.

5.2 Air Oxidation of Steam-Preoxidized Capsules

5.2.1 300-600°C

The steam-preoxidized M5 capsules were oxidized in air at 300, 400, 500, and 600°C for times shown in Table 2.10. The exposed capsules were sectioned and mounted for metallographic examination and oxide thickness measurements. Figure 5.4 shows the weight change data obtained during air oxidation of the steam-preoxidized M5 specimens. Air oxidation data was also generated for Zircadyne 702 at temperatures in the range of 300-900°C and this information was used to apply a correction to the observed weight change for the M5 specimens in air. Similar to Zircaloy-4 and Zirlo oxidation, M5 also exhibits a breakaway trend (see data for 500 and 600°C) even though the specimens were preoxidized in steam. The data obtained at 400 and 300°C did not show a breakaway trend for the duration of oxidation conducted in the present study.

In general, the kinetics of oxidation of M5 specimens were derived from weight change data by plotting the weight change against square root of exposure time and fitting the data by two lines to depict before and after

breakaway. The slopes of both fitted lines were used to develop rate constants for the oxidation process. A comparison of the data for M5 with those reported earlier for Zircaloy-4 and Zirlo showed that the post-breakaway rates are significantly lower for M5 at all temperatures studied; however. Table 5.1 lists the rates, calculated from the weight change data, for oxidation in air for all three alloys that were initially in the steam-preoxidized condition with nominally similar initial thickness of oxide. Results indicate that the oxidation rates for M5 in air are much lower than those for Zircaloy-4 and Zirlo at all temperatures in the range of 300-600°C. Furthermore, M5 did not exhibit breakaway trend at 400°C in the exposure times used in the present study while the other two alloys did show such a trend under similar exposure conditions.

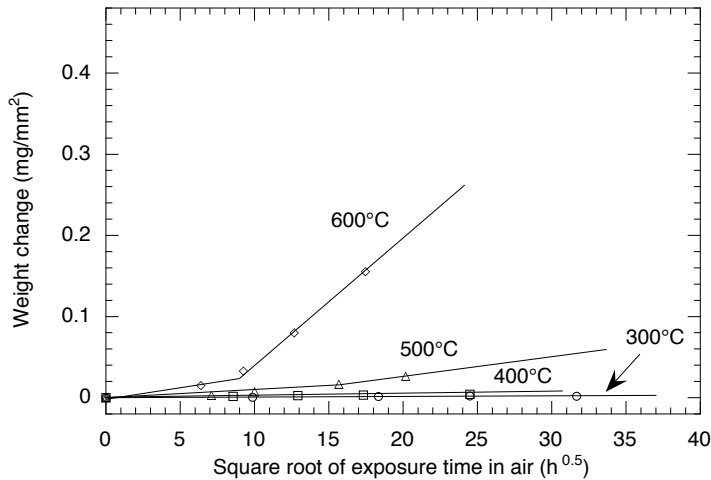


Figure 5.4. Weight change data during air oxidation of steam-preoxidized M5 capsule specimens

Table 5.1. Oxidation rates (based on weight change) in air for steam-preoxidized Zircaloy-4, Zirlo, and M5 specimens

Specimen Treatment	Pre- or Post-breakaway	Oxidation rate ($\text{kg}^2/\text{m}^4\cdot\text{s}$) at temperature			
		600°C	500°C	400°C	300°C
Air oxidation of steam-preoxidized Zircaloy-4 ¹	Pre-breakaway	8.4×10^{-9}	2.8×10^{-10}	4.3×10^{-12}	5.7×10^{-12}
	Post-breakaway	7.2×10^{-8}	1.9×10^{-9}	6.4×10^{-11}	NB ³
Air oxidation of steam-preoxidized Zirlo ¹	Pre-breakaway	1.8×10^{-8}	1.1×10^{-10}	2.6×10^{-11}	1.4×10^{-12}
	Post-breakaway	1.9×10^{-7}	8.2×10^{-10}	4.6×10^{-11}	NB ³
Air oxidation of steam-preoxidized M5 ²	Pre-breakaway	8.2×10^{-10}	1.3×10^{-10}	1.3×10^{-11}	5.4×10^{-13}
	Post-breakaway	3.4×10^{-8}	8.0×10^{-10}	NB ³	NB ³

¹Steam preoxidation condition for Zircaloy-4 and Zirlo: 140 h at 550°C; oxide thickness ≈ 30 and $27 \mu\text{m}$ for Zircaloy-4 and Zirlo, respectively.

²Steam preoxidation condition for M5: 427 h at 550°C; oxide thickness $\approx 25 \mu\text{m}$.

³Breakaway oxidation was not observed in the exposure times used in the present study.

Figures 5.5-5.8 show the SEM photomicrographs of cross sections of steam-preoxidized M5 specimens after oxidation in air for different times at 600, 500, 400, and 300°C, respectively. Several conclusions were drawn from these photomicrographs:

- Though the initial oxide scale, developed by 427-h exposure in steam at 550°C, was adherent and relatively free, the oxide tended to crack (both axially and radially, see Fig. 5.5) in air at 600°C.

- The thickness of the oxide developed during air exposure increased significantly with time, and the transverse cracks persisted over the entire thickness of the scale, as evidenced by the micrograph of the specimen exposed to air for 305 h at 600°C. However, the propagation of the transverse cracks seem to stop on the oxide side of the scale/metal interface..
- The growth rate for oxide at 500°C in air was much less, and the scales exhibited little cracking, if any.
- The oxidation rates in air for steam-preoxidized specimens were minimal to negligible at 400 and 300°C after exposure times of 600 and 1003 h, respectively.

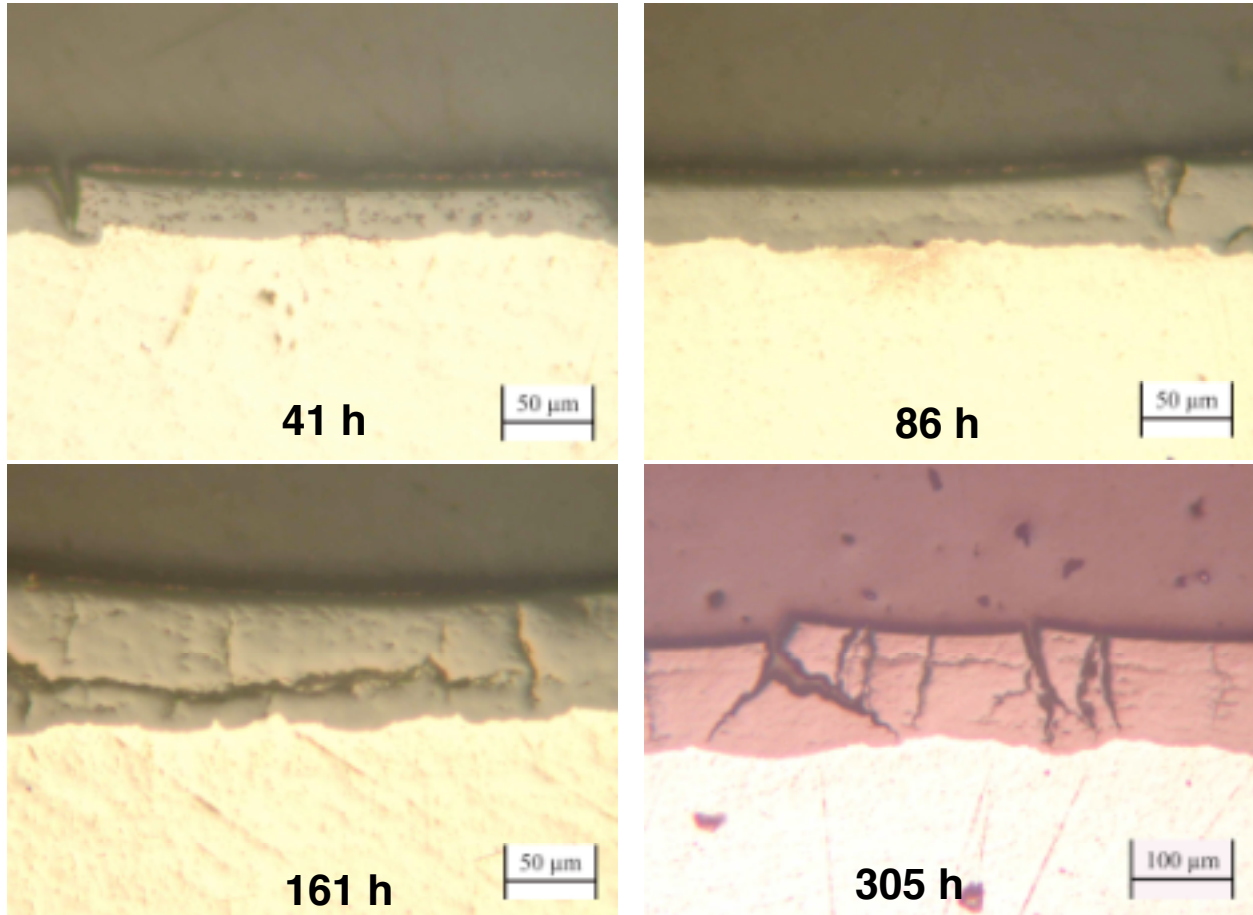


Figure 5.5. SEM photomicrographs of cross sections of steam-preoxidized M5 after oxidation in air for 41, 86, 161, and 305 h at 600°C.

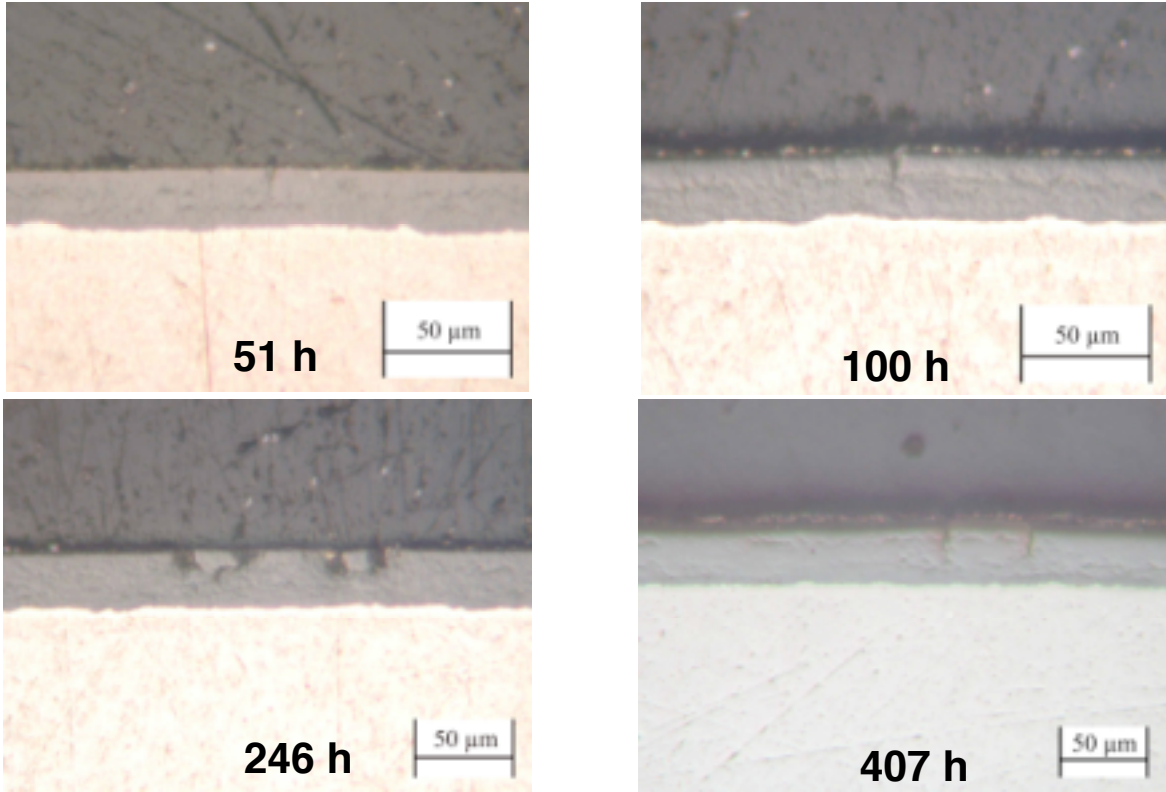


Figure 5.6. SEM photomicrographs of cross sections of steam-preoxidized M5 after oxidation in air for 51, 100, 246, and 407 h at 500°C.

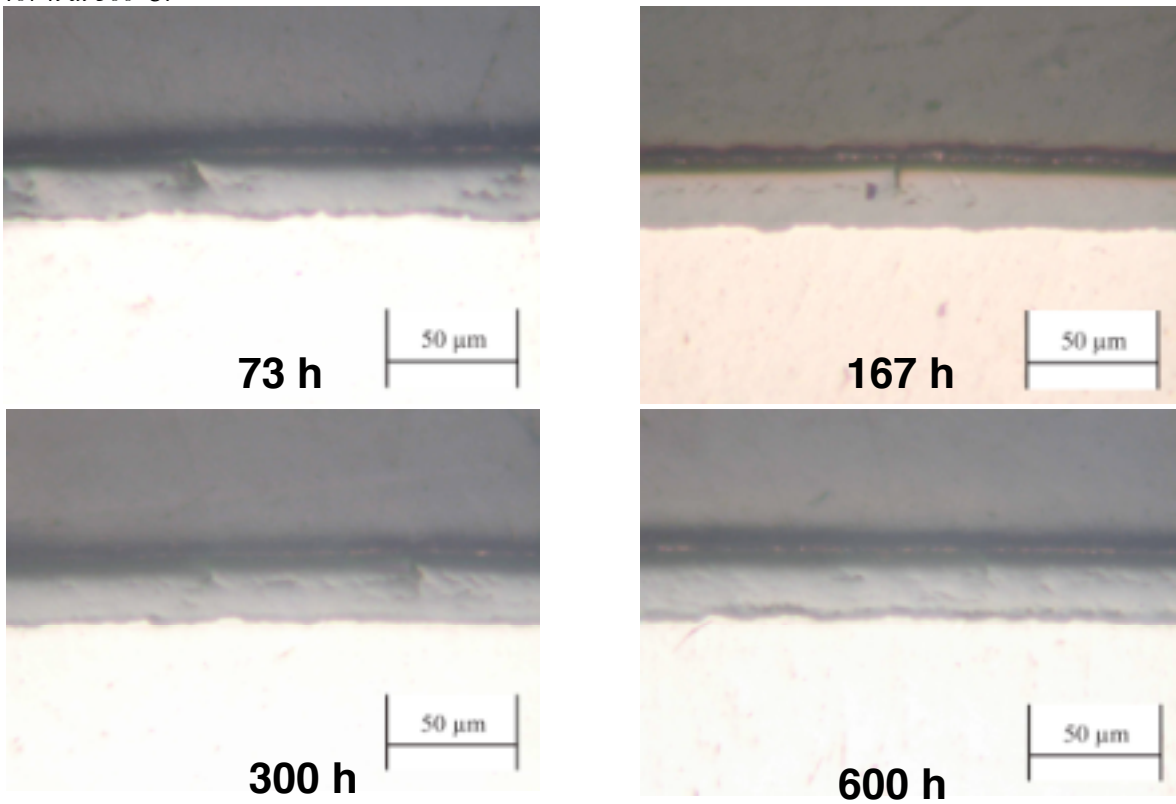


Figure 5.7. SEM photomicrographs of cross sections of steam-preoxidized M5 after oxidation in air for 73, 167, 300, and 600 h at 400°C.

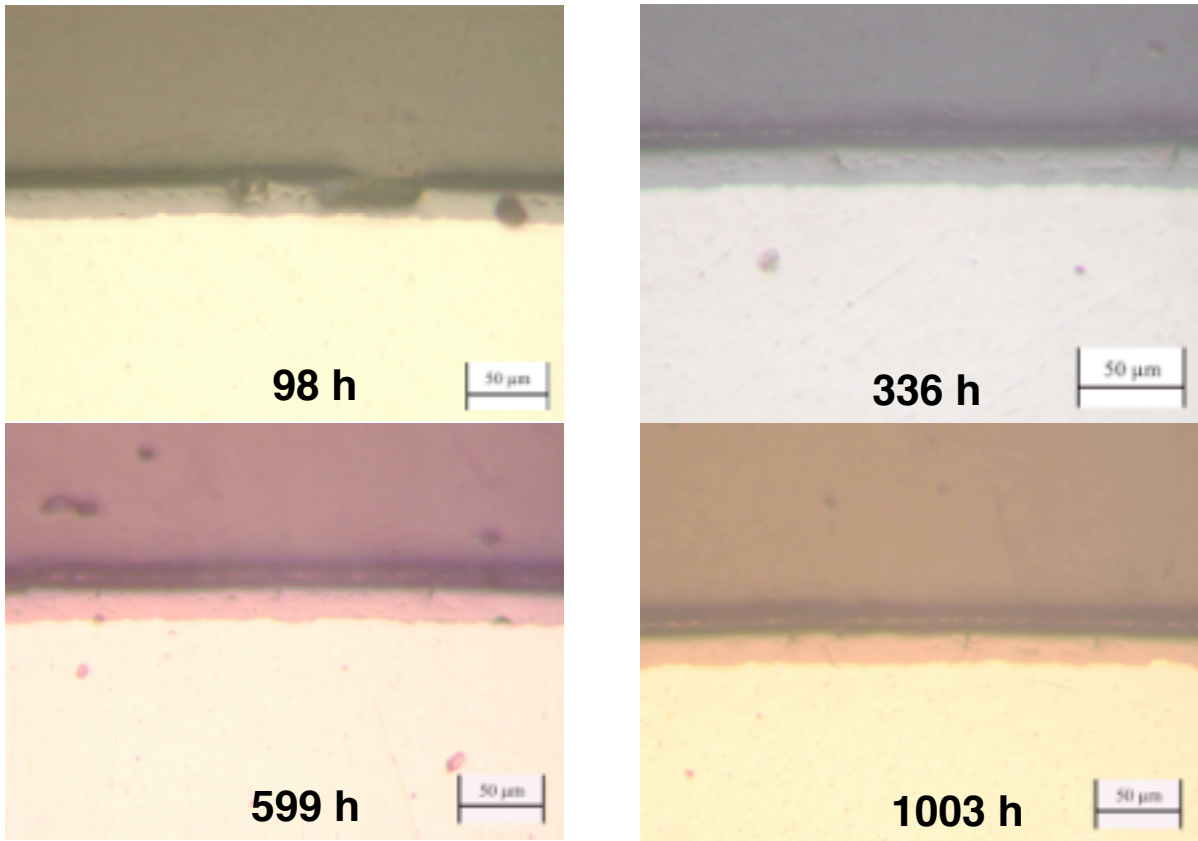


Figure 5.8. SEM photomicrographs of cross sections of steam-preoxidized M5 after oxidation in air for 98, 336, 599, and 1003 h at 300°C.

Figure 5.9 shows oxide thicknesses that were measured in the 75-mm-long capsules of steam-preoxidized M5 after various oxidation times in air at temperatures of 300, 400, 500, and 600°C. These thickness values are for the oxide that grew during air oxidation only and do not include the $\approx 25\text{-}\mu\text{m}$ -thick oxide that was developed during steam preoxidation. The thickness results showed good agreement with the corrected data on weight change.

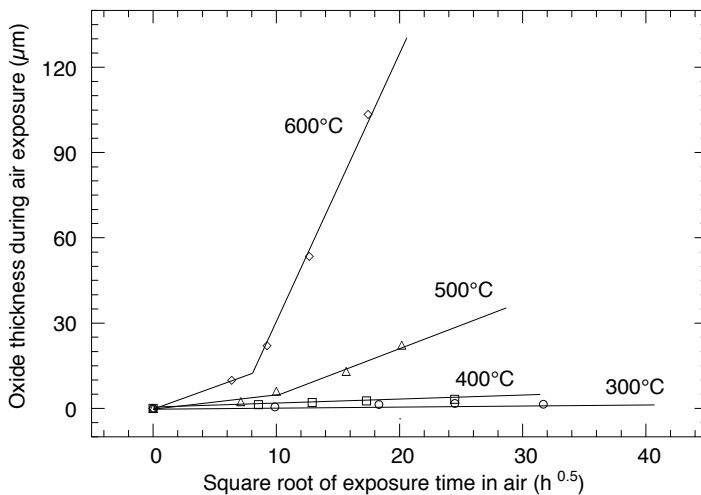


Figure 5.9. Oxide thickness for air oxidation of steam-preoxidized M5 capsule specimens at several temperatures.

5.2.2 700-900°C

Table 2.12 lists the exposure times used for evaluating the air oxidation characteristics of steam-preoxidized M5 at 700, 800, and 900°C. A single specimen was used at each temperature, and the weight change as a function of exposure time was obtained by periodic retrieval and weighing of the specimen. The exposures were terminated when the oxidation became substantial and/or when the specimen deformed significantly. Oxide thickness was measured on the specimens, if possible, after the final time of exposure at each temperature. Figure 5.10 shows the corrected weight change data as a function of square root of time at the three temperatures.

Oxide thickness was calculated from the corrected weight change data as a function of square root of time at the three exposure temperatures. Figure 5.11 shows a plot of the oxide thickness as a function of square root of time. The calculated oxide thickness after 46.2-h exposure in air at 700°C was 95.4 μm , and the total (in steam plus in air) calculated thickness was 120.7 μm . This compares with a measured value of 133.1 μm after 46.2-h exposure at 700°C. The calculated oxide thickness after 8.3-h exposure in air at 800°C was 166.9 μm , and the total (in steam plus in air) calculated thickness was 191.3 μm . This compares with a measured value of 152.1 μm after 8.6-h exposure at 800°C; the discrepancy between the measured and calculated values is primarily due to excessive spallation of the scale at 800°C. The calculated oxide thickness after 1.7-h exposure in air at 900°C was 156.7 μm , and the total (in steam plus in air) calculated thickness was 182.0 μm . This compares with a measured value of 170.8 μm for the total thickness after 1.7-h exposure at 900°C.

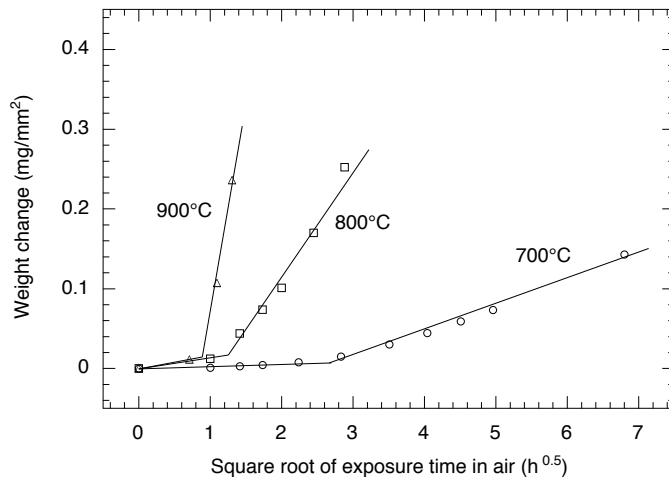


Figure 5.10. Weight change during air oxidation of steam-preoxidized M5 capsule specimens at 700, 800, and 900°C.

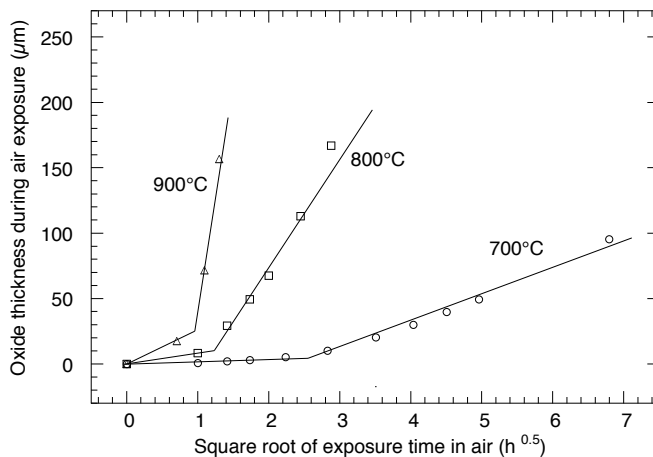


Figure 5.11. Oxide thickness calculated from the weight change data for air oxidation of steam-preoxidized M5 capsule specimens at 700, 800, and 900°C.

5.2.3 Oxygen Analysis

Several air-oxidized specimens of M5 were analyzed for oxygen and nitrogen concentrations. The oxygen values were compared with those calculated from the weight change data, assuming all of the weight change in the specimen is due to oxygen ingress. The sample is reacted with carbon by rapidly heating it to over 2700°C in a helium-purged graphite crucible. The evolved carbon monoxide is carried by helium to a copper oxide furnace, where carbon monoxide is converted to carbon dioxide. The concentration of carbon dioxide is measured by an infrared cell and reported in terms of oxygen concentration. The nitrogen gas that evolved on combustion is measured by a thermal conductivity detector.

Table 5.2 shows the oxygen concentration values that were calculated from the weight change data along with the analyzed values for specimens air oxidized at 300-600°C. The specimens were analyzed twice. In general, agreement between the calculated and measured values was good for all the specimens tested, except when the oxide was thick and/or had a tendency to spall (e.g., specimens exposed for 407 h at 500°C and 161 and 305 h at 600°C).

Table 5.2. A comparison of the oxygen concentration values calculated from the weight change data with the measured values for steam-preoxidized M5 specimens after air oxidation

Air exposure temperature (°C)	Air exposure time (h)	Calculated oxygen content (wt.%)	Analyzed oxygen content (wt.%)	Analyzed nitrogen content (wt.%)
300	97.5	0.85	1.05, 0.82	0.11, 0.11
300	336	0.79	0.64, 0.86	0.16, 0.18
300	599	0.76	1.06, 0.78	0.22, 0.23
300	1003	0.73	0.78, 1.04	0.23, 0.26
400	73	0.87	0.95	0.07
400	167	0.90	0.62, 1.05	0.31, 0.31
400	300	0.93	0.96, 0.87	0.30, 0.32
400	600	0.97	1.0, 1.24	0.23, 0.28
500	51	0.83	0.98, 1.09	0.31, 0.36
500	100	0.91	1.18, 1.17	0.33, 0.33
500	246	1.00	1.21, 0.87	0.36, 0.43
500	407	1.28	1.42, 1.43	-
600	41	1.18	0.85, 1.6	-
600	86	1.77	1.54, 1.67	-
600	161	2.84	1.31, 1.99	-
600	305	4.19	2.68, 2.04	-

5.3 Air Oxidation of Bare Alloy

5.3.1 300-600°C

Table 2.11 lists the exposure times used for evaluating the air oxidation characteristics of bare M5 at 300, 400, 500, and 600°C. A single specimen was used at each temperature, and weight-change data as a function of exposure time were obtained by periodic retrieval and weighing of the specimen. Exposures were, in general,

complementary to those conducted on air oxidation of steam-preoxidized specimens. Oxide thickness was measured on the specimens after the final time of exposure at each temperature. Figure 5.12 shows the corrected weight change data as a function of square root of time at the four temperatures.

Oxide thickness was calculated from the weight change data as a function of time at the four exposure temperatures. Figure 5.13 shows oxide thickness as a function of square root of time. The calculated oxide thickness after 300-h exposure in air at 600°C was 132.7 μm . This compares with a measured value of 123.0 μm . The calculated oxide thickness after 580-h exposure in air at 500°C was 31.0 μm , and the measured value was 24.3 μm . The calculated value after 643 h at 400°C was 3.9 μm , whereas the measured value was 5.4 μm . The specimens exposed at 300°C was not examined since the oxide thickness in it was negligibly small.

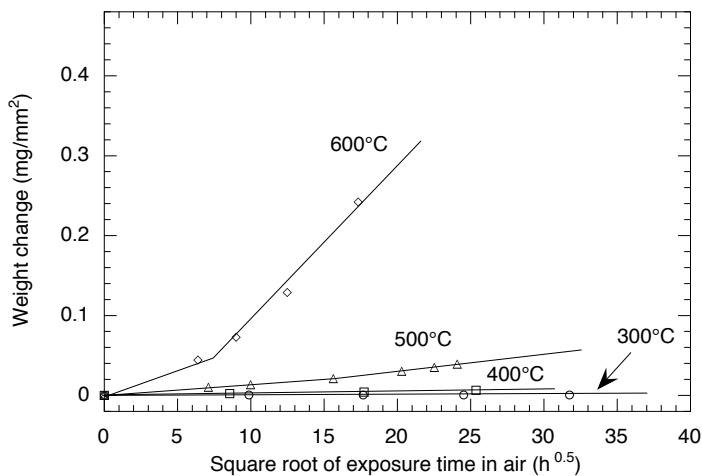


Figure 5.12. Corrected weight change during oxidation of bare M5 capsule specimens at 300, 400, 500, and 600°C.

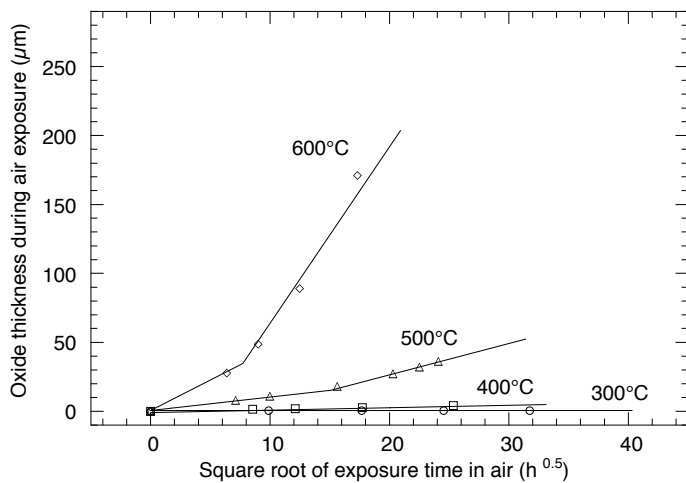


Figure 5.13. Oxide thickness calculated from the weight change data for air oxidation of bare M5 capsule specimens at 300, 400, 500, and 600°C.

5.3.2 700-900°C

Table 2.12 lists the exposure times used for evaluating the air oxidation characteristics of bare M5 at 700, 800, and 900°C. A single specimen was used at each temperature, and the weight change as a function of exposure time was obtained by periodic retrieval and weighing of the specimen. The exposures were terminated when the oxidation became substantial and/or when the specimen deformed significantly. Oxide thickness was measured on the specimens, if possible, after the final time of exposure at each temperature. Figure 5.14 shows the weight change data as a function of square root of time at the three temperatures.

Oxide thickness was calculated from the weight change data as a function of time at the three exposure temperatures. Figure 5.15 shows a plot of the oxide thickness as a function of square root of time. The calculated oxide thickness after 46.2-h exposure in air at 700°C was 152.9 μm . This compares with a measured value of 144.8 μm . The calculated oxide thickness after 10.3-h exposure in air at 800°C was 197.8 μm , whereas the measured value was 190.2 μm . The calculated oxide thickness after 1.7-h exposure in air at 900°C was 221.2 μm , whereas the measured value was 195.4 μm .

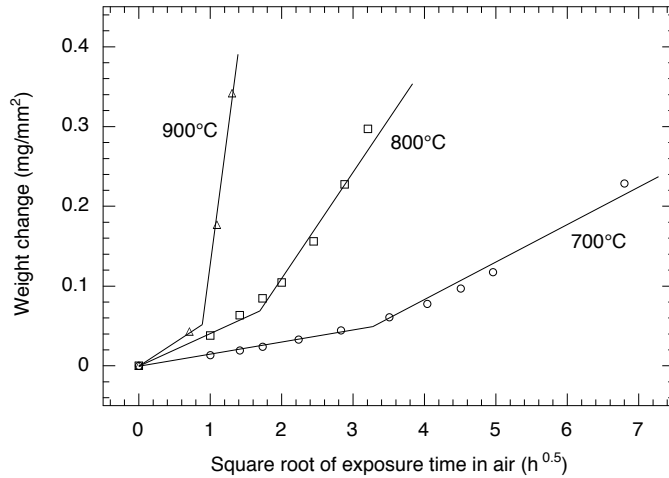


Figure 5.14. Weight change during oxidation of bare M5 capsule specimens at 700, 800, and 900°C.

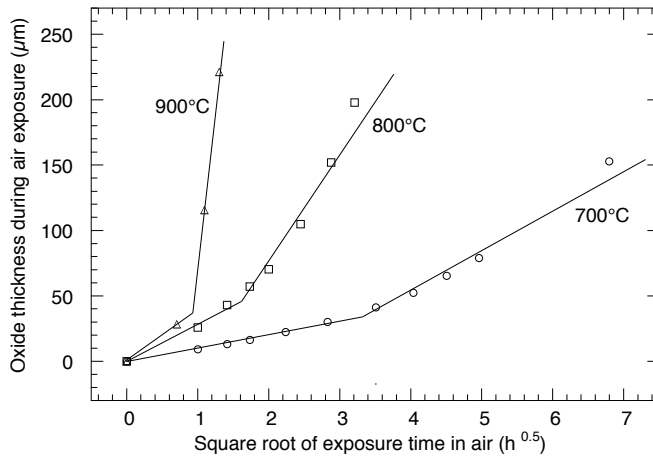


Figure 5.15 Oxide thickness calculated from the weight change data for air oxidation of bare M5 capsule specimens at 700, 800, and 900°C.

6 Correlations for Oxidation Kinetics

6.1 Zircaloy-4

In general, the kinetics of oxidation of Zircaloy-4 specimens were derived from weight change data by plotting the weight change against square root of exposure time and fitting the data by two lines to depict pre- and post-breakaway kinetics. The slopes of both fitted lines were calculated and were used to develop rate constants for the oxidation process. Data presented in the earlier sections were used to develop correlations that relate oxidation rate and temperature. Weight change data for the air oxidation of steam-preoxidized Zircaloy-4 for 300-600°C and for 700-900°C are presented in Figs. 3.10 and 3.17, respectively. Oxide thickness data for the air oxidation of steam-preoxidized Zircaloy-4 for 300-600°C and for 700-900°C are presented in Figs. 3.15 and 3.18, respectively.

6.1.1 Oxidation Rate Correlations

In general, the rates developed using the weight change data at different temperatures were curve fitted in an Arrhenius-type formalism,

$$\text{Rate constant} = A \exp(-B/TK) \quad (6.1)$$

where A and B are constants.

The equations for the air oxidation of steam-preoxidized Zircaloy-4 specimens in the low temperature range are

$$\text{Rate constant (in kg}^2\text{/m}^4\text{·s)} = 0.386 \exp(-16070/TK) \text{ for pre-breakaway, } 573 \geq TK \leq 873 \quad (6.2)$$

$$\text{Rate constant (in kg}^2\text{/m}^4\text{·s)} = 187.3 \exp(-19245/TK) \text{ for post-breakaway, } 673 \geq TK \leq 873 \quad (6.3)$$

The equations for the air oxidation of bare Zircaloy-4 specimens in the low temperature range are

$$\text{Rate constant (in kg}^2\text{/m}^4\text{·s)} = 1.12 \times 10^4 \exp(-23950/TK) \text{ for pre-breakaway, } 573 \geq TK \leq 873 \quad (6.4)$$

$$\text{Rate constant (in kg}^2\text{/m}^4\text{·s)} = 7.6 \times 10^4 \exp(-24040/TK) \text{ for post-breakaway, } 673 \geq TK \leq 873 \quad (6.5)$$

The temperature range is only 400-600°C because the oxidation rate for the bare alloy at 300°C was negligibly small. Figures 6.1 and 6.2 show the data points and the curve-fit lines for the steam-preoxidized and bare Zircaloy-4, respectively.

Correlations were also developed to depict the kinetics over the entire temperature range of 300-900°C. Figures 6.3 and 6.4 show the data developed along with curve-fit lines for the data for the steam-preoxidized and bare Zircaloy-4, respectively. The equations for the air oxidation of steam-preoxidized Zircaloy-4 specimens in a wider temperature range are

$$\text{Rate constant (in kg}^2\text{/m}^4\text{·s)} = 3.3 \exp(-17490/TK) \text{ for pre-breakaway, } 573 \geq TK \leq 1173 \quad (6.6)$$

$$\text{Rate constant (in kg}^2\text{/m}^4\text{·s)} = 367 \exp(-19680/TK) \text{ for post-breakaway, } 673 \geq TK \leq 1173 \quad (6.7)$$

The equations for the air oxidation of bare Zircaloy-4 specimens are

$$\text{Rate constant (in kg}^2\text{/m}^4\text{.s)} = 8.1 \exp(-18620/\text{TK}) \text{ for pre-breakaway, } 673 \geq \text{TK} \leq 1173 \quad (6.8)$$

$$\text{Rate constant (in kg}^2\text{/m}^4\text{.s)} = 1096 \exp(-20900/\text{TK}) \text{ for post-breakaway, } 673 \geq \text{TK} \leq 1173 \quad (6.9)$$

Correlations were also developed to depict the kinetics of oxide scale growth over the temperature range of 300-600°C and 300-900°C. Figures 6.5 and 6.6 show the temperature dependence of the oxide growth rate during air oxidation of initially steam-preoxidized Zircaloy-4 in the temperature ranges of 300-600°C. Equations for oxide growth are as follows:

$$\text{Oxide growth rate constant (in } \mu\text{m}^2\text{/s)} = 10720 \exp(-13870/\text{TK}) \text{ for pre-breakaway, } 573 \geq \text{TK} \leq 873 \quad (6.10)$$

$$\text{Oxide growth rate constant (in } \mu\text{m}^2\text{/s)} = 1.08 \times 10^{10} \exp(-23460/\text{TK}) \text{ for post-breakaway, } 673 \geq \text{TK} \leq 873 \quad (6.11)$$

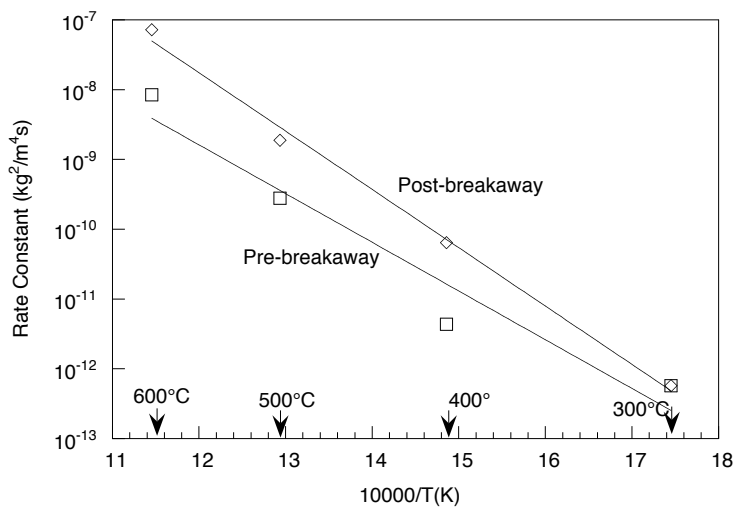


Figure 6.1. Temperature dependence of rate constant for the air oxidation of steam-preoxidized Zircaloy-4 capsule specimens in the temperature range 300-600°C.

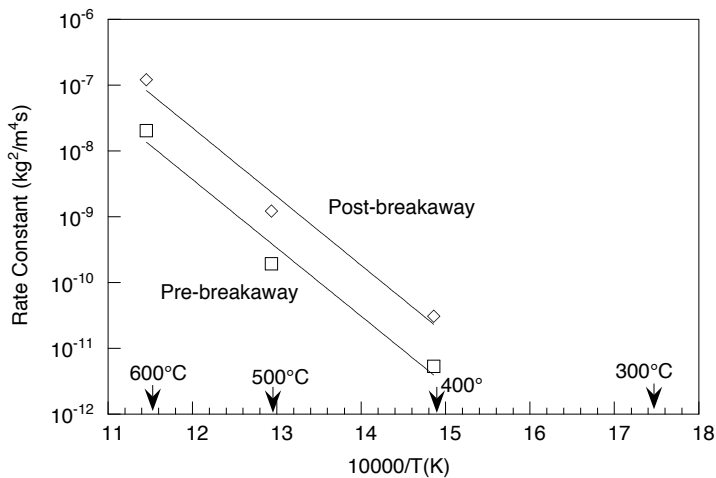


Figure 6.2. Temperature dependence of rate constant for the air oxidation of bare Zircaloy-4 capsule specimens in the temperature range 400-600°C.

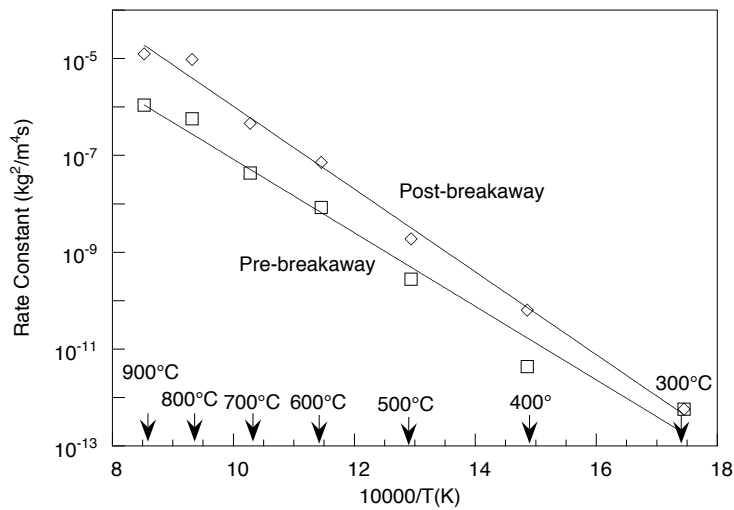


Figure 6.3. Temperature dependence of rate constant for the air oxidation of steam-oxidized Zircaloy-4 capsule specimens in the temperature range 300-900°C.

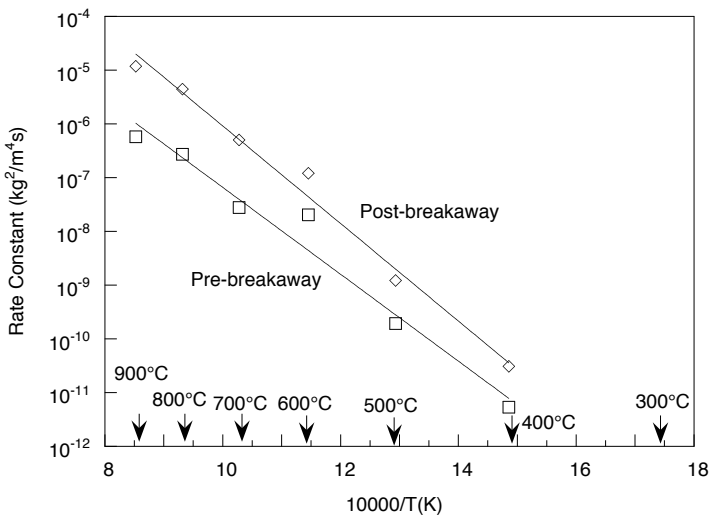


Figure 6.4. Temperature dependence of rate constant for the air oxidation of bare Zircaloy-4 capsule specimens in the temperature range 400-900°C.

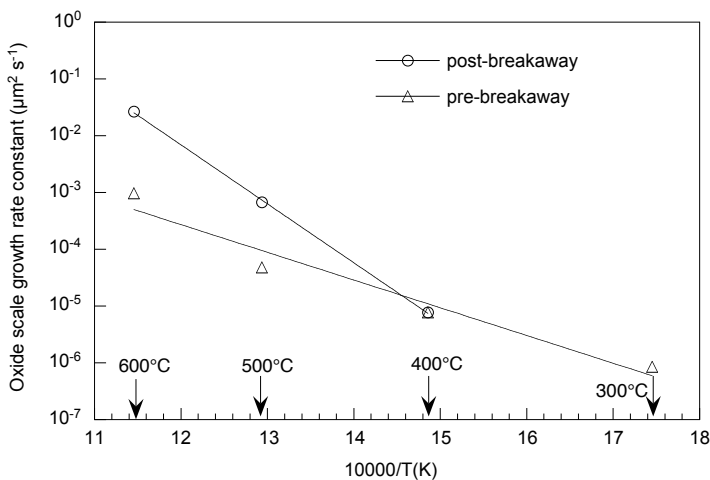


Figure 6.5. Temperature dependence of rate constant for oxide growth during air oxidation of steam-preoxidized Zircaloy-4 capsule specimens in the temperature range of 300-600°C.

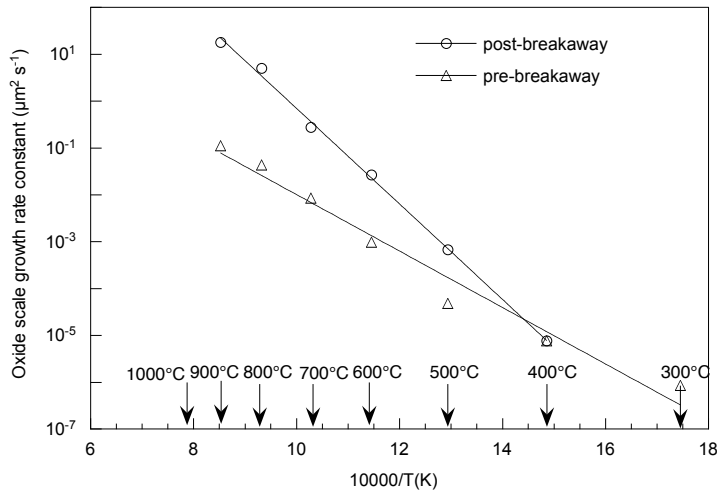


Figure 6.6. Temperature dependence of rate constant for oxide growth during air oxidation of steam-preoxidized and Zircaloy-4 capsule specimens in the temperature range of 300-900°C.

6.1.2 Comparison with Nureg Correlations

Oxidation rate correlations, developed using the data generated in this project, were compared with several Nureg correlations. The rate constants (in kg²/m⁴·s), based on parabolic models, are Nureg1 (also Powers), Nureg2 (cited by Shepherd), and CODEX.

The correlations used for comparison are:

- Nureg1 and Powers: $k_{\text{Nureg1}}(T) = 1.292 \exp(-15630/TK)$ (6.12)

- Nureg2: $k_{\text{Nureg2}}(T) = 30900 \exp(-28485/TK)$ (6.13)

- CODEX: $k_{\text{CODEX}}(T) = 63645 \exp(-29054/TK)$ (6.14)

For the temperature range of 300-600°C for steam-preoxidized and 400-600°C for bare alloy,

- ANL: Steam-preoxidized $k_{\text{ANL}}(T) = 0.386 \exp(-16070/TK)$ for pre-breakaway (6.15)

$$k_{\text{ANL}}(T) = 187.3 \exp(-19245/TK) \text{ for post-breakaway} \quad (6.16)$$

- ANL: Bare $k_{\text{ANL}}(T) = 1.12 \times 10^4 \exp(-23950/TK)$ for pre-breakaway (6.17)

$$k_{\text{ANL}}(T) = 7.6 \times 10^4 \exp(-24040/TK) \text{ for post-breakaway} \quad (6.18)$$

For the temperature range of 300-900°C for steam-preoxidized and 400-900° for bare alloy,

- ANL: Steam-preoxidized $k_{\text{ANL}}(T) = 3.3 \exp(-17490/TK)$ for pre-breakaway (6.19)

$$k_{\text{ANL}}(T) = 367 \exp(-19680/TK) \text{ for post-breakaway} \quad (6.20)$$

- ANL: Bare $k_{\text{ANL}}(T) = 8.1 \exp(-18620/TK)$ for pre-breakaway (6.21)

$$k_{\text{ANL}}(T) = 1096 \exp(-20900/TK) \text{ for post-breakaway} \quad (6.22)$$

Figures 6.7 and 6.8 show data developed on steam preoxidized (at 300-600°C) and bare (400-600°C) specimens, respectively, along with Nureg correlations. The results show that the correlation developed from the oxidation data generated in the current project is in fair agreement with that based on Nureg1 and Powers. The predictions based on Nureg2 and CODEX correlations are several orders of magnitude lower than those based on current work, especially at lower temperatures.

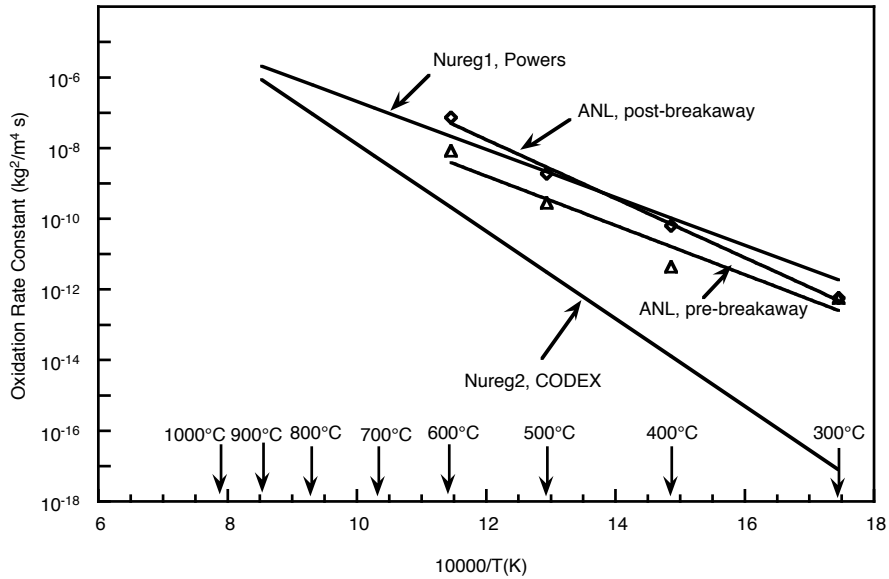


Figure 6.7. A comparison of the temperature dependence of the oxidation rate constant for air oxidation of steam-preoxidized Zircaloy-4 at 300-600°C derived from this project with those based on Nureg1 (Powers), Nureg2, and CODEX.

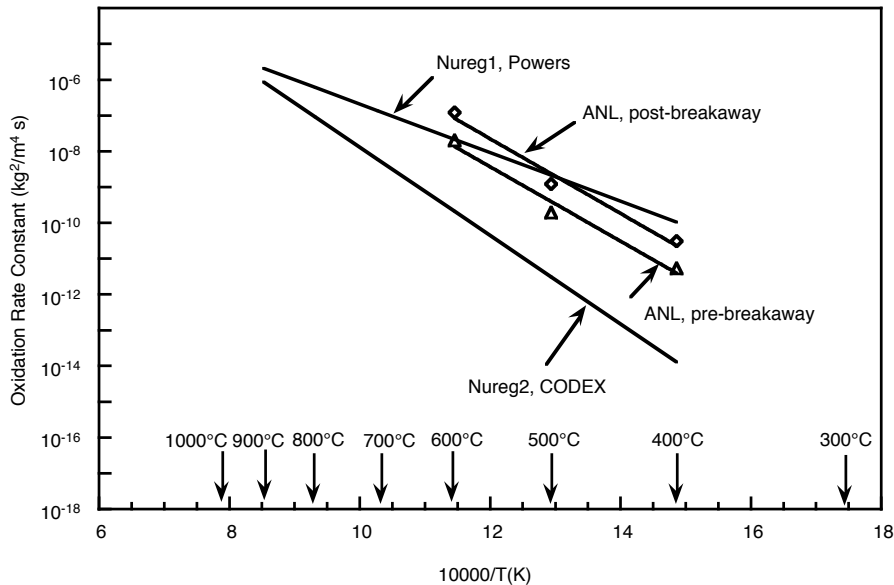


Figure 6.8. A comparison of the temperature dependence of the oxidation rate constant for air oxidation of bare Zircaloy-4 at 400-600°C derived from this project with those based on Nureg1 (Powers), Nureg2, and CODEX.

Figures 6.9 and 6.10 show comparative plots of the data developed in the entire temperature range of 300-900°C for the steam-preoxidized and 400-900°C for the bare specimens along with the Nureg correlations. It is evident that the rates are somewhat higher than the Nureg1 values at temperatures >500°C. Figure 6.11 is a comparative plot of data developed on steam-preoxidized and bare alloy in the post-breakaway region along with the Nureg correlations. In general, the air oxidation rates for steam-preoxidized material are somewhat higher than those for the bare alloy.

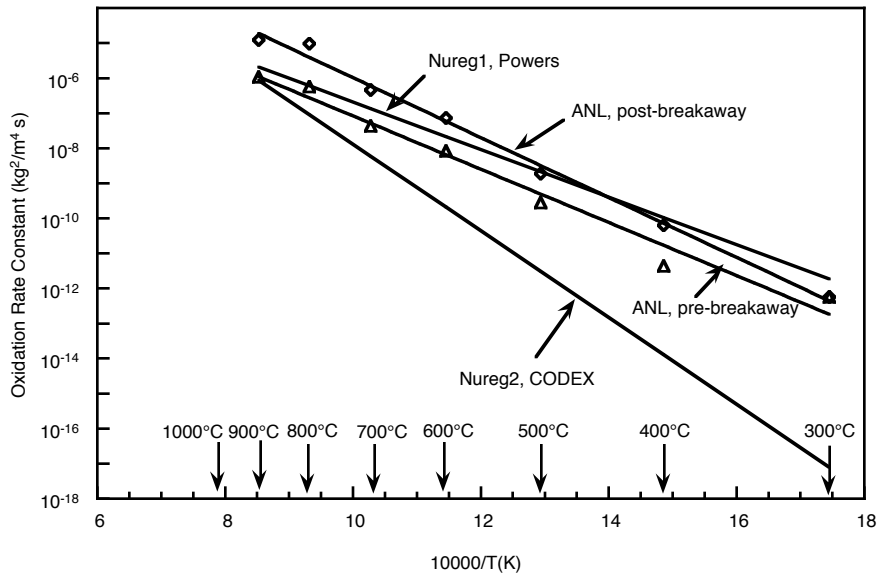


Figure 6.9. A comparison of the temperature dependence of the oxidation rate constant for air oxidation of steam-preoxidized Zircaloy-4 at 300-900°C derived from this project with those based on Nureg1 (Powers), Nureg2, and CODEX.

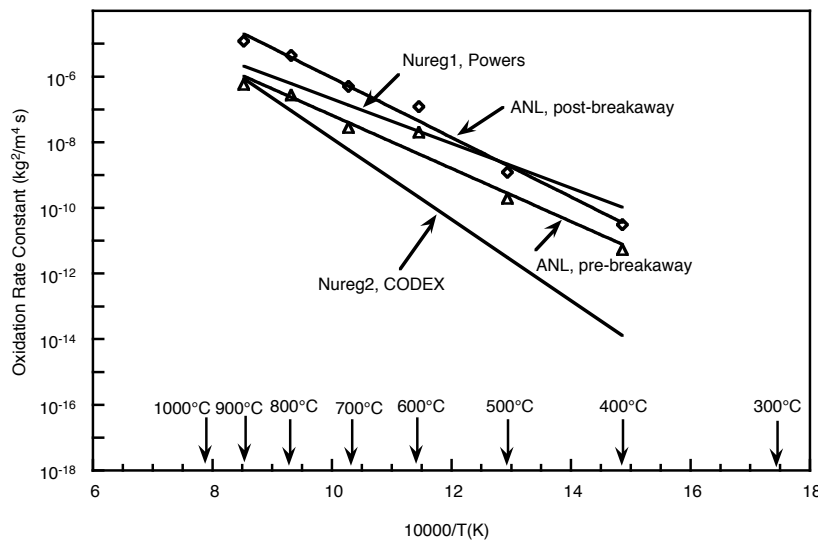


Figure 6.10. A comparison of the temperature dependence of the oxidation rate constant for air oxidation of bare Zircaloy-4 at 400-900°C derived from this project with those based on Nureg1 (Powers), Nureg2, and CODEX.

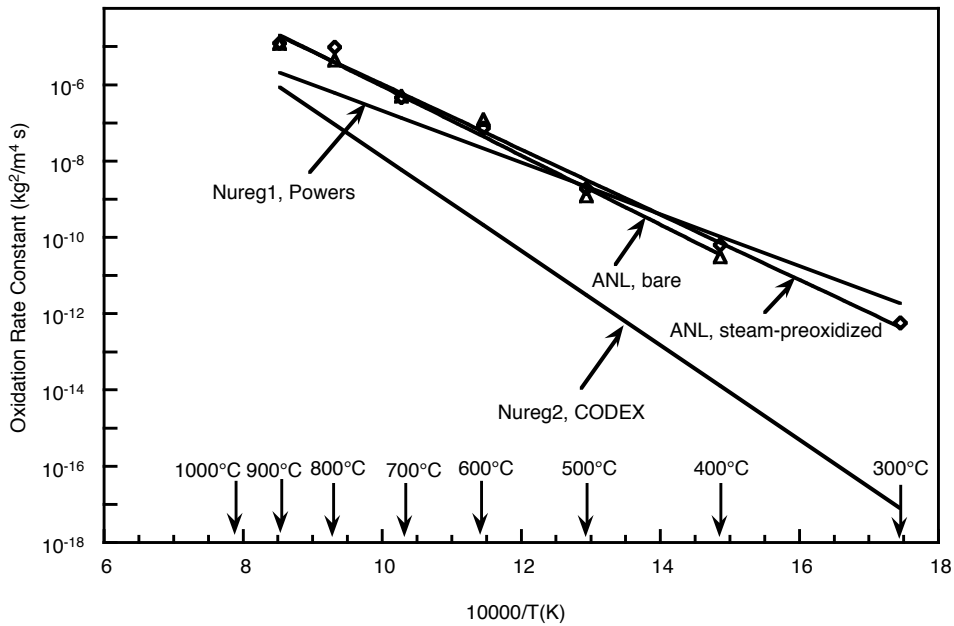


Figure 6.11. A comparison of the temperature dependence of the oxidation rate constant for air oxidation of steam-preoxidized and bare Zircaloy-4 at 300-900°C derived from this project with those based on Nureg1 (Powers), Nureg2, and CODEX.

6.2 Oxidation Rate Correlations for Zirlo

Data presented in the earlier sections were used to develop correlations that relate oxidation rate (in terms of weight change and oxide thickness) and temperature. Weight change data for the air oxidation of steam-preoxidized Zirlo for 300-600°C and for 700-900°C are presented in Figs. 4.3 and 4.9, respectively. Oxide thickness data for the air oxidation of steam-preoxidized Zirlo for 300-600°C and for 700-900°C are presented in Figs. 4.8 and 4.10, respectively.

Equations for the air oxidation of steam-preoxidized Zirlo specimens in the low-temperature range are

$$\text{Rate constant (in kg}^2\text{/m}^4\text{·s)} = 0.07 \exp(-14430/\text{TK}) \text{ for pre-breakaway, } 573 \geq \text{TK} \leq 873 \quad (6.23)$$

$$\text{Rate constant (in kg}^2\text{/m}^4\text{·s)} = 8.33 \times 10^4 \exp(-24000/\text{TK}) \text{ for post-breakaway, } 673 \geq \text{TK} \leq 873 \quad (6.24)$$

Equations for the air oxidation of bare Zirlo specimens in the low-temperature range are

$$\text{Rate constant (in kg}^2\text{/m}^4\text{·s)} = 0.057 \exp(-14240/\text{TK}) \text{ for pre-breakaway, } 573 \geq \text{TK} \leq 873 \quad (6.25)$$

$$\text{Rate constant (in kg}^2\text{/m}^4\text{·s)} = 1.03 \times 10^5 \exp(-24580/\text{TK}) \text{ for post-breakaway, } 673 \geq \text{TK} \leq 873 \quad (6.26)$$

Note that the oxidation rate for the bare alloy at 300°C was negligibly small and not included in the analysis. Figures 6.12 and 6.13 show the data points and the curve-fit lines for steam-preoxidized and bare Zirlo, respectively.

Correlations were also developed to depict the kinetics over the entire temperature range of 300-900°C, which was used in the present study. Figures 6.14 and 6.15 show the data developed along with curve-fit lines for

the steam-preoxidized and bare Zirlo, respectively. The equations for the air oxidation of steam-preoxidized Zirlo specimens over a wider temperature range are

$$\text{Rate constant (in kg}^2\text{/m}^4\cdot\text{s)} = 0.86 \exp(-16100/\text{TK}) \text{ for pre-breakaway, } 573 \geq \text{TK} \leq 1173 \quad (6.27)$$

$$\text{Rate constant (in kg}^2\text{/m}^4\cdot\text{s)} = 1.72 \times 10^4 \exp(-22865/\text{TK}) \text{ for post-breakaway, } 673 \geq \text{TK} \leq 1173 \quad (6.28)$$

The equations for the air oxidation of bare Zirlo specimens are

$$\text{Rate constant (in kg}^2\text{/m}^4\cdot\text{s)} = 0.46 \exp(-15610/\text{TK}) \text{ for pre-breakaway, } 573 \geq \text{TK} \leq 1173 \quad (6.29)$$

$$\text{Rate constant (in kg}^2\text{/m}^4\cdot\text{s)} = 1.30 \times 10^4 \exp(-22830/\text{TK}) \text{ for post-breakaway, } 773 \geq \text{TK} \leq 1173 \quad (6.30)$$

Correlations were also developed to depict the kinetics of oxide scale growth over the temperature range of 300-600°C and 300-900°C. Figures 6.16 and 6.17 show the temperature dependence of the oxide growth rate during air oxidation of initially steam-preoxidized Zirlo in the temperature range of 300-600°C and 300-900°C, respectively. Equations for oxide growth are as follows:

$$\text{Oxide growth rate constant (in } \mu\text{m}^2\text{/s)} = 2662 \exp(-12790/\text{TK}) \text{ for pre-breakaway, } 573 \geq \text{TK} \leq 873 \quad (6.31)$$

$$\text{Oxide growth rate constant (in } \mu\text{m}^2\text{/s)} = 1.44 \times 10^8 \exp(-19610/\text{TK}) \text{ for post-breakaway, } 673 \geq \text{TK} \leq 873 \quad (6.32)$$

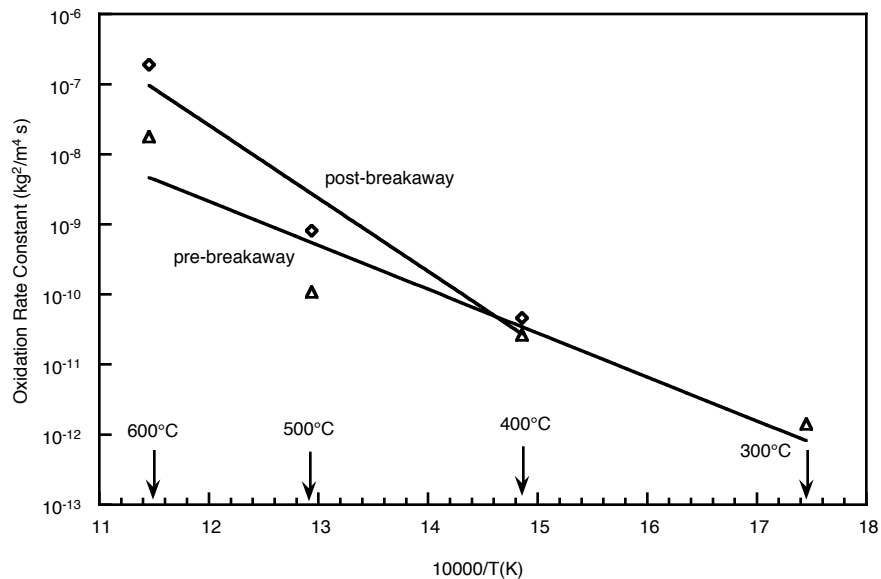


Figure 6.12. Temperature dependence of rate constant for the air oxidation of steam-preoxidized Zirlo capsule specimens in the temperature range of 300-600°C.

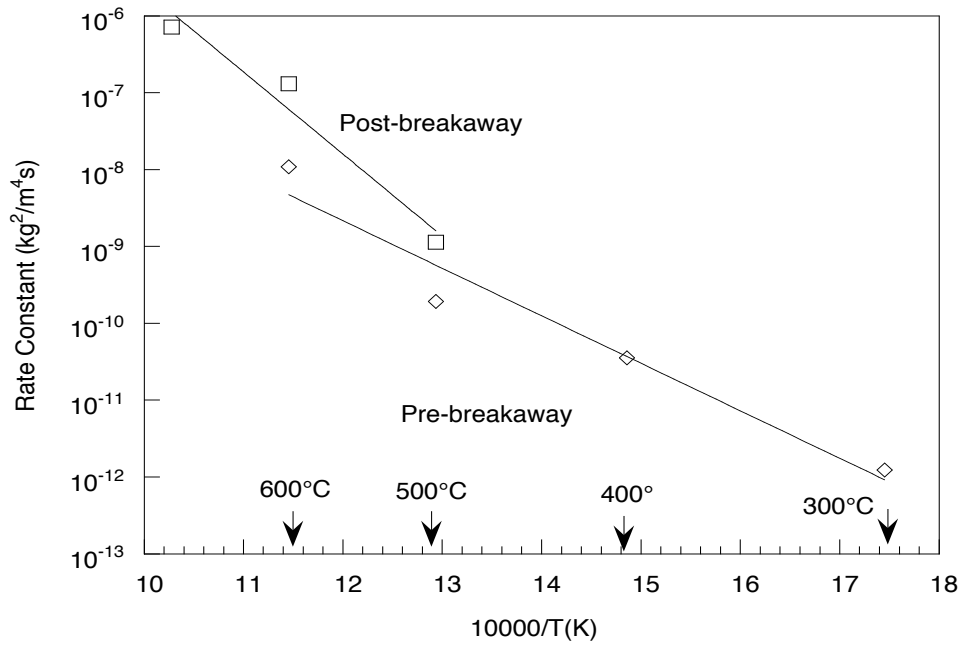


Figure 6.13. Temperature dependence of rate constant for the air oxidation of bare Zirlo capsule specimens in the temperature range of 300-700°C.

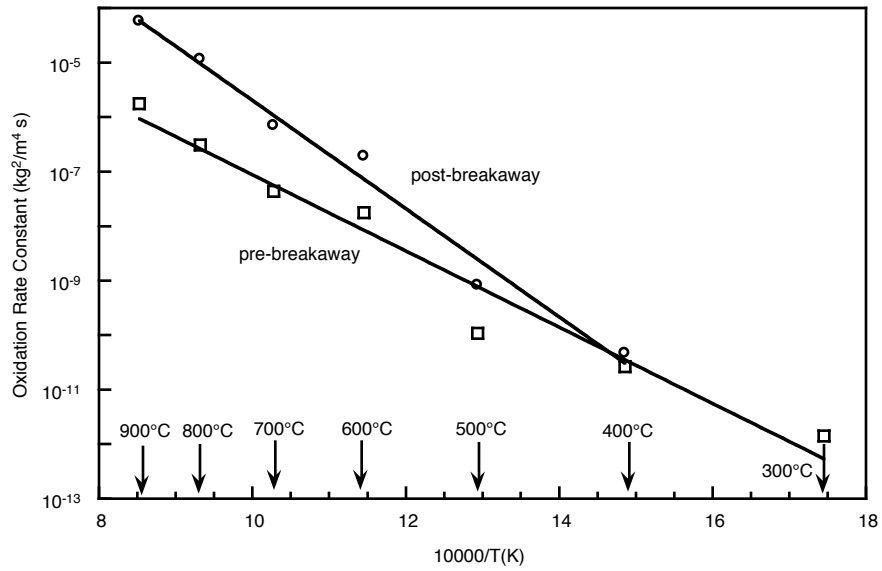


Figure 6.14. Temperature dependence of rate constant for the air oxidation of steam-preoxidized Zirlo capsule specimens in the temperature range of 300-900°C.

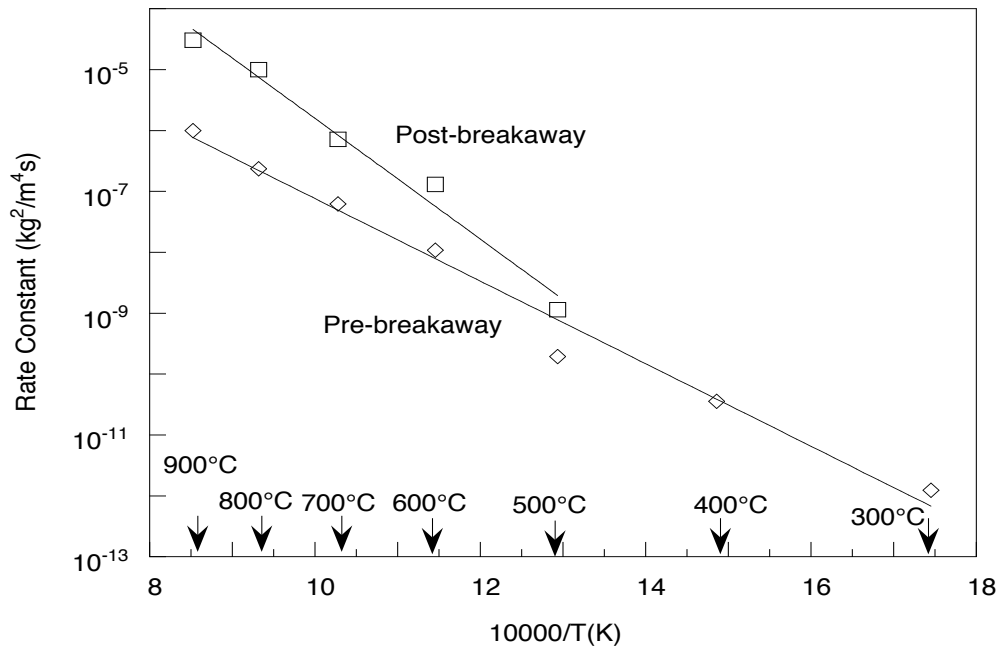


Figure 6.15. Temperature dependence of rate constant for the air oxidation of bare Zirlo capsule specimens in the temperature range of 300-900°C.

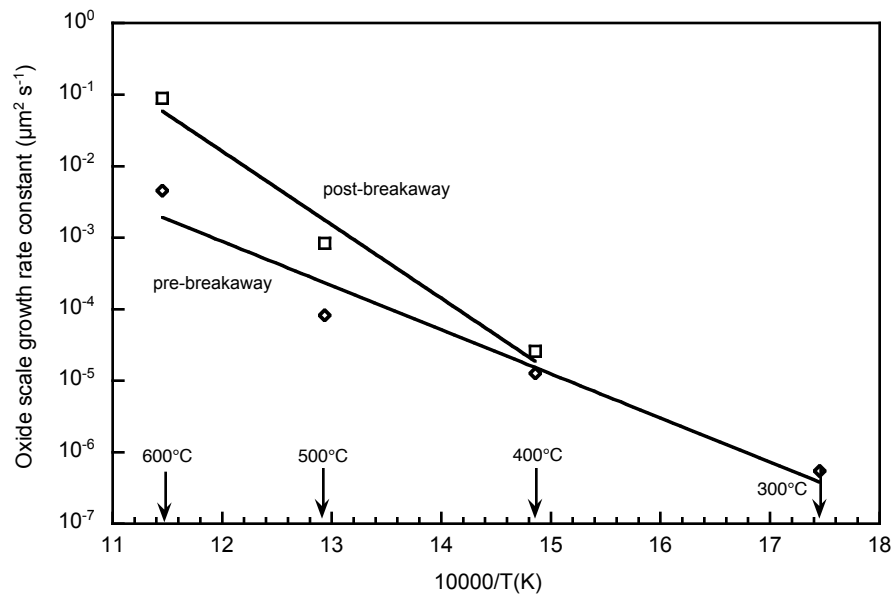


Figure 6.16. Temperature dependence of rate constant for oxide growth during air oxidation of steam-preoxidized Zirlo capsule specimens in the temperature range of 300-600°C.

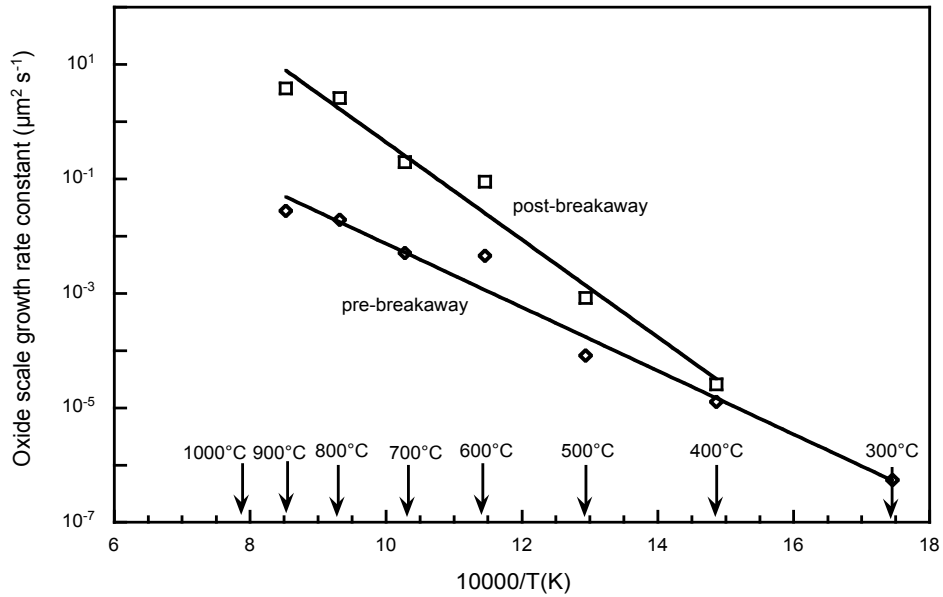


Figure 6.17. Temperature dependence of rate constant for oxide growth during air oxidation of steam-preoxidized Zirlo capsule specimens in the temperature range of 300-900°C.

6.3 Oxidation Rate Correlations for M5

Data presented in the earlier sections were used to develop correlations that relate oxidation rate (in terms of weight change and oxide thickness) and temperature. Weight change data for the air oxidation of steam-preoxidized M5 for 300-600°C and for 700-900°C are presented in Figs. 5.4 and 5.10, respectively. Oxide thickness data for the air oxidation of steam-preoxidized M5 for 300-600°C and for 700-900°C are presented in Figs. 5.9 and 5.13, respectively.

Equations for the air oxidation of steam-preoxidized M5 specimens in the low-temperature range are

$$\text{Rate constant (in kg}^2/\text{m}^4\cdot\text{s)} = 1.0 \times 10^{-3} \exp(-12230/\text{TK}) \text{ for pre-breakaway, } 573 \geq \text{TK} \leq 873 \quad (6.33)$$

$$\text{Rate constant (in kg}^2/\text{m}^4\cdot\text{s)} = 1.3 \times 10^5 \exp(-25290/\text{TK}) \text{ for post-breakaway, } 773 \geq \text{TK} \leq 873 \quad (6.34)$$

Equations for the air oxidation of bare M5 specimens in the low-temperature range are

$$\text{Rate constant (in kg}^2/\text{m}^4\cdot\text{s)} = 68.4 \exp(-19620/\text{TK}) \text{ for pre-breakaway, } 573 \geq \text{TK} \leq 873 \quad (6.35)$$

$$\text{Rate constant (in kg}^2/\text{m}^4\cdot\text{s)} = 1.2 \times 10^7 \exp(-28680/\text{TK}) \text{ for post-breakaway, } 773 \geq \text{TK} \leq 873 \quad (6.36)$$

Note that the oxidation rate for the bare alloy at 300°C was negligibly small and not included in the analysis. Figure 6.18 shows the data points and the curve-fit lines for steam-preoxidized M5. Figure 6.19 shows a comparison of air oxidation data that were developed for the steam-preoxidized and bare M5 alloy.

Correlations were also developed to depict the kinetics over the entire temperature range of 300-900°C, which was used in the present study. The equations for the air oxidation of steam-preoxidized and bare M5 specimens in the temperature range of 500-900°C in the post-breakaway region are

$$\text{Rate constant (in kg}^2\text{/m}^4\text{.s)} = 3.5 \times 10^3 \exp(-22660/\text{TK}) \text{ for steam preoxidized, } 773 \geq \text{TK} \leq 1173 \quad (6.37)$$

$$\text{Rate constant (in kg}^2\text{/m}^4\text{.s)} = 5.8 \times 10^3 \exp(-22600/\text{TK}) \text{ for bare, } 773 \geq \text{TK} \leq 1173 \quad (6.38)$$

Correlations were also developed to depict the kinetics of oxide scale growth over the temperature range of 300-600°C and 300-900°C. Figures 6.20 shows the temperature dependence of the oxide growth rate during air oxidation of initially steam-preoxidized and bare M5. Equations for oxide growth for the steam-preoxidized M5 are as follows:

$$\text{Oxide growth rate constant (in } \mu\text{m}^2\text{/s)} = 8.0 \times 10^3 \exp(-14040/\text{TK}) \text{ for pre-breakaway, } 573 \geq \text{TK} \leq 1173 \quad (6.39)$$

$$\text{Oxide growth rate constant (in } \mu\text{m}^2\text{/s)} = 9.6 \times 10^8 \exp(-22090/\text{TK}) \text{ for post-breakaway, } 773 \geq \text{TK} \leq 1173 \quad (6.40)$$

Equations for oxide growth for the bare M5 are as follows:

$$\text{Oxide growth rate constant (in } \mu\text{m}^2\text{/s)} = 4.9 \times 10^6 \exp(-18410/\text{TK}) \text{ for pre-breakaway, } 573 \geq \text{TK} \leq 1173 \quad (6.41)$$

$$\text{Oxide growth rate constant (in } \mu\text{m}^2\text{/s)} = 2.0 \times 10^9 \exp(-22370/\text{TK}) \text{ for post-breakaway, } 773 \geq \text{TK} \leq 1173 \quad (6.42)$$

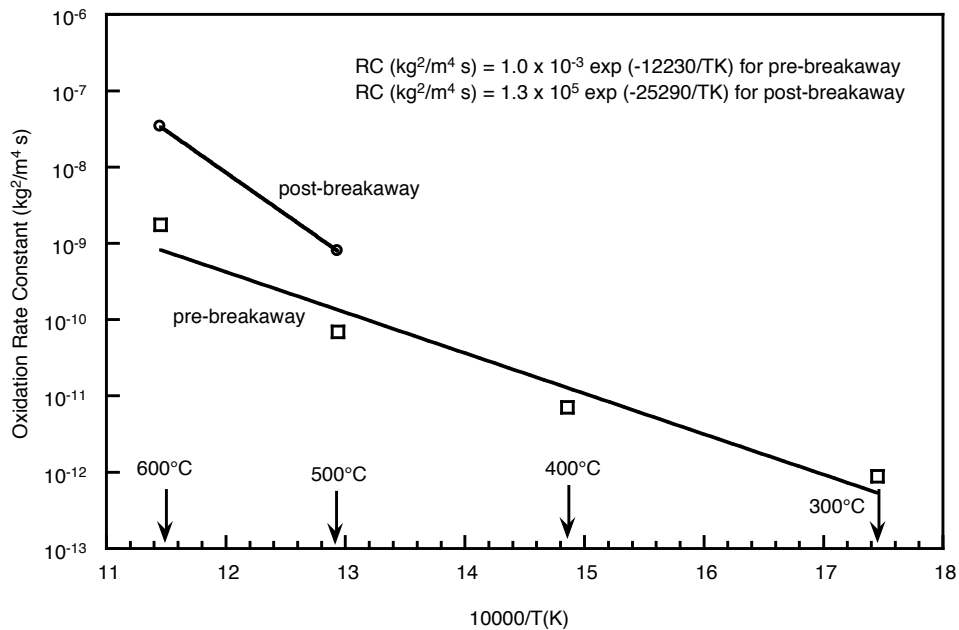


Figure 6.18. Temperature dependence of rate constant for the air oxidation of steam-preoxidized M5 capsule specimens in the temperature range of 300-600°C.

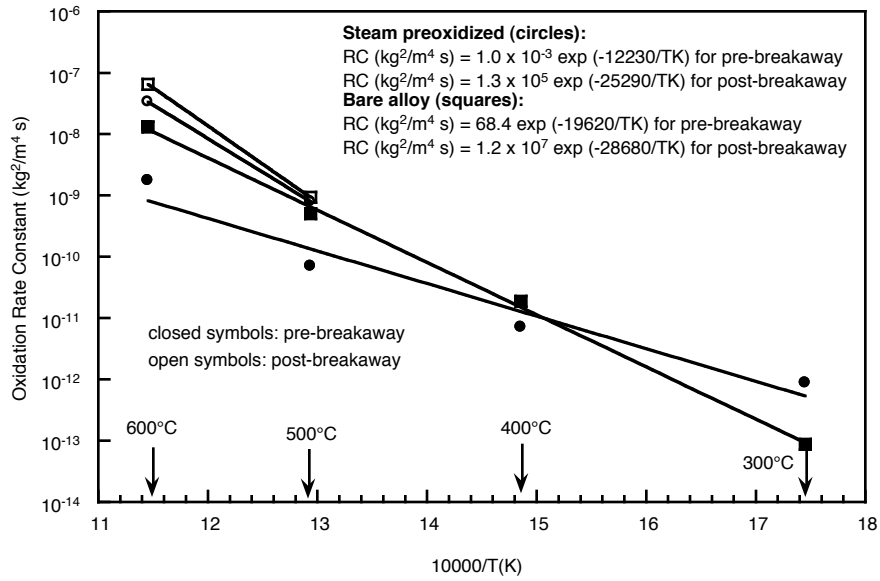


Figure 6.19. Temperature dependence of rate constant for the air oxidation of steam preoxidized and bare M5 capsule specimens in the temperature range of 300-600°C.

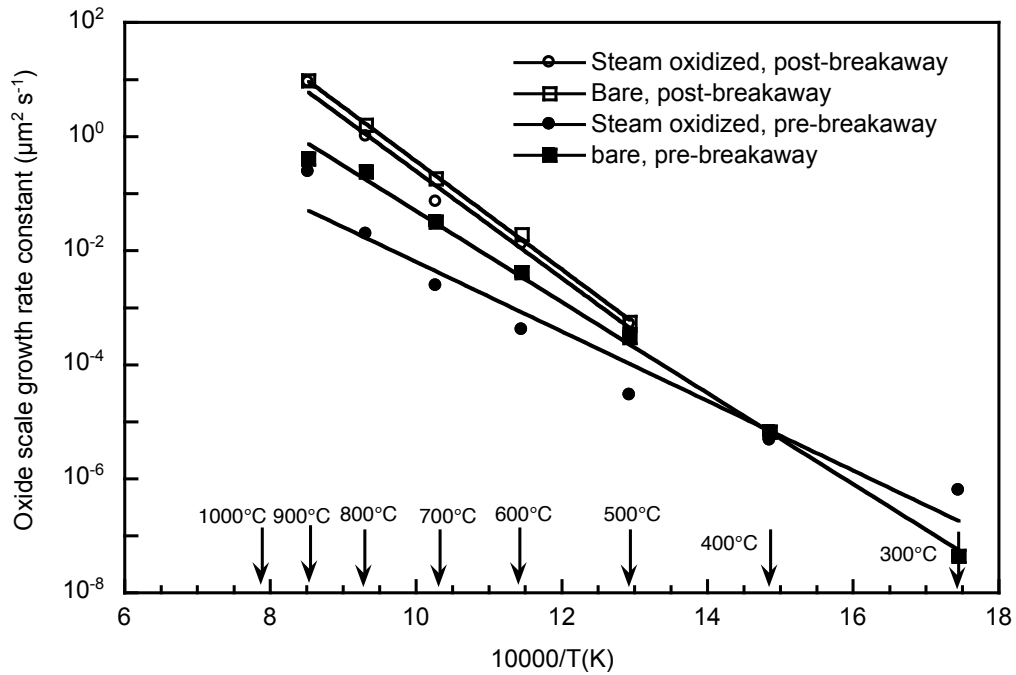


Figure 6.20. Temperature dependence of oxide scale growth rate constant for the air oxidation of steam-preoxidized M5 capsule specimens in the temperature range of 300-900°C.

6.4 Oxidation Comparison between Zircaloy-4, Zirlo, and M5

The oxidation performance of Zircaloy-4, Zirlo, and M5 can be compared since the data for all three materials were developed under similar conditions. All three alloys were preoxidized in steam at 550°C to develop $\approx 25\text{-}30\ \mu\text{m}$ oxide layer. The steam-preoxidized specimens of all three alloys were air oxidized at temperatures of 300, 400, 500, and 600°C for times up to ≈ 1000 h.

Figures 6.21 and 6.22 show a comparison of the air oxidation rate in the temperature range of 300-600°C and 300-900°C, respectively, for all three materials, which were initially in steam-preoxidized condition. Figure 6.23 shows the temperature dependence of the oxide growth rate during air oxidation of initially steam-preoxidized Zircaloy-4, Zirlo, and M5.

Several conclusions can be drawn from the current air oxidation study on the three alloys.

- The data showed that in the pre-breakaway region, oxygen ingress into Zirlo occurs at a faster rate than in Zircaloy-4. In the post-breakaway region, the rates for Zirlo are somewhat lower than for Zircaloy-4 at $T \leq 500^\circ\text{C}$; however, at $T \geq 600^\circ\text{C}$, the rates for Zirlo are higher than for Zircaloy-4.
- After exposures at temperatures $\geq 600^\circ\text{C}$, the oxide scales that developed exhibited multitude of radial cracks that extended to the substrate alloy; at 500°C, the radial cracks traveled only part way from the external surface even after 429 h exposure.
- The oxidation rate data developed in this project were used to develop correlations that relate rates (based on weight change and oxide thickness) and temperature. Correlations were developed for two temperature regimes namely 300-600°C (low-temperature oxidation regime) and over a wide temperature range of 400-900°C. Correlations were developed for both pre- and post-breakaway regimes.
- M5 alloy did not exhibit breakaway trend at 300 and 400°C during the exposure times used in the current study. The oxidation rates (in the post-breakaway region) for M5 are consistently lower than for other two alloys at 500 and 600°C.

6.5 Comparison with Nureg Correlations

Figure 6.24 shows a comparative plot of data developed on steam preoxidized (300-600°C) specimens, along with Nureg correlations. The results show that the correlation developed for Zircaloy-4 from the oxidation data generated in the current project is in fair agreement with that based on Nureg1 and Powers. The predictions based on Nureg2 and CODEX correlations for Zircaloy-4 are several orders of magnitude lower than those based on current work, especially at lower temperatures. Figure 6.25 shows a comparative plot of the data (in the post-breakaway region) developed for the steam-preoxidized Zircaloy-4, Zirlo, and M5 specimens at temperatures between 400-900°C along with the Nureg correlations. The data for the steam-preoxidized Zircaloy-4 and Zirlo showed higher oxidation rate than that based on correlation by Nureg1 and Powers for Zircaloy-4 at temperatures $\geq 600^\circ\text{C}$.

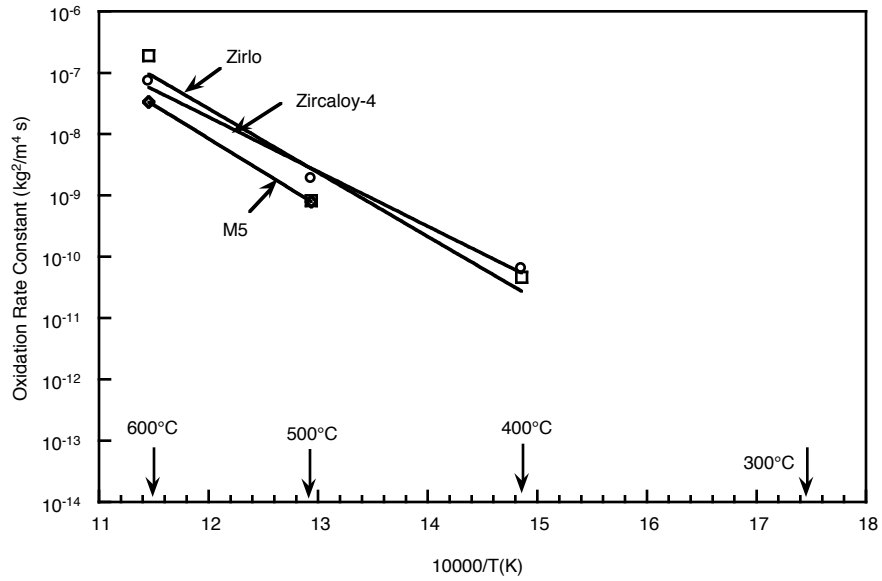


Figure 6.21. Temperature dependence of rate constant (in the post-breakaway region) for the air oxidation of steam-preoxidized Zircaloy-4, Zirlo, and M5 capsule specimens in the temperature range of 400-600°C.

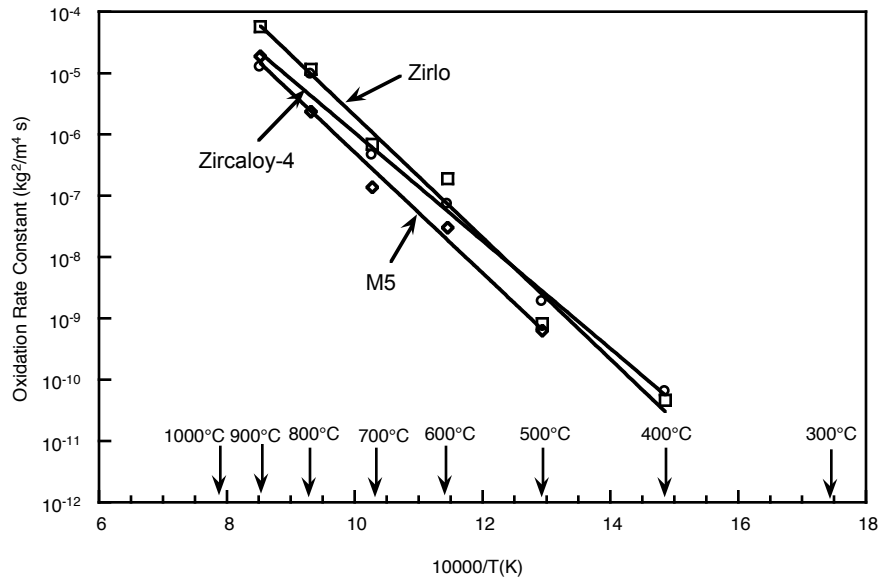


Figure 6.22. Temperature dependence of rate constant for the air oxidation of steam-preoxidized Zircaloy-4, Zirlo, and M5 capsule specimens in the temperature range of 400-900°C.

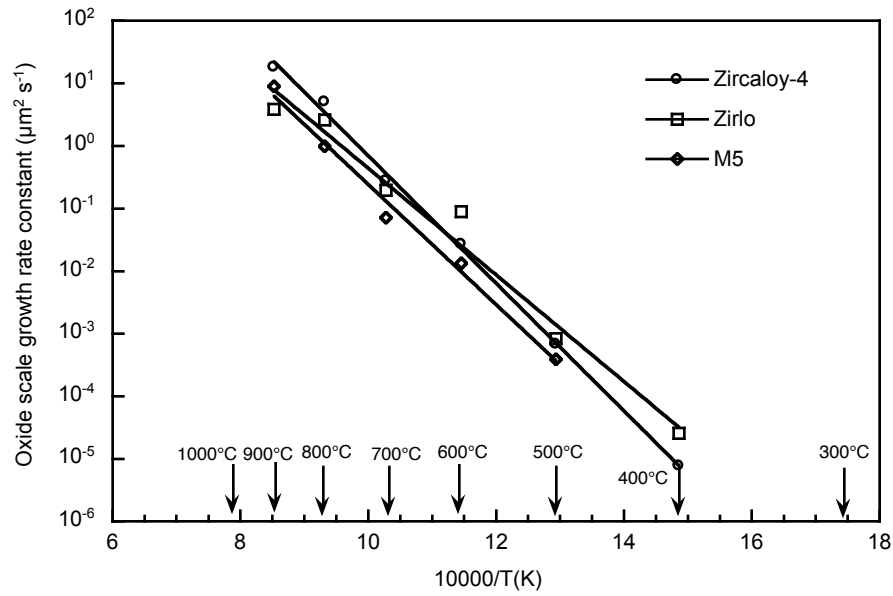


Figure 6.23. Temperature dependence of rate constant for oxide growth rate during air oxidation of steam-preoxidized Zircaloy-4, Zirlo, and M5 capsule specimens in the temperature range of 400-900°C.

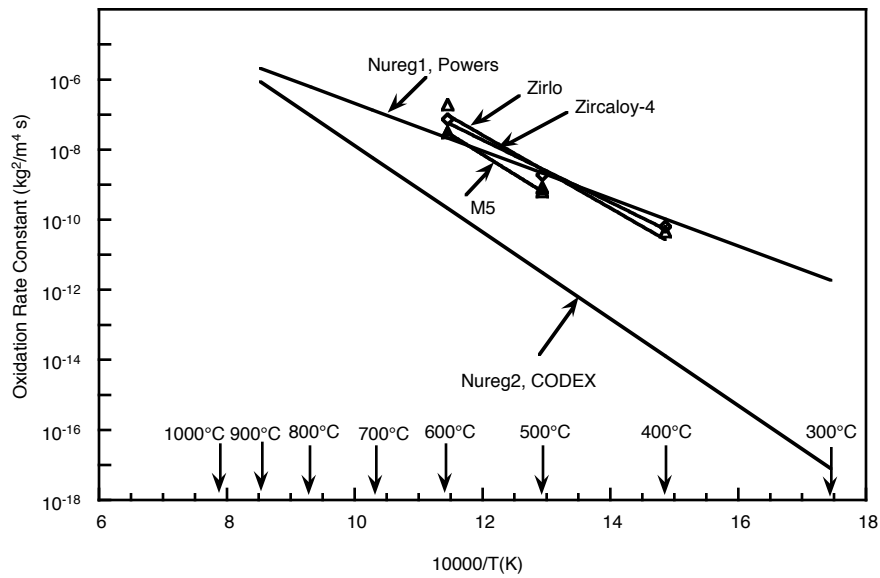


Figure 6.24. A comparison of the temperature dependence of the oxidation rate constant for air oxidation of steam-preoxidized Zircaloy-4, Zirlo, and M5 at 400-600°C derived from this project with those for Zircaloy-4, based on Nureg1 (Powers), Nureg2, and CODEX.

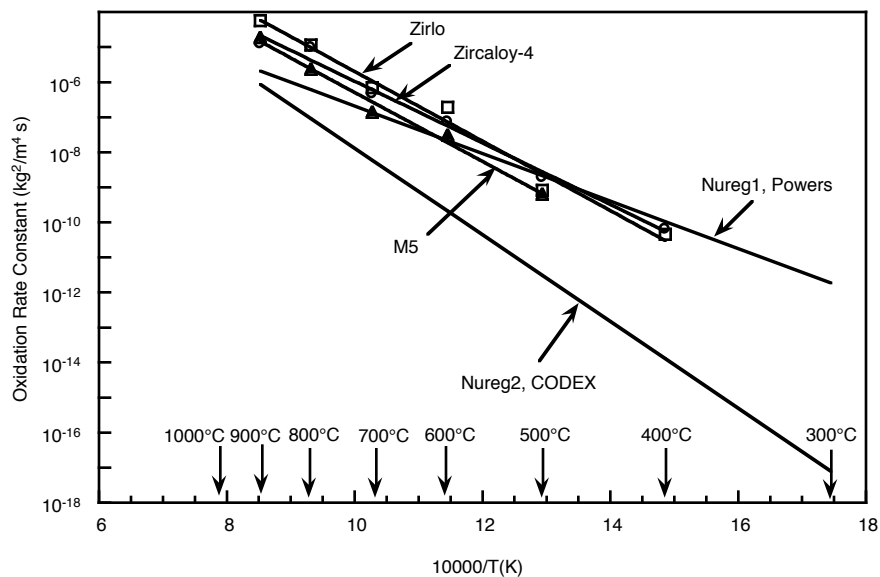


Figure 6.25. A comparison of the temperature dependence of the oxidation rate constant (in post-breakaway region) for air oxidation of steam-preoxidized Zircaloy-4, Zirloy, and M5 at 400-900°C derived from this project with those for Zircaloy-4, based on Nureg1 (Powers), Nureg2, and CODEX.

6.6 Oxide Thickness Growth

The results discussed thus far shows that all three alloys, initially in steam-preoxidized condition, can undergo further oxidation in the event of air ingress. The rate at which the oxide scale grows is dependent on the cladding temperature, exposure time, and alloy composition. The data and correlations on oxide scale development (presented in earlier sections of this report) in the three alloys are used to evaluate the time dependence cladding oxidation for the three cladding materials with nominal wall thickness and to calculate the section loss of the cladding as a function of time and temperature. Based on the air oxidation test data for internally pressurized steam-preoxidized Zircaloy-4 specimens (see Tables 3.3 and 3.4), an internal pressure of 400 psig at room temperature would result in rupture of the cladding within 43 h at 600°C. In order to evaluate the effect of air oxidation without cladding failure, 600°C was selected as the upper-bound temperature. Figures 6.26-6.28 show the calculated oxide thickness for steam-preoxidized Zircaloy-4, Zirloy, and M5, respectively, at several temperatures. For example, the calculations indicate that Zircaloy4 cladding would develop an additional oxide of 100 μm in 150 h at 600°C and $\approx 50 \mu\text{m}$ in 1000 h at 500°C, due to air ingress. Under similar conditions, Zirloy would develop an oxide of 170 μm at 600°C, 150 h and 55 μm at 500°C, 1000 h. Values for M5 are 65 μm at 600°C, 150 h and 45 μm at 500°C, 1000 h.

Figure 6.29 shows a comparison of the oxidation behavior of Zircaloy-4, Zirloy, and M5, and can be used to assess the time available to implement mitigating cladding failure under different time-temperature scenarios. Figure 6.30 shows a plot of cladding wall thickness (in percent) that would undergo oxidation when subjected to air ingress at various temperatures. Data and correlations for Zirloy, and M5, developed in this project, are applicable to the advanced claddings for use under high burnup conditions.

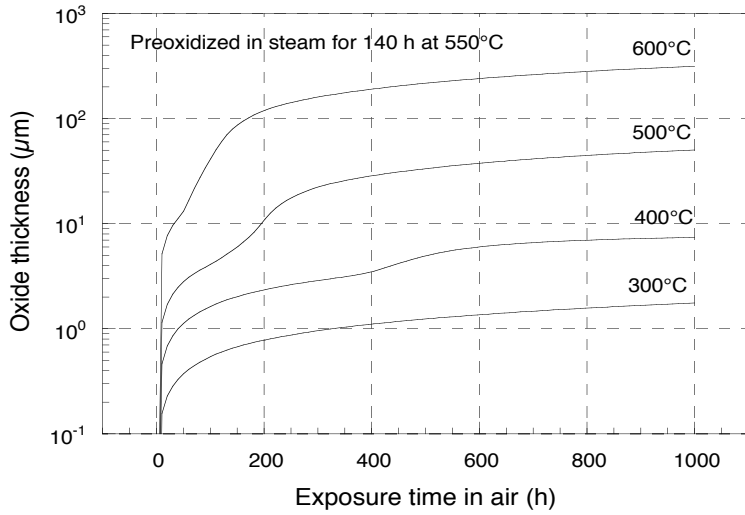


Figure 6.26. Oxide thickness growth as a function of exposure time in air at several temperatures for steam-preoxidized Zircaloy-4.

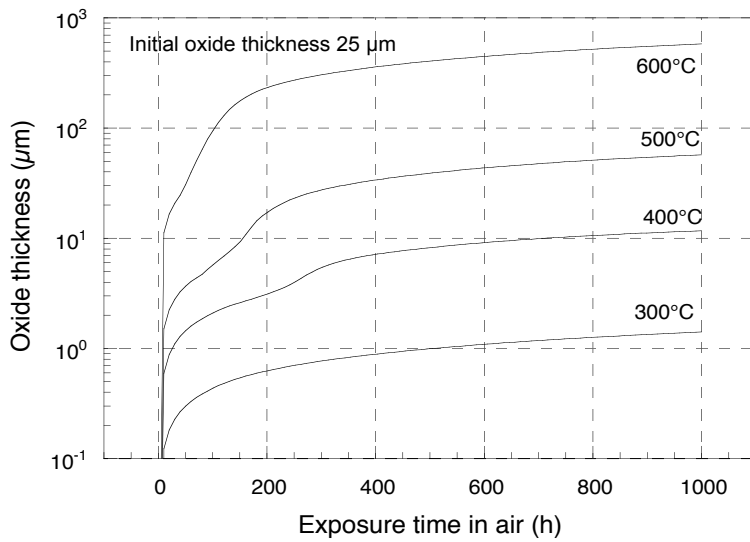


Figure 6.27. Oxide thickness growth as a function of exposure time in air at several temperatures for steam-preoxidized Zirlo.

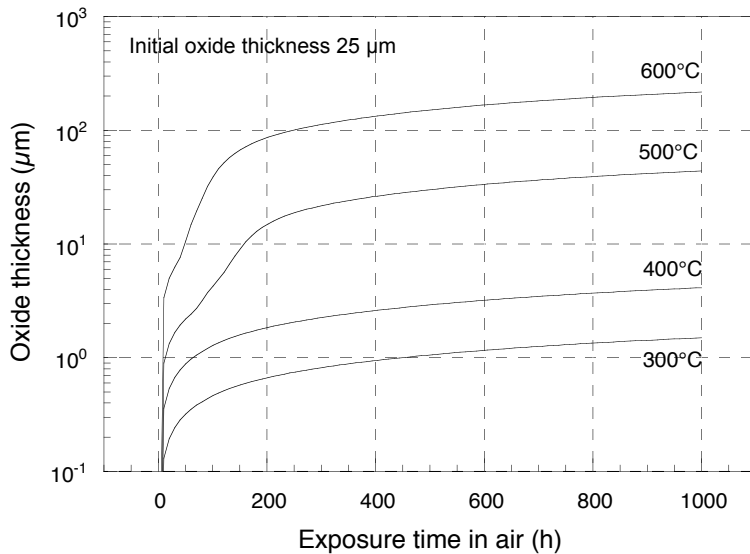


Figure 6.28. Oxide thickness growth as a function of exposure time in air at several temperatures for steam-preoxidized M5.

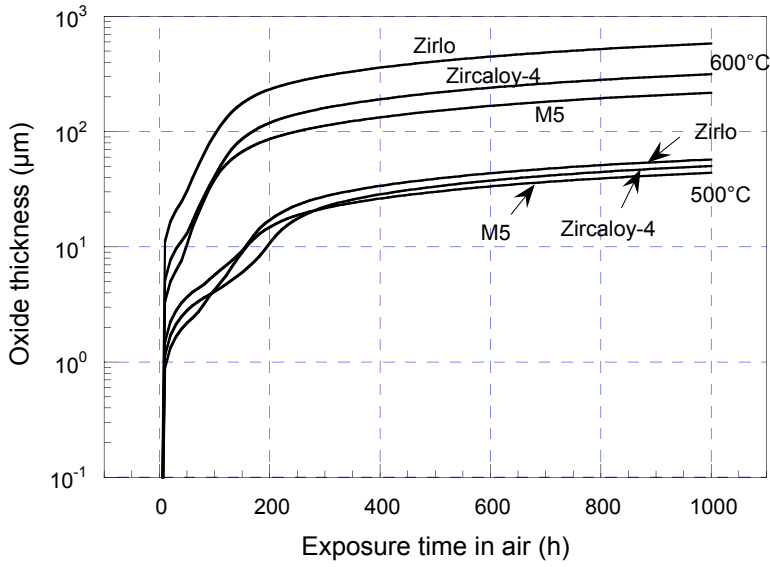


Figure 6.29. Comparison of oxide thickness growth for steam-preoxidized Zircaloy-4, Zirlo, and M5 as a function of exposure time in air at 500 and 600°C.

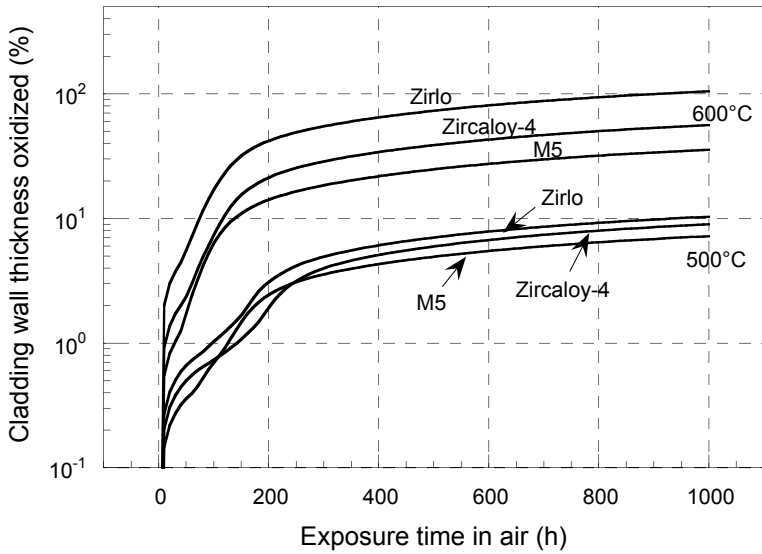


Figure 6.30. Cladding wall thickness (in percent) oxidized in air at 500 and 600°C for initially steam-preoxidized Zircaloy-4, Zirlo, and M5.

7 Summary and Conclusions

An extensive oxidation study was conducted on Zircaloy-4, Zirlo, and M5 cladding materials to establish the air kinetics of oxidation for the alloys in both bare and steam-preoxidized conditions. Weight change and oxide thickness data were developed over a wide temperature range, and the results were used to develop oxidation rate correlations for all three materials. The following is a summary of the information developed for both the alloys.

7.1 Zircaloy-4

Several conclusions were drawn from the oxidation study on bare and steam-preoxidized Zircaloy-4 specimens and in different exposure environments:

- At 600°C, the oxidation rate of the bare alloy in air was 2 to 4 times higher than that of the bare alloy oxidized in steam. Also, the rate in air for the bare alloy was ≈ 2 times higher than the rate for steam-preoxidized condition.
- At temperatures $\leq 500^\circ\text{C}$, the oxidation rates for the bare alloy in air were factors of 2-10 lower than those observed for the bare alloy oxidized in steam. Also, the oxidation rates for the bare alloy in air were comparable to (or only slightly higher than) the rates obtained for the air oxidation of steam-preoxidized specimens.
- The observed oxidation rates in the low- O_2 environment for the steam-preoxidized alloy were comparable to (or slightly lower than) the air oxidation rates of steam-preoxidized specimens.
- At 600°C, the major cause for the differences in the oxidation rates for the specimens with different pretreatment is the development and propagation of transverse cracks in the oxide scales after only 80 hours of exposure.
- At temperatures $\leq 500^\circ\text{C}$, metallographic examination of the specimens (that were exposed for times up to 400 h at 500°C and ≥ 1000 h at 300°C) showed the oxide scales to be adherent and virtually crack-free.
- At temperatures $\geq 600^\circ\text{C}$, the bare and steam-preoxidized Zircaloy-4 oxidized rapidly in air; the steam-oxidized material seemed to oxidize faster than the bare alloy, probably due to the increased propensity for cracks to develop in the preformed oxide than in the in-situ developed oxide.
- In order to evaluate the role, if any, of the oxygen-deficient and nitrogen-enriched gas mixture in the oxidation of Zircaloy-4, limited tests were conducted in a 2.5 vol.% $\text{O}_2\text{-N}_2$ gas mixture at 400 and 600°C. At 600°C, the weight change data indicated that the rates are somewhat slower in the low- O_2 environment when compared with those in air. The rates were almost the same in both environments at 400°C.
- Isothermal oxidation tests were conducted with tube specimens of steam-preoxidized Zircaloy-4 with internal pressures in the range of 50-400 psig at 600 to 900°C. Extensive metallography was used on the tested specimens to examine the oxide scale development, pin-hole rupture morphology, and oxide cracking propensity. The data indicated that the oxide thickness is somewhat larger ($\approx 20\%$ in the post-breakaway region) in the tests conducted with high internal pressure than that obtained in the absence of it, especially at 600 and 700°C. The increase is attributed to microcracks in the oxide (and associated oxidation) that results from increased deformation in the specimen due to pressurization.

- In the temperature range 300-600°C, the results showed that the correlation, developed from the oxidation data for the steam-preoxidized Zircaloy-4, generated in the current project is in fair agreement with that based on Nureg1 and Powers.
- Weight change and oxide thickness data, developed in the present program, were used to develop correlations to depict the air oxidation behavior of the alloys as a function of time and temperature. The results showed that the correlation developed for Zircaloy-4 in the current project is in fair agreement with that based on Nureg1 and Powers. The predictions based on Nureg2 and CODEX correlations for Zircaloy-4 are several orders of magnitude lower than those based on current work, especially at lower temperatures.
- At temperatures $\geq 600^\circ\text{C}$, the present data for both the steam-preoxidized and bare Zircaloy-4 showed a higher oxidation rate than that based on the correlation by Nureg1 and Powers.

7.2 Zirlo

Several conclusions were drawn from the oxidation study on bare and steam-preoxidized Zirlo specimens:

- From the steam oxidation standpoint, the oxidation rate for Zirlo is $\approx 10\%$ less than that for Zircaloy-4 under similar exposure conditions; the oxide thickness ranged from 26-30 μm in Zirlo and 28-32 μm in Zircaloy-4 after 140 h exposure at 550°C.
- At temperatures $>400^\circ\text{C}$, the weight change and oxide thickness data for steam-preoxidized Zirlo exhibited a breakaway trend, similar to that observed for Zircaloy-4. The data obtained up to 1013 h (the longest time in the present study) at 300°C did not show a breakaway trend.
- The weight change data showed good agreement with the measured oxide thickness values for specimens exposed at temperatures between 300 and 700°C. At temperatures of 800 and 900°C, the oxide scales exhibited significant spallation and fracturing. As a result, reliable measurements on oxide thickness could not be made in these specimens.
- The oxidation rate for Zirlo in the post-breakaway region were lower than those reported earlier for Zircaloy-4 at $T \leq 500^\circ\text{C}$; however, the rates are higher for Zirlo than for Zircaloy-4 at $T \geq 600^\circ\text{C}$.
- After exposures at temperatures $\geq 600^\circ\text{C}$, the oxide scales that developed exhibited a multitude of radial cracks that extended to the substrate alloy; at 500°C, the radial cracks traveled only part way from the external surface, even after 429 h exposure.
- The oxidation rate data developed in this project were used to develop correlations that relate rates (based on weight change and oxide thickness) and temperature. Correlations were developed for two temperature regimes, namely, 300-600°C (low-temperature oxidation regime) and 300-900°C. Correlations were developed for both pre- and post-breakaway regimes.
- The data showed that in the pre-breakaway region, oxygen ingress into Zirlo occurs at a higher rate than in Zircaloy-4. In the post-breakaway region, the rates for Zirlo are somewhat lower than those for Zircaloy-4 at $T \leq 500^\circ\text{C}$; however, at $T \geq 600^\circ\text{C}$, the rates for Zirlo are higher than for Zircaloy-4.

7.3 M5

Several conclusions were drawn from the oxidation study on bare and steam-preoxidized M5 specimens and in different exposure environments:

- From the steam oxidation standpoint, the oxidation rate for M5 is substantially less than that for either for Zircaloy-4 or Zirlo. For example, it took 427 h at 550°C to obtain $\approx 25\text{-}\mu\text{m}$ -thick oxide in M5 whereas a similar thickness is achieved in 140 h at 550°C in Zirlo and Zircaloy-4.
- In the pre-breakaway region, the air oxidation rate for steam-preoxidized M5 is comparable to that of Zirlo in the temperature range 300-500°C but it is somewhat higher than that of Zircaloy-4, possibly due to the presence of Nb in the advanced alloys. At 600°C, the rate for M5 was less than that for either Zircaloy-4 or Zirlo.
- In the post-breakaway region, the air oxidation rate was similar for M5 and Zirlo at 500°C; at 600°C, the rate for M5 was less than that for Zircaloy-4 or Zirlo. M5 did not exhibit breakaway oxidation trend at 400 and 300°C in the time periods used in the present study.
- The weight change data showed good agreement with the measured oxide thickness values for specimens exposed at temperatures between 300 and 700°C. After 161 and 305 h exposures at 600°C, the oxide scale on M5 exhibited significant axial and transverse cracks and its protective capacity seemed inadequate.
- At 500°C and below, the oxide developed in during air oxidation seemed adherent and relatively crack free in the time periods used in the current study.

The study showed that all three alloys, initially in steam-preoxidized condition, can undergo further oxidation in the event of air ingress. The rate at which the oxide scale grows is dependent on the cladding temperature, exposure time, and alloy composition. The data and correlations on oxide scale development, presented in various sections of this report, in the three alloys are used to evaluate the time dependence cladding oxidation for the three cladding materials with nominal wall thickness and to calculate the section loss of the cladding as a function of time and temperature. Data and correlations for Zirlo, and M5, developed in this project, are applicable to the advanced claddings for use under high burnup conditions.

References

- Com-Nougue, J., K. Omo, B. de Gelas, G. Beranger, and P. Lacombe, 1969, *J. Less-Common Metals*, 19, 259.
- Cubicciotti, D., 1950, *J. Am. Chem. Soc.*, 72, 4138.
- Godlewski, J., 1994, "How the Tetragonal Zirconia is Stabilized in the Oxide Scale that is Formed on a Zirconium Alloy Corroded at 400°C in Steam," *Zirconium in the Nuclear Industry*, ASTM STP 1245, p. 663.
- Gulbransen, E. A. and K. F. Andrew, 1957, *Trans. Metall. Soc. AIME*, 209, 394.
- Kidson, G. V., 1966, *Electrochemical Technology*, 4, 193.
- Leistikow, S. and H. v. Borg, 1987, "Investigation under Nuclear Safety Aspects of Zircaloy-4 Oxidation Kinetics at High Temperatures in Air," 2nd Workshop of German and Polish Research on High Temperature Corrosion of Metals, eds. W. J. Quadackers, H. Schuster, and P. J. Ennis, Julich, Germany.
- Leistikow, S., R. Kraft, and E. Pott, 1980, "The Interaction between Corrosion and Mechanical Stress at High Temperatures," *Proc. Eur. Symp.*, Petten, p. 123.
- Leistikow, S., G. Schanz, and H. V. Borg, 1978, "Kinetik und Morphologie der Isothermen Dampf-Oxidation von Zircaloy-4 bei 700-1300°C," *KfK 2587*, Germany.
- Mackay, T. L., 1963, *Trans. Metall. Soc. AIME*, 227, 1184.
- Moalem, M. and D. R. Olander, 1991, "Oxidation of Zircaloy by Steam," *J. Nucl. Mater.* 182 p. 170.
- Pawel, R. E., 1979, *J. Electrochem. Soc.*, 126, 1111.
- Pawel, R. E. and J. J. Campbell, 1980, *J. Electrochem. Soc.*, 127, 2188.
- Pemslar, J. P., 1962, *J. Nucl. Mater.*, 7, 16.
- Pemslar, J. P., 1964, *J. Electrochem. Soc.*, 111, 1185.
- Powers, D. A., L. N. Kmetyk, and R. C. Schmidt, 1994, "A Review of the Technical Issues of Air Ingression During Severe Reactor Accidents," Sandia National Laboratories, Albuquerque, NM, SAND94-0731.
- Rosa, C. J., and W. W. Smeltzer, 1980, "The Oxidation of Zirconium in Oxygen/Nitrogen Atmospheres," *Z. Metallkunde*, p. 470.
- Wallwork, G. R., W. W. Smeltzer, and C. J. Rosa, 1964, *Acta Metall.*, 12, 409.

APPENDIX

Parabolic rate constants, based on weight change and oxide thickness, for air oxidation of Zircaloy-4, Zirlo, and M5 cladding

Initial condition	Air oxidation temperature (°C)	Parabolic rate constant (kg ² /m ⁴ ·s)		Oxide thickness rate constant (μm ² /s)	
		Pre-breakaway	Post-breakaway	Pre-breakaway	Post-breakaway
Zircaloy-4					
Steam preoxidized	900	1.1 x 10 ⁻⁶	1.2 x 10 ⁻⁵	1.1 x 10 ⁻¹	18.1
	800	5.7 x 10 ⁻⁷	9.6 x 10 ⁻⁶	4.3 x 10 ⁻²	5.0
	700	4.3 x 10 ⁻⁸	4.6 x 10 ⁻⁷	8.6 x 10 ⁻³	2.8 x 10 ⁻¹
	600	8.4 x 10 ⁻⁹	7.2 x 10 ⁻⁸	9.8 x 10 ⁻⁴	2.7 x 10 ⁻²
	500	2.8 x 10 ⁻¹⁰	1.9 x 10 ⁻⁹	4.8 x 10 ⁻⁵	6.8 x 10 ⁻⁴
	400	4.3 x 10 ⁻¹²	6.4 x 10 ⁻¹¹	7.7 x 10 ⁻⁶	7.7 x 10 ⁻⁶
	300	5.7 x 10 ⁻¹³	-	8.6 x 10 ⁻⁷	-
Bare	900	5.1 x 10 ⁻⁷	7.1 x 10 ⁻⁶	2.2 x 10 ⁻¹	2.6
	800	1.3 x 10 ⁻⁷	1.6 x 10 ⁻⁶	9.8 x 10 ⁻²	2.0
	700	2.8 x 10 ⁻⁸	5.7 x 10 ⁻⁷	1.9 x 10 ⁻²	3.1 x 10 ⁻¹
	600	2.0 x 10 ⁻⁸	1.2 x 10 ⁻⁷	9.6 x 10 ⁻³	6.6 x 10 ⁻²
	500	1.9 x 10 ⁻¹⁰	1.1 x 10 ⁻⁹	8.6 x 10 ⁻⁵	4.9 x 10 ⁻⁴
	400	4.3 x 10 ⁻¹²	2.9 x 10 ⁻¹¹	3.1 x 10 ⁻⁶	1.8 x 10 ⁻⁵
	300	4.2 x 10 ⁻¹³	-	3.1 x 10 ⁻⁷	3.1 x 10 ⁻⁷
Zirlo					
Steam preoxidized	900	1.8 x 10 ⁻⁶	5.7 x 10 ⁻⁵	2.8 x 10 ⁻²	3.8
	800	3.1 x 10 ⁻⁷	1.2 x 10 ⁻⁵	1.9 x 10 ⁻²	2.6
	700	4.3 x 10 ⁻⁸	6.9 x 10 ⁻⁷	5.1 x 10 ⁻³	2.0 x 10 ⁻¹
	600	1.8 x 10 ⁻⁸	1.9 x 10 ⁻⁷	4.6 x 10 ⁻³	9.0 x 10 ⁻²
	500	1.1 x 10 ⁻¹⁰	8.2 x 10 ⁻¹⁰	8.3 x 10 ⁻⁵	8.4 x 10 ⁻⁴
	400	2.6 x 10 ⁻¹¹	4.6 x 10 ⁻¹¹	1.3 x 10 ⁻⁵	2.6 x 10 ⁻⁵
	300	1.4 x 10 ⁻¹²	-	5.5 x 10 ⁻⁷	-
Bare	900	1.0 x 10 ⁻⁶	3.0 x 10 ⁻⁵	3.9 x 10 ⁻¹	11.3
	800	2.4 x 10 ⁻⁷	9.9 x 10 ⁻⁶	6.3 x 10 ⁻²	4.8
	700	6.3 x 10 ⁻⁸	7.2 x 10 ⁻⁷	1.1 x 10 ⁻²	2.7 x 10 ⁻¹
	600	1.1 x 10 ⁻⁸	1.3 x 10 ⁻⁷	3.9 x 10 ⁻³	5.5 x 10 ⁻²
	500	1.9 x 10 ⁻¹⁰	1.1 x 10 ⁻⁹	1.2 x 10 ⁻⁴	6.0 x 10 ⁻⁴
	400	3.5 x 10 ⁻¹¹	-	2.9 x 10 ⁻⁶	-
	300	1.2 x 10 ⁻¹²	-	1.7 x 10 ⁻⁷	-
M5					
Steam preoxidized	900	6.3 x 10 ⁻⁸	1.9 x 10 ⁻⁵	2.4 x 10 ⁻¹	8.9
	800	4.3 x 10 ⁻⁸	2.4 x 10 ⁻⁶	1.9 x 10 ⁻²	9.9 x 10 ⁻¹
	700	3.8 x 10 ⁻⁹	1.4 x 10 ⁻⁷	2.4 x 10 ⁻³	7.2 x 10 ⁻²
	600	1.5 x 10 ⁻⁹	3.0 x 10 ⁻⁸	4.2 x 10 ⁻⁴	1.3 x 10 ⁻²
	500	6.9 x 10 ⁻¹¹	6.3 x 10 ⁻¹⁰	2.9 x 10 ⁻⁵	3.9 x 10 ⁻⁴
	400	7.1 x 10 ⁻¹²	-	4.7 x 10 ⁻⁶	-
	300	8.8 x 10 ⁻¹³	-	6.2 x 10 ⁻⁷	-
Bare	900	8.6 x 10 ⁻⁷	3.4 x 10 ⁻⁵	4.7 x 10 ⁻¹	1.7 x 10 ⁺¹
	800	4.4 x 10 ⁻⁷	2.7 x 10 ⁻⁶	2.2 x 10 ⁻¹	1.1
	700	5.7 x 10 ⁻⁸	3.5 x 10 ⁻⁷	3.0 x 10 ⁻²	1.5 x 10 ⁻¹
	600	1.3 x 10 ⁻⁸	6.5 x 10 ⁻⁸	4.1 x 10 ⁻³	1.9 x 10 ⁻²
	500	5.0 x 10 ⁻¹⁰	9.3 x 10 ⁻¹⁰	3.0 x 10 ⁻⁴	5.6 x 10 ⁻⁴
	400	1.9 x 10 ⁻¹¹	-	6.6 x 10 ⁻⁶	-
	300	8.7 x 10 ⁻¹⁴	-	4.4 x 10 ⁻⁸	-

BIBLIOGRAPHIC DATA SHEET
(See instructions on the reverse)

1. REPORT NUMBER
(Assigned by NRC. Add Vol., Supp., Rev.,
and Addendum Numbers, if any.)

NUREG/CR-6846
ANL-03/32

2. TITLE AND SUBTITLE

Air Oxidation Kinetics for Zr-Based Alloys

3. DATE REPORT PUBLISHED

MONTH	YEAR
June	2004

4. FIN OR GRANT NUMBER

Y6707, Y6512

5. AUTHOR(S)

K. Natesan and W. K. Soppet

6. TYPE OF REPORT

Technical

7. PERIOD COVERED (Inclusive Dates)

8. PERFORMING ORGANIZATION – NAME AND ADDRESS (If NRC, provide Division, Office or Region, U.S. Nuclear Regulatory Commission, and mailing address; if contractor, provide name and mailing address.)

Argonne National Laboratory
9700 South Cass Avenue
Argonne, IL 60439

9. SPONSORING ORGANIZATION – NAME AND ADDRESS (If NRC, type "Same as above"; if contractor, provide NRC Division, Office or Region, U.S. Nuclear Regulatory Commission, and mailing address.)

Division of Systems Analysis and Regulatory Effectiveness
Office of Nuclear Regulatory Research
U.S. Nuclear Regulatory Commission
Washington, DC 20555-0001

10. SUPPLEMENTARY NOTES

S. Basu, NRC Project Manager

11. ABSTRACT (200 words or less)

An experimental program was conducted to generate data on the air oxidation kinetics of unirradiated cladding of Zr-based alloys (such as Zircaloy-4, Zirlo, and M5) with an oxide layer that is representative of the current inventory of spent fuel discharged after a medium or high level of fuel burnup. The oxide layer that forms on the cladding while in the spent fuel pool was simulated by a preoxidation step in a steam environment for 140 h at 550°C for Zircaloy-4 and Zirlo and for 427 h at 550°C for M5. The steam-preoxidized specimens were subsequently oxidized in air at temperatures in the range of 300-900°C. Oxidation tests in air emphasized temperatures in the range of 300-600°C, which is representative of cladding heatup in the event of a partial or full draining of spent fuel pool coolant. Weight change and oxide thickness measurements were made on the specimens exposed at various times to establish the kinetics of the scaling process as a function of temperature. Bare capsules of the three alloys were also exposed in air for comparison of the oxidation behavior of the alloys with and without steam preoxidation. Limited tests were conducted at 400 and 600°C to evaluate the oxidation performance of Zircaloy-4 in a low-oxygen high-nitrogen environment. Isothermal oxidation tests were also conducted with tube specimens of steam-preoxidized Zircaloy-4 with internal pressures in the range of 50-400 psig at 600 to 900°C. Extensive metallography was used on the tested specimens to examine the oxide scale development, pin-hole rupture morphology, and oxide cracking propensity. The results showed that the correlation, developed for Zircaloy-4 from the oxidation data generated in the current project, is in fair agreement with that based on Nureg1 and Powers. The predictions based on Nureg2 and CODEX correlations for Zircaloy-4 are several orders of magnitude lower than those based on current work, especially at lower temperatures. A comparison of the oxidation data for Zirlo with those for Zircaloy-4 showed that the post-breakaway rates are somewhat lower for Zirlo at T ≤ 500°C; however, the rates are higher for Zirlo than for Zircaloy-4 at T ≥ 600°C. The oxidation rates (in the post-breakaway region) for M5 are consistently lower than for other two alloys at 500 and 600°C. Oxide scale thickness data, developed on the three materials during air exposure, are used to evaluate the time- and temperature-dependence of oxidation of cladding of typical wall thickness.

12. KEY WORDS/DESCRIPTORS (List words or phrases that will assist researchers in locating this report.)

Air Oxidation
Zr-Based Alloys
Oxide Thickness
Weight Change
Oxidation Correlations
Zircaloy-4
Zirlo
M5

13. AVAILABILITY STATEMENT

Unlimited

14. SECURITY CLASSIFICATION

(This Page)

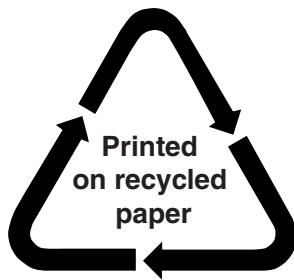
Unclassified

(This Report)

Unclassified

15. NUMBER OF PAGES

16. PRICE



Federal Recycling Program